Partial Oxidation and Autothermal Reforming of Heavy Hydrocarbon Fuels with Non-Equilibrium Gliding Arc Plasma for Fuel Cell Applications

A Thesis

Submitted to the Faculty

of

Drexel University

by

Michael J. Gallagher, Jr.

in partial fulfillment of the

requirement for the degree

of

Doctor of Philosophy

February 2010

Acknowledgements

I would like to express my sincerest gratitude to my Ph.D. advisors Dr. Alexander Fridman and Dr. Alexander Gutsol for all of their help and guidance over these past years. Working with them was a rewarding challenge and I had the privilege to participate in interesting research projects, travel to many interesting places, and be introduced to many of their friends and colleagues in the plasma community.

I would like to especially thank my Ph.D. Committee: Dr. Alex Fridman, Dr. Nick Cernansky, Dr. Alex Rabinovich, Dr. Gary Friedman, and Dr. Alex Dolgopolsky. All of them have contributed greatly to my development at Drexel in many ways from teaching interesting courses, providing excellent research advice, and giving important career advice.

I would also like to thank my fellow graduate students in the Mechanical Engineering Department and within the Drexel Plasma Institute. They are too numerous to name here, so I will just say thank you for your support, creative ideas, and encouragement.

I also would like to thank my family who has supported and guided me throughout my lifetime and especially my parents, for without their hardwork and dedication to their children, I would never have made it this far.

Finally, I would like to thank my wife Angela. You are everything to me and if it weren't for your constant love and encouragement, I never would have finished this doctoral thesis.

Table of Contents

List of Tables

List of Figures

Abstract

Synthesis Gas Production through Partial Oxidation and Autothermal Reforming of Heavy Hydrocarbon Fuels with Non-Equilibrium Gliding Arc Plasma Reactors for Fuel Cell Applications

Michael J. Gallagher, Jr.
Advisor: Dr. Alexander Fridman

Non-thermal plasma fuel reforming technology has several advantages over traditional catalytic or thermal processes including fast start time, high productivity, relatively low electrical energy costs to operate. Several novel gliding arc plasma reformers were developed and investigated for the partial oxidation of several fuels including n-Tetradecane, Diesel, and JP-8 in the partial oxidation and autothermal reforming regimes. High conversion was achieved with efficiencies greater than 80 percent. The results show that gliding arc systems are capable of reforming heavy hydrocarbon fuels with high conversion efficiency and are an important piece of technology for on-board vehicular reforming systems that should be further developed and optimized.

1. Introduction to Plasma-assisted Synthesis Gas Production for Fuel Cell Applications

1.1 Introduction

In the search for cleaner, more efficient energy-producing technologies, the fuel cell stands out as one that has the potential to revolutionize how energy is produced throughout the world. In the transportation industry, some researchers and engineers are seeking ways to combine fuel cells with electric motors on-board vehicles in hopes of replacing the internal combustion engine and significantly reducing local carbon and nitrogen oxide emissions. There are several technological barriers to incorporating fuel cells onto vehicles; currently there is no refueling infrastructure where consumers can readily purchase hydrogen, and storage of pure hydrogen gas in a tank on a vehicle is possible, but very expensive due to the extremely high pressures required to achieve an energy density that is comparable to petroleum fuels. As an intermediate step to avoid these problems, some researchers have developed on-board fuel reformers that can convert widely available petroleum fuels (gasoline, diesel, natural gas) into hydrogen rich synthesis gas (H_2 + CO), which can then be utilized in a fuel cell to generate the required electrical power.

The types of fuel reformers that are available for onboard syngas production include catalytic [1-3], non-catalytic (superadiabatic) [4-6], and plasma reformers [7-9]. Each type of reformer has its advantages and disadvantages with regard to performance, capital cost, lifetime, and feasibility for integration into a vehicular system. Catalytic reformers have shown the best results thus far in terms of hydrogen selectivity; however, they have several drawbacks that include high capital costs to construct (because of expensive rare metals employed) and a limited lifetime due to poisoning from sulfur and soot produced as byproducts during reforming.

Catalytic reformers also have a high metal capacity and equipment size that requires long pre-heating times and low specific productivity as the product gas stream must have good contact with the densely packed catalyst metal surfaces. Non-catalytic reformers use a dense, flow-restricting packed bed or monolith structure made from inert materials to provide efficient heat recuperation and minimize heat losses in the reaction zone. By using this scheme, researchers claim that it is possible to achieve superadiabatic temperature conditions that can accelerate reforming reaction kinetics [6]. Using such structures, however, can create large pressure drops within the system, reduce the overall productivity, and make integration into a vehicular onboard unit more challenging. Alternatively, non-thermal plasma systems are typically small and compact with relatively simple power supplies, which make them ideal for integration onto a vehicle. In addition, plasma reformers can have a wide dynamic range of operation that allows for high productivity of syngas at low electrical energy cost, and they have low capital costs to build and have a very long operational lifetime. Plasmas have been involved in fuel conversion and combustion systems over a century and were originally used as a convenient thermal energy source to ignite/initiate combustion reactions. Recently, plasmas have been investigated for their potential to exhibit catalytic effects primarily because of complex interactions of their excited species (electrons, ions, radicals) in fuel conversion reactions. Some evidence has been found for the plasma catalysis effect in lowering the required ignition temperatures for combustion systems; however more work is needed to elucidate the catalytic effects in fuel-rich syngas production systems.

Over the past two decades, plasma researchers have investigated the reforming capability of nearly all types of plasma, from thermal to non-thermal ones, in fuel conversion systems with many types of hydrocarbon fuels. In addition, plasma researchers have utilized various reforming schemes such as partial oxidation, dry (CO_2) reforming, steam reforming, and steam-oxidative reforming to test the limits of plasma's capabilities to act as a catalyst and even possibly replace

traditional metal catalysis-based systems. The focus of this plasma fuel reforming research has largely been on finding the best plasma discharge for fuel reforming and improving the energy efficiency of those systems, namely keeping the electrical energy cost to produce the plasma as low as possible (1-5% of the heating values of the product stream) while still achieving good conversion. The two best plasma discharges that have produced the best results for conversion to syngas with acceptable energy efficiency are gliding arc (transitional arcs) and microwave plasmas. The reasons why these discharges are the most suitable for syngas production will be discussed in later sections including an explanation of why the simpler to organize gliding arc discharge was chosen as the focus of this thesis. Gliding arc plasma systems for syngas production were first developed with a simple 2D-planar geometry and reforming results produced by these systems were good [10]. However, it was later discovered that organizing gliding arc in a 3D cylindrical geometry within a vortex chamber provided for better mixing and contact of reactants with the plasma discharge [11]. Such an installation was first designed at Drexel University for investigating methane conversion to syngas using a partial oxidation reforming scheme which was stabilized in reverse vortex flow [12].

In this thesis, the focus was on designing smaller and compact vortex-based reformers for use on-board vehicles. In addition, a new type of plasma-based auxiliary power system was developed to generate electrical power from hydrocarbon fuels onboard military tanks. Several design challenges were overcome including incorporating exhaust gas recirculation from a solid oxide fuel cell as reactants in an autothermal reforming scheme. The results presented here show that vortex-based gliding arc systems are capable of reforming heavy hydrocarbon fuels with high conversion efficiency and are an important piece of technology for on-board vehicular reforming systems that should be further developed and optimized.

1.2 What is Plasma?

Plasma is often described as the fourth state of matter and this refers to the chemical, thermal, or electrical breakdown of a gas, often forming a luminous ionized state comprised of a mix of particles: positive ions, negatively charged electrons, radicals, and neutral gas atoms and molecules [13]. The act of ionization, when an electron is separated from an atom or molecule leaving a positive ion behind (or attached, thereby creating a negative ion), can be created by means of chemical and/or thermal energy or the electro-dynamic forces from an electric field. A flame is a well-known type of weakly-ionized, low-temperature plasma consisting primarily of a heated pool of radicals and molecules and small amounts of electrons and ions created from chemical and thermal ionization processes [14]. Other types of man-made and some naturally occurring plasmas are created by a strong electric field generated by high potential from the accumulation of charge (e.g. lightning in clouds) or a high voltage source. The electrons within the background gas near the electric field absorb energy from the field, ionize, and then establish a flow of current within channels of the electrically conductive ions and electrons.

Plasmas are categorized as thermal or non-thermal, with the primary difference being how energy is deposited into the plasma gas stream. In thermal plasmas, energy is spent to heat the entire gas stream, and temperatures often range from 10,000-100,000K (10-100 electron volts (eV)). The joule heating effect is responsible for high gas temperatures in thermal plasmas where power is initially transferred from the electric field to electrons and then to the background neutral gas species by way of a large number of electron-neutral collisions [15]. In thermal plasmas, the temperatures of all of the plasma components approach thermal equilibrium, which is why these plasmas are often referred to as *equilibrium* plasmas. In non-thermal plasmas, also referred to as *non-equilibrium* plasmas, the temperatures of the plasma components are not the same, and electrons often have greater temperatures than the other gas components. The

background gas molecules in non-thermal plasmas are often at or near room temperature; however, they can become excited and/or store energy in their thermodynamic energy modes (rotational, vibrational, and electronic). In addition, high energy electrons produced in non-thermal plasma can influence processes such as molecular dissociation and can lead to the formation of active chemical species that act as aggressive oxidizing and reducing agents. Radicals, such as atomic oxygen (O) and hydroxyl (OH), and electronically excited oxygen ($O_1\Delta G$) are among the many species that are known to influence the kinetics of fuel conversion reactions. Plasma-generated radicals and ions behave very much like catalysts, as they can participate in chain reactions that promote or accelerate reaction pathways.

Both thermal and non-thermal plasmas have many commercial and industrial applications, and measurements of their effectiveness and efficiency are often based on the energy cost to include them in a process. For example, thermal plasmas have useful applications in metallurgy where high temperatures are needed to separate aluminum from the naturally occurring mineral bauxite (aluminum oxide). However, such high temperatures can be unsuitable for hydrocarbon conversion and hydrogen production processes because the electrical power that is spent to create the plasma is comparable to the energy value of the obtained products. Also since non-thermal plasmas are considered as weakly ionized plasmas, that is, they produce very small amounts of high-energy ionized species, the price to generate one radical or ion can be very high (3-30 eV or 30-3000 kJ/mol). It is often beneficial for the plasma active species to participate in multiple reactions or chain reactions, thereby increasing their effectiveness and reducing their specific energy cost to produce the desired products. The specific energy cost, which is defined as the ratio of plasma power to the number of syngas molecules produced, should be comparable to, if not much less than, the thermodynamic enthalpy of the process. Non-thermal plasmas, in general, are very suitable for fuel conversion applications with high

productivity because they have low power levels (30-300W) that usually comprise only a small fraction (2-5%) of the power of the syngas product stream.

1.3 Types and Classifications of Plasmas

There are a variety of thermal and non-thermal plasma discharges that have been used for fuel conversion applications. The most well-known thermal plasma used for this purpose is the arc plasma, followed by the lesser known radio frequency inductively-coupled plasma (RF ICP), and thermal microwave plasma. Among the non-thermal plasmas investigated for fuel conversion, most researchers have focused on using the gliding arc discharge, pulsed corona, dielectric barrier discharge (DBD), spark discharges, and the RF capacitively-coupled plasma (CCP) discharge. In the section that follows, a brief introduction of each type of discharge will be presented to highlight its characteristics and demonstrate the benefits for fuel conversion applications.

1.3.1 Arc Plasmas

Thermal arc plasmas have been used in many industrial and commercial applications throughout history including metallurgy, waste disposal, lighting applications, and ignition systems in vehicles. Arc plasmas are high-current (30A – 30kA), low-voltage (10 – 100V) discharges that attain very high gas temperatures (10,000 – 100,000K or 10 - 100 eV) due to the high degree of joule heating from the discharge current. Their initial high temperature also contributes to sustaining high current by influencing the mechanism by which electrons are supplied to the discharge, namely the thermionic field emission mechanism. Essentially, the thermionic mechanism relies on the synergistic combination of high metal electrode temperature and help from the external electric field which allows a large number of electrons to escape the electrode metal surface and provides a high flux of current into the discharge [13]. The high

temperatures of thermal plasmas can lead to problems such as, evaporation and erosion of electrodes that can only be prevented by employing cooling systems. Thermal plasmas are favorable for certain fuel conversion applications, such as gasification of solid fuels like coal or biomass, because they can rapidly accelerate reactions. But they have the significant drawback of high electrical energy cost to operate them and therefore have limited applications in syngas and hydrogen production systems.

1.3.2 Non-Thermal Gliding Arc Plasmas

An alternative to high power thermal arc systems is a type of transitional non-equilibrium plasma called gliding arc. This is an auto-oscillating discharge that begins as a thermal arc plasma, and through the force of convective air flow or a magnetic field it is elongated and cooled until it transitions into a non-thermal plasma. Gliding arc plasmas are sometimes referred to as *warm* plasmas because they have translational gas temperatures in the range of 1000-3000K, which are in between the gas temperatures of cold plasmas (300K) and thermal plasmas (≥10,000K) [16]. A non-equilibrium temperature distribution between the other degrees of freedom was demonstrated [17] with vibrational temperatures of approximately 4500K, and average electron energies in the range of 1.4-2.1 eV [18]. Figure 1a shows a schematic of a planar gliding arc discharge configuration, and Figure 1b depicts an image of several arcs at various lengths between two diverging electrodes.

Gliding arc plasmas are often arranged in cylindrical geometry in which the discharge is rotated using a vortex flow scheme (Figure 2). These vortex-based gliding arc reformers have the advantage of providing good mixing and contact of reactants with the plasma discharge. Figure 3 shows a schematic of a typical vortex-based gliding arc plasma reactor [19]. Gliding arc plasmas have shown some of the best reforming results in terms of syngas conversion and low electrical energy cost for syngas production [9].

1.3.3 Microwave and Radio-Frequency Plasma Discharges

Plasma discharges that are sustained with high frequency electromagnetic fields have been employed in various syngas production systems [16]. Radio frequency (RF) and microwave discharges are the two major types used for this purpose and they have the unique advantage that the plasma does not need to be in direct contact with the electrodes. Electrode-less operation is often preferred for extremely high temperature reforming applications because it can eliminate the need for complicated electrode cooling. Initiating high frequency plasmas is more challenging than DC plasmas because they require complex and somewhat more expensive power supplies that include a high frequency generator, and more importantly, the plasma must be coupled as a load in the power circuit. In RF plasmas, the electromagnetic fields generated by the power supply interacts with the plasma through processes known as inductive or capacitive coupling, with the former used to generate thermal discharges and the latter primarily used for generating non-thermal plasmas. The idea of coupling the electromagnetic field to the plasma discharge is very important because the plasma is sustained by the energy absorbed by the field, and poor coupling means that the efficiency of the power supply and the overall circuit is low. The frequencies used to generate RF plasmas are typically in the range between 0.1 to 100 MHz.

In microwave plasmas, the wavelengths are very small, on the order of centimeters, and approach the dimensions of the reactor itself. Often, waveguides are used to collect and concentrate the electromagnetic waves within the reactor, and the waves are then are able to transfer power within the discharge. Not all of the wave power is dissipated in the discharge however; typically about half is absorbed, a quarter of it is transmitted through the discharge, and another quarter is reflected. The benefit of using complex discharges such as microwave plasmas is that the high degree of coupling between the electromagnetic field and the discharge creates conditions of strong non-equilibrium with a high degree of ionization. This is much better than

the previously described non-thermal plasmas, where energy density is low and ionization is weak, with only a small fraction of high energy electrons created. In microwave plasmas, increased energy input is used very efficiently in producing a larger fraction of high energy electrons along with higher amounts of vibrationally excited species as compared to other non-thermal plasmas. High power microwave discharges with 95% efficiency have been developed [20] and the increased amount of energetic species can boost the plasma catalysis effect, although the cost of such improvements is a more complex design and more expensive power generation equipment. Figure 4 shows microwave plasma configurations in low, moderate, and high pressure as well as a photograph of a low pressure microwave discharge

1.3.4 Dielectric Barrier Discharge Plasmas

The dielectric barrier discharge (DBD) is a well-known commonly used non-thermal plasma discharge that is employed in many industrial processes related to surface treatments of materials such as polymers and textiles [21-22], ozone generation [23-24], and air sterilization in heating, ventilation, and air conditioning (HVAC) systems [25]. DBD plasmas have a layered electrode structure in which two metal electrodes are separated by a thin layer of dielectric material, often made from ceramic, quartz, or glass (Figure 5). The dielectric barrier acts to limit current flow once the plasma discharge is ignited and prevents the discharge from transitioning into a plasma spark, which can result in local overheating, shock waves, and noise. DBD plasmas typically operate with either an AC frequency (0.5 to 500 kHz) or in a pulsed DC mode and most often have a non-uniform, filamentary structure consisting of a series of microdischarges.

DBD plasmas are non-equilibrium and can generate a significant fraction of active chemical species that are beneficial in fuel ignition and conversion reactions; however they have had limited success in fuel conversion applications. The oxygen dissociation mechanism in DBD plasmas can be quite efficient (up to 85%) [26] and can result in relatively high atomic oxygen

and ozone production levels. These aggressive oxidizers tend to act quickly and combust fuels to CO_2 and H_2O, rather than promoting direct partial oxidation with formation of CO and H_2. Another limitation of DBDs in fuel conversion applications is their low power density due to their limited current and low gas temperatures. Since partial oxidation (POX) and steam reforming reactions require an elevated initial temperature to proceed (800-1100K), non-thermal DBD systems usually require additional energy to be spent for pre-heating.

1.3.5 Continuous & Pulsed Corona Discharges

The corona discharge is a weak plasma typically found in regions of high electric field strength near sharp edges, points, or thin wires. A corona discharge can be created with a strong, continuous DC electric field and often requires only one electrode. The space surrounding the high voltage electrode can itself function as a sink for charged particles, thus completing the circuit. Figure 6 shows an example of a corona plasma discharge. Man-made corona discharges are typically arranged with a point-to-plane geometry or as a concentric annulus (thin wire inside of a tube). The strong non-uniformity of the electric field between the two electrodes is the driving force that makes a corona discharge ignite; to achieve such non-uniformity, the characteristic size of the high voltage electrode should be much less than the distance between electrodes. The corona discharge can become unstable if additional voltage or current is applied causing breakdown between electrodes forming a strong plasma channel, known as a spark. Spark formation should be avoided because it causes local overheating of the gas and non-uniformity of treatment, which is undesirable for many applications. Continuous coronas are then limited in terms of power input; however, they are strongly non-equilibrium and can provide high concentrations of active chemical species and radicals that are useful in a variety of chemical and industrial processes. One way to increase the power of corona discharges while avoiding spark formation is to use a pulsed power supply to deliver high amplitude voltage (steep wave front)

with short rise times. Pulsed-periodic voltage delivers fast and effective power transfer into the discharge, but stops short of spark formation as long as the pulse width is shorter than the transition time (on the order of 100-300 nanoseconds with electrode distances at 1-3 cm) [15]. Corona discharges are attractive for fundamental studies of the plasma catalysis effect in combustion and fuel conversion due to their high degree of non-equilibrium and good spatial uniformity. Researchers in this area have had success integrating pulsed-corona discharges in shock tubes to study the effect of plasma active species on ignition delay times [27].

1.4 Chemical Reactions in Fuel Processing

The following section highlights the important chemical reactions that are utilized in fuel processing systems. The stoichiometric equations involving combustion, partial oxidation, steam reforming, steam-oxidative reforming, and dry (CO_2) reforming are explained as well as basic definitions of parameters such as the oxygen-to-carbon and steam-to-carbon ratios. Examples of specific chemical reactions along with their reaction enthalpies are listed in Table 1 below.

1.4.1 Combustion of Hydrocarbons

Combustion is a well-known phenomenon where a hydrocarbon fuel is completely oxidized to the products of CO_2 and H_2O in an exothermic reaction. The general stoichiometric equation for hydrocarbon oxidation in air is as follows:

$$C_xH_y + \left(x + \frac{y}{4}\right)(O_2 + 3.76N_2) \rightarrow xCO_2 + \left(\frac{y}{2}\right)H_2O + \left(x + \frac{y}{4}\right)(3.76N_2) \qquad (1\text{-}1)$$

1.4.2 Partial Oxidation of Hydrocarbons

The partial oxidation of hydrocarbons occurs when a sub-stoichiometric amount of oxygen is supplied to the reaction thus causing partial combustion to occur. Similar to

combustion, partial oxidation is also an exothermic reaction, however; the amount of heat released is considerably less than the heat release caused during complete combustion of the fuel. The primary products are hydrogen and carbon monoxide (also known as synthesis gas). The general relation of the partial oxidation of hydrocarbons is as follows [28]:

$$C_xH_y + \frac{x}{2}(O_2 + 3.76N_2) \rightarrow xCO + \frac{y}{2}H_2 + \frac{x}{2}(3.76N_2) \quad (1\text{-}2)$$

Partial oxidation reactions are thought to proceed in two distinct phases; a rapid, highly exothermic combustion phase where all free oxygen is consumed to form heat and the products of CO_2 and H_2O; and a much slower endothermic reforming phase where residual unconverted fuel reacts with the CO_2 and H_2O plus the reaction heat to form syngas products H_2 and CO [29-32].

1.4.3 Steam Reforming of Hydrocarbons

Steam reforming of hydrocarbons occurs when H_2O is used as an oxidizer to produce hydrogen and carbon monoxide as products. This reaction is endothermic and requires a source of heat energy to drive the reaction.

$$C_xH_y + xH_2O \rightarrow xCO + (x + \frac{y}{2})H_2 \quad (1\text{-}3)$$

1.4.4 Oxidative Steam Reforming of Hydrocarbons

Oxidative steam reforming combines traditional steam reforming with some additional amount of air or oxygen to provide a supplementary source of exothermic reaction heat to assist in the completion of the steam conversion reactions. It is possible to balance the amount of heat released by exothermic partial oxidation with the endothermic energy consumption from the

steam reforming reactions such that the reaction is theoretically self-sustaining [28]. This process is known at Autothermal reforming and the net enthalpy change for the process is zero (ΔH = 0).

$$C_xH_y + \ n(O_2 + \ 3.76N_2) + \ (x - 2n)H_2O \rightarrow xCO + \ \left(x - 2n + \frac{y}{2}\right)H_2 + \ 3.7nN_2 \qquad (1\text{-}4)$$

1.4.5 Dry (CO_2) Reforming of Hydrocarbons

Dry reforming is a process that utilizes carbon dioxide as an oxidant to convert hydrocarbon fuels into syngas. The process is similar to steam reforming in that it is endothermic; however it usually requires greater energy input for the reaction to proceed. The general reaction scheme for dry (CO_2) reforming is as follows:

$$C_xH_y + \ xCO_2 \rightarrow 2xCO + \ \frac{y}{2}H_2 \qquad (1\text{-}5)$$

1.4.6 Water gas shift reaction

The water gas shift (WGS) reaction is an important part of the fuel conversion process because it is possible that a portion of the syngas produced may react with residual CO_2 or H_2O causing a shift in the concentrations of CO and H2 through the following:

$$CO + H_2O \leftrightarrow CO_2 + \ H_2 \qquad (1\text{-}6)$$

The WGS reaction is often used to purify syngas streams to eliminate CO and produce additional hydrogen. The reaction is slightly exothermic (ΔH = -41 kj/mol) and typically occurs at low temperatures (T ≈ 400°C). The WGS reaction is reversible at very high temperatures (T>1000C).

1.4.7 Oxygen-to-Carbon Ratio

The oxygen-to-carbon (O/C) ratio is the ratio of twice the molar oxygen flow rate versus the molar flow rate of the fuel carbon within a hydrocarbon oxidation reaction scheme. It is also an important parameter used to identify the regime of the hydrocarbon oxidation system (i.e. combustion versus partial oxidation regimes). For example, an O/C ratio of 1 denotes the stoichiometric partial oxidation point of a fuel conversion process where exactly one mole of carbon is combined with one mole of atomic oxygen to from CO as a product.

$$\frac{O}{C}ratio = \frac{2\dot{n}_{O_2}}{x\dot{n}_{C_xH_y}} \tag{1-7}$$

1.4.8 Steam-to-Carbon Ratio

Similar to the O/C ratio, the steam-to-carbon ratio (S/C) is the ratio of the molar flow rate of H_2O to the molar flow rate of the fuel carbon:

$$\frac{S}{C}ratio = \frac{n_{H_2O}}{x\dot{n}_{C_xH_y}} \tag{1-8}$$

Table 1. List of reaction enthalpies involving methane in various fuel conversion systems

Conversion Process		Reaction Enthalpy (eV/mol)
Direct Decomposition:	$CH_4 \rightarrow C(s) + 2H_2$	$\Delta H = 0.7\ eV/mol$
Dry reforming:	$CH_4 + CO_2 \rightarrow 2CO + 2H_2$	$\Delta H = 2.6\ eV/mol$
Steam reforming:	$CH_4 + H_2O \rightarrow CO + 3H_2$	$\Delta H = 2.2\ eV/mol$
Partial Oxidation:	$CH_4 + 1/2\ O_2 \rightarrow CO + 2H_2$	$\Delta H = -0.2\ eV/mol$
Water-gas shift reaction:	$CO + H_2O \rightarrow CO_2 + H_2$	$\Delta H = -0.4\ eV/mol$

1.5 Important Equations to Measure Reforming Performance

1.5.1 Specific Energy Requirement

One important parameter to measure the effectiveness heat utilization during fuel reforming is the specific energy requirement. For plasma systems, this calculation includes the energy input as electrical power from the plasma discharge plus any additional heating supplied to sustain the process. The specific energy requirement is often described in terms of electron volts per molecule of hydrogen produced (eV/mol H_2) for plasma systems, but others use more familiar units such as kWh/m^3 and kJ/mol (for reference: 1 eV/molecule ≈ 1.2 kWh/m^3 and 100 kJ/mol ≈ 1 eV/molecule). Since the specific energy required to produce syngas is dependent on the amount of syngas produced, it is inherently tied to the physical conversion for each set of conditions for each system. In other words, if the specific energy requirement for a particular system is high, the system may have had poor physical conversion of fuel to syngas, and therefore the energy cost per mole of syngas produced is high. The specific energy requirement can be used to compare the costs of plasma with other technologies such as thermal or catalytic reformers.

1.5.2 Product yield

The product yield is defined as the amount of desired reagent produced divided by the maximum possible amount of reagent that could be yielded by the input fuel. Using hydrogen as an example:

$$H2\ Yield\ (\%) = \frac{mol_{H2}\ produced}{mol_{H2}\ in\ fuel} \times 100 \tag{1-9}$$

1.5.3 Product Selectivity

Product selectivity is a measure of how much of one particular reagent is produced as compared to all of the reagents. Hydrogen selectivity is then:

$$Selectivity\ (\%) = \frac{mol_{H2}\ produced}{total\ mol_{H2}\ in\ products} \times 100 \tag{1-10}$$

1.5.4 Energy conversion efficiency

The energy conversion efficiency is an important parameter to estimate conversion of fuel to products in terms of energy by using the lower heating values (LHV) of each component.

$$Energy\ Conversion\ Efficiency\ (\%) = \frac{(Mol_{Syngas}\ \times LHV_{Syngas})}{Mol_{Fuel} \times LHV_{Fuel}} \times 100 \tag{1-11}$$

1.6 Plasma as an alternative to traditional catalyst in fuel reforming

The kinetic limitations of fuel conversion processes often require higher reaction temperatures than what is necessary to produce the same results when the system is at thermodynamic equilibrium. Lower reaction temperatures are desired, not only from the obvious viewpoint of improving energy efficiency, but because higher temperatures can open reaction pathways that may ultimately lead to undesirable soot formation in hydrocarbon reforming systems. Therefore, many modern fuel conversion systems incorporate a catalyst of some kind in order to lower activation energy barriers and thus lower the required reaction temperatures and avoid unwanted by-product formation.

Researchers that incorporate plasma into fuel reforming systems claim that plasma behaves like a catalyst. The effect of *plasma catalysis*, in essence, is caused by the interaction of charged and excited particles generated by plasma that allow for the reduction or removal of activation energy barriers in fuel conversion reactions. It was demonstrated long ago that most exothermic ion-molecule reactions have no activation energy requirement and therefore proceed without barrier [33]. This is because the charge-dipole attraction in plasma-induced ion-molecular reactions is stronger than the quantum-mechanical repulsion between molecules, and thus overrules most barriers for exothermic reactions to proceed [15].

The major drawback of using plasma for its catalytic properties is that it requires a constant (electrical) energy source in order to sustain it. Some plasma active species have long lifetimes once they are generated, for example nitrogen oxide (NO) and ozone (O_3) can survive for several minutes and travel long distances from the plasma source. But most of the highly reactive plasma species have very short lifetimes and recombination occurs in short distances within the plasma itself or near the plasma boundaries and reactor walls. One could even describe plasma as a catalyst that needs constant regeneration from the continuous loss of

electrons, ions, and radicals through recombination processes. The need for constant energy input to sustain the plasma raises questions about the economics and the energy cost of using plasma in fuel conversion systems. The cost of using plasma as a catalyst in fuel conversion systems is dependent on how well its active species, particularly ions, participate in fuel conversion reactions. The energy cost to create one ion is high, around 10-30eV, and therefore the ion should participate in multiple chain reactions to be cost effective. It is possible to organize such chain reactions in fuel conversion systems; however, many of the kinetic mechanisms involving plasma active species in fuel-rich hydrocarbon conversion reactions are still unknown. Much of the plasma fuel conversion and syngas production research over the past decade has been focused on designing engineering systems that are capable of producing more syngas at higher conversion rates while operating with lower plasma energy cost. In order to maximize the catalytic effect of plasma, more focus is needed to identify the key reaction mechanisms and pathways for product formation in plasma-assisted fuel conversion processes.

Alternatively, there has been a greater emphasis on identifying plasma mechanisms for the enhancement of ignition and combustion, where reaction mechanisms involving plasma active species and fuels, such as hydrogen and methane, have been identified [34-36]. In the field of plasma-assisted combustion, researchers have discovered that plasma-induced gas excitation can significantly reduce ignition temperature by as much as 600K and increase a flame's blow off velocity with very high energy efficiency (less than 1% of burner power is input as plasma power) [14]. Such breakthroughs were made possible through support from the aerospace industry and large contributions from the U.S. and foreign government military research institutions for projects related to jet engine ignition at high altitudes. In addition, plasma combustion researchers have investigated the effects of non-thermal plasma on ignition and stabilization of flames [37-38] and combustion in supersonic flows [39-40], moderate pressures, and lean mixtures [41]. These researchers employed experimental installations such as shock

tubes with advanced diagnostics, to specifically isolate and prove the plasma effect for ignition enhancement. The plasma-assisted fuel conversion community should follow the example of the plasma combustion/aerospace industry in order to answer the most important questions related to the plasma influenced mechanisms of syngas production and the overall significance of plasma for fuel conversion.

1.6.1 Thermal versus non-thermal mechanisms of plasma catalysis

As stated in the previous section, most of what is known about the plasma catalysis effect is related to mechanisms for *fuel-lean* (or *oxygen-rich*) ignition/combustion of hydrocarbons. These mechanisms, however, overlap *fuel-rich* conversion processes such as partial oxidation (POX), since POX is known to begin with a short combustion phase where nearly all oxidizers are consumed to form a small amount of combustion products (H_2O, CO_2) and higher temperatures [31]. In this section, we discuss the specific mechanisms of plasma catalysis related to ignition/combustion and review the postulated mechanisms related to plasma-assisted fuel reforming processes such as POX and steam (H_2O) and dry (CO_2) reforming.

Plasma-assisted ignition and combustion systems are driven by two types of kinetic mechanisms, thermal and non-thermal. The thermal mechanism, in which plasma's contribution is through gas heating alone, results in a local temperature increase, exponential acceleration of elementary combustion reactions, chain propagation of fuel oxidation, and ultimately stable combustion [16]. This mechanism is well known and one of its earliest applications was the spark ignition in internal combustion engines [42]. The thermal ignition mechanism is not very relevant for applications because, although it is the easiest to organize, it has a high energy cost since electrical energy from the plasma is spent non-selectively and is distributed into many degrees of freedom that are irrelevant for ignition and combustion (i.e. heating of inert nitrogen). Alternatively, non-thermal plasma mechanisms for ignition and combustion have been shown to

induce oxidation reactions as a result of interactions between active species, such as excited particles and ions. Often, significant fractions of neutral chemical species acquire and store energy internally (through vibrational or electronic excitation) resulting from collisions between ions and electrons in plasma. This stored energy may be used to overcome activation energy barriers for reactants otherwise in their ground states [43]. Additionally, the non-thermal ignition mechanism allows plasma energy to be used selectively in the creation of these useful active species.

1.6.2 Non-thermal plasma-induced mechanisms of ignition and stabilization of flames

There are several known reaction pathways in which the various active particles generated by non-equilibrium plasmas can participate in the stimulation of ignition and combustion of hydrocarbon fuels [16]. Amongst these options, there are three primary groups of important plasma species, namely excited species, radicals, and ions. The effect generated by the plasma active species in ignition systems is related to shifting the ignition limit, where chain branching and terminating reactions are balanced. The classical results demonstrating the effect of electrical discharges on the explosion limits for an H_2-O_2 mixture [42, 44-45] is shown in Figure 4. The effect of increasing plasma current is shown, including the case of "0A" (i.e. no current), which is the conventional H_2-O_2 explosion limit (typically referred to as the S-shaped curve). In the area to the right of the curves, corresponding to higher temperatures, the chain-branching reactions dominate and this is known as the explosive region. As demonstrated from Figure 7, plasma lowers the threshold temperature required for autoignition, an effect otherwise known as sub-threshold ignition. In essence, plasma active species are able to accelerate chain branching reactions faster than chain terminating reactions at temperatures below the predicted autoignition temperature, where traditional chemical kinetics predicts that ignition is impossible.

1.6.3 Effect of excited species on subthreshold ignition in H_2-O_2 mixtures

Chain branching and terminating reactions for H_2-O_2 mixtures can be controlled by suppressing the formation of the relatively stable chain-terminating hydroperoxy radical (HO_2), or by accelerating chain-branching radical formation (H, OH). The most important chain-propagating reactions are described in Table 1.

Stimulation of chain branching reactions can occur by means of employing vibrationally or electronically excited particles to destroy the metastable HO_2^* complex, thereby recovering the chain-branching radicals O and OH:

$$H + O_2 \rightarrow HO_2^* \quad (1\text{-}12)$$

$$HO_2^* + P^* \rightarrow OH + O + P \quad (1\text{-}13)$$

whereas P^* represents an excited plasma particle [46]. An additional mechanism to avoid the formation of the HO_2 radical involving vibrationally excited nitrogen (N_2^*) is accomplished through the reaction [47]:

$$H + O_2 + N_2^* \rightarrow OH + O + N_2 \quad (1\text{-}14)$$

In addition to suppressing formation of the HO_2 radical, it is possible to stimulate the dissociation of HO_2 through vibrational excitation in the following plasma-induced mechanism:

$$HO_2 + N_2^* \rightarrow OH + O + N_2 \quad (1\text{-}15)$$

It should be noted that vibrationally excited nitrogen is included in the above mechanisms because it is considered as one of the most stable of the vibrational species produced by plasma.

Table 2. Chain propagating reactions in H_2-O_2 ignition processes

Chain-branching	$H + O_2 \rightarrow OH + O$	(1-16)
	$O + H_2 \rightarrow H + OH$	(1-17)
Chain-terminating	$H + O_2 + M \rightarrow HO_2 + M$	(1-18)

1.6.4 Effect of ions on subthreshold ignition in H_2-O_2 mixtures

The role of plasma-generated ions in fuel conversion and combustion reactions was previously discussed and relates to charge attractive forces that can overcome quantum-mechanical reaction barriers resulting in the plasma-catalysis effect. Kosarev et al. [48] proposed a low-temperature hydrogen oxidation mechanism involving negative ions from plasma:

$$e + O_2 + M \rightarrow O_2^- + M \quad (1\text{-}19)$$

$$O_2^- + H_2 \rightarrow OH^- + OH \quad (1\text{-}20)$$

$$OH + H_2 \rightarrow H_2O + H \quad (1\text{-}21)$$

$$H + O_2 + M \rightarrow HO_2 + M \quad (1\text{-}22)$$

$$OH^- + H \rightarrow H_2O + e \quad (1\text{-}23)$$

$$OH^- + HO_2 \rightarrow H_2O + O_2 + e \quad (1\text{-}24)$$

The effectiveness of this mechanism is limited by competition between electron detachment and the fast recombination processes of reactions (8-12) and (8-13) [16]. Other ionic mechanisms similar to this one may be responsible for the effects related to sub-threshold ignition and can be applied to ignition and combustion of hydrocarbons. More investigation is needed in this area to further understand the effects of ions and to apply these principles to fuel conversion and hydrogen production systems.

1.6.5 Effect of radicals and other long-lived species on subthreshold ignition

Plasma-generated oxidizing radicals such as atomic oxygen (O), ozone (O_3), nitrogen oxide (NO), and other hydrocarbon radicals like CH_2, CH_3, and CH have been investigated to provide insight into their influence on the kinetic pathways of ignition and combustion [41, 49]. Starikovskaia et al. [34] performed an efficiency analysis of the effects of atomic oxygen on ignition of H_2-O_2 mixtures at various initial temperatures and found that, at lower temperatures, the main effect of ignition acceleration was caused by fast local gas heating upon recombination of atomic oxygen to O_2. Following on this concept, a plasma-related variant of the thermal ignition mechanism known as the radical-thermal bootstrap mechanism was developed to explain some of the subthreshold ignition results. Again, the idea is that instantaneous thermalization of plasma energy caused by heating upon recombination and relaxation of plasma radicals can boost temperatures from subthreshold to above-threshold conditions. The radical-thermal bootstrap mechanism is considered a thermal mechanism for ignition; however, it is possible to accelerate the bootstrap effect by using non-thermal plasmas through short oxidation chains below the autoignition limit, thereby increasing the energy efficiency over the thermal ignition mechanism alone [16].

An additional mechanism involving the long-lived NO radical has also been shown to improve subthreshold ignition by suppressing chain-terminating processes through the following mechanism:

$$NO + HO_2 \rightarrow NO_2 + OH \quad (1\text{-}25)$$

$$H + NO_2 \rightarrow NO + OH \quad (1\text{-}26)$$

The above mechanism can be effective for stimulating ignition, not only because NO has a long lifetime, but also because it is produced with relatively high concentrations in combustion

systems. Furthermore, this mechanism has been shown to occur in ignition systems utilizing hydrogen, ethylene, and other hydrocarbon fuel sources.

1.6.6 Effect of plasma active species on hydrogen-rich syngas production systems

All of the previously described mechanisms explained the effect of some of the plasma active species on ignition and combustion of primarily hydrogen-oxygen systems. Less is known about the effect of plasma active species on conversion of hydrocarbon fuels to hydrogen-rich synthesis gas (H_2, CO); however, there are a few research groups that are making progress in identifying plasma's role in these reactions [50-51]. Many investigations have focused on methane conversion in plasma-assisted processes such as direct decomposition (pyrolysis) [52-57]; methane oxidative conversion using air and pure O_2 [58-61], H_2O and CO_2 [62]; and steam-oxidative reforming [63-65]. The following sections provide an overview of the mechanisms of plasma catalysis as they relate to these syngas production processes.

1.6.7 Plasma catalysis of direct decomposition (pyrolysis) of methane

Direct non-oxidative conversion of methane with the plasma-catalysis effect can occur with the production of hydrogen and soot:

$$CH_4 \rightarrow C(s) + 2H_2 \qquad (1\text{-}27)$$

This process has the potential to produce CO_2-free hydrogen although it is endothermic and requires thermal energy input ($\Delta H = 0.7$ eV/mol) to sustain the process. Experimental work using non-thermal plasmas for pyrolysis was performed by Givotov et al. [66] using microwave plasmas with some preheating of reactants. It was found that the addition of plasma energy caused a decrease in the reaction temperature, and it is believed that a fraction of the input plasma energy (<20%) is spent in catalytic stimulation of reaction 8-16. Givotov et. al. postulated several possible mechanisms of plasma-stimulated pyrolysis including process stimulation from

non-uniform temperature distribution in the discharge, effect of plasma radicals and excited species, CH_4 decomposition on the surface of carbon clusters, and the ion-Winchester mechanism. The methyl ion radical CH_3^+ was found to provide the most effective chain stimulation for the production of hydrogen and multiple carbon cluster growth to sizes up to C_{20}. The ion-Winchester mechanism is thought to have the strongest effect in CH_4 decomposition and it begins with dissociative ionization by electron impact:

$$e + CH_4 \rightarrow CH_3^+ + H + e + e \quad (1\text{-}28)$$

Carbon cluster formation with hydrogen production then proceeds through the following:

$$CH_3^+ + CH_4 \rightarrow C_2H_5^+ + H_2 \quad (1\text{-}29)$$

Increasing growth of carbon clusters occurs through the attachment of CH_2 groups, with additional hydrogen production occurring through two pathways:

$$C_nH^+_{2n+1} + CH_4 \rightarrow C_{n+1}H^+_{2n+3} + H_2 \quad (\text{for } n>1) \quad (1\text{-}30)$$

$$C_nH^+_{2n+1} + CH_4 \rightarrow [C_{n+1}H^+_{2n+5}]^* \quad (1\text{-}31)$$

Chain termination of this process occurs due to recombination of charged particles:

$$e + C_{n+1}H^+_{2n+3} \rightarrow C_{n+1}H^+_{2n+2} + H \quad (1\text{-}32)$$

$$e + CH_3^+ \rightarrow CH_2 + H \quad (1\text{-}33)$$

The experimental results of plasma-assisted pyrolysis are described in section 8.X.

1.6.8 Plasma Catalysis of Partial Oxidation (POX) of methane

There have been fewer studies on the mechanisms of the plasma catalysis effect for the partial oxidation of methane and other hydrocarbon fuels as compared to pyrolysis and ignition/combustion studies. This may be due to the fact that several of the reaction mechanisms

for plasma stimulation of pyrolysis (non-oxidative) and ignition/combustion (highly-oxidative) overlap within the partial oxidation (moderately-oxidative) processes. Partial oxidation begins with a rapid-oxidation phase in which nearly all free oxygen is consumed to form the combustion products H_2O and CO_2 [31-32]. Because of this rapid combustion phase, regions of fuel-rich mixtures are created in which almost no oxidizers are present, and pyrolysis reactions can occur almost simultaneously. Nair et al. suggested that the mechanisms of plasma stimulated partial oxidation of methane begin with the following four reactions [65]:

$$e + CH_4 \rightarrow CH_3 + H + e \quad (1\text{-}34)$$

$$e + CH_4 \rightarrow CH_2 + H_2 + e \quad (1\text{-}35)$$

$$e + CH_4 \rightarrow CH + 3H + e \quad (1\text{-}36)$$

$$e + O_2 \rightarrow 2O + e \quad (1\text{-}37)$$

In this mechanism, electrons from the plasma are postulated to play an important role in non-oxidative CH_4 decomposition, while free oxygen is converted into aggressive oxygen radicals.

Nair et. al. combined experimental investigation of methane partial oxidation in DBD plasma at low temperatures (<200C) with a kinetic model, which included over 180 reactions with 29 species. Their investigation showed that at low temperatures, C_1 oxygenated species (such as, CH_2O, CH_3O) are formed as intermediate products, and are then further oxidized to syngas products CO and H_2. They also noted that the greatest limitation of plasma-assisted POX is low selectivity toward H_2 because of the plasma's affinity to oxidize H_2 to H_2O; however, this may be improved by moving to a combined steam-oxidative reforming process [65].

Rusanov et. al. described a short-chain mechanism for the non-thermal plasma conversion of methane that includes intermediate products acetylene and ethylene [67]. This process is described in the framework of several conversion zones within a plasma reformer: the zone ahead of the combustion wave front, the high temperature zone immediately behind the

combustion front, and the zone beyond (far behind) the combustion front. The zone beyond the combustion front includes some amount of combustion products from the rapid oxidation phase (CO_2, H_2O), some partial oxidation products (CO, H_2) and some amount of pyrolysis products (C_2H_2, C_2H_4). The process also includes a short chain mechanism that describes the creation and destruction of the intermediate residual hydrocarbons by the following:

$$H_2O + H \rightarrow OH + H_2^* \quad (1\text{-}38)$$

$$2C_2H_2 + 2OH \rightarrow 2CO + 2CH_3 \quad (1\text{-}39)$$

$$2CH_3 \rightarrow C_2H_4 + H_2 \quad (1\text{-}40)$$

$$C_2H_4 + M \rightarrow C_2H_3 + H + M \quad (1\text{-}41)$$

$$C_2H_3 + M \rightarrow C_2H_2 + H + M \quad (1\text{-}42)$$

This process can also be used to describe acetylene conversion to syngas.

Researchers are currently continuing efforts to indentify and understand the underlying mechanisms related to plasma-assisted partial oxidation, steam, and CO_2 reforming. Greater knowledge of these mechanisms will ultimately help scientists and engineers to optimize future plasma-assisted reforming systems. In the meantime, the existing experimental plasma reforming systems can provide valuable information about the effects such as temperature, plasma energy input, and other factors, which are known to have a direct impact on the efficiency of plasma reformers.

1.7 Other Advantages of Plasma Catalysis in Fuel Reforming Systems

There are several other important factors that contribute to the advantages of using plasma for fuel-cell-based conversion systems. These factors are particularly important for transportation applications where plasma reformers are combined with vehicles. The following sections highlight these important factors.

1.7.1 No Inertia (Preheating) Required

Traditional thermal catalytic systems require long preheating times in order to reach the required activation temperatures for the metal catalysts to become effective. These temperatures are in the range of 900-1300K [68], and given the typical high density of packed-bed and monolith-structured catalyst systems, this can require preheating times on the order of tens of minutes to hours in duration. The principle advantage of plasma reformer systems is that the plasma has a near-instantaneous response and requires no preheating to initiate fuel conversion reactions. This is especially important for on-board reformers for vehicles where plasma reformers generate hydrogen or hydrogen-rich syngas for fuel cells.

1.7.2 No Sensitivity to Sulfur or Other Contaminates

Most metal-based catalyst systems suffer from deactivation problems due to impurities in the fuel feedstock stream which can bind with active sites on the catalyst surface [69]. Deactivation by sulfur, which is commonly found in liquid hydrocarbon fuels such as Diesel and JP-8, is often irreversible and can render the catalyst useless. Catalyst deactivation can also occur from coke and carbonaceous deposits on catalyst surfaces that can occur during reforming reactions; however it is possible to regenerate by increasing oxygen and temperature and burning off the coke/soot [70]. Plasma-based fuel conversion systems do not suffer from these limitations because it is a gaseous-phase, volumetric catalyst with no surfaces with which these compounds can bind.

1.7.3 No Soot Formation

Many researchers report observations of little or no soot formation in rich and ultra-rich plasma-assisted fuel conversion systems [11, 19, 58]. One explanation of this observed effect is that plasma is strongly oxidative and can provide fast oxidation of soot precursors. The strong

oxidative effect is due in part to the acidic nature of air-driven plasmas. The acidic nature of plasma begins with the ionization of air (21% O_2-79% N_2) and leads to a large production of N_2^+ ions, which can then easily react with water due through the following:

$$N_2^+ + H_2O \rightarrow N_2 + H_2O^+ \quad (1\text{-}43)$$

Although water is only present in small quantities in air, the presence of water ions leads to interactions with neutral water molecules forming hydronium ions and hydroxyl radicals:

$$H_2O^+ + H_2O \rightarrow H_3O^+ + OH \quad (1\text{-}44)$$

The efficiency of production of H_3O^+ and OH from these reaction mechanisms determines the level of acidity of air plasmas and defines plasma's overall oxidative nature.

As previously mentioned, the surfaces of metal catalysts can induce soot formation because they can act as deposition sites where carbon products and soot prefer to condense. Some researchers have combined plasma and metal catalysts, in so-called plasma-catalytic reformers, in order to eliminate soot formation while still realizing the benefits of catalyst reforming. In this way, plasma acts as an initiator of reforming reactions, preventing soot formation on the catalyst surface, while the catalyst itself acts to improve heat transfer in the post-plasma region and complete the reforming reactions. Plasma-catalytic reforming is described in more detail in the following sections.

1.7.4 Plasma Reformers are Small and Compact

The characteristic size of atmospheric pressure plasma reformers for syngas production can be quite small and compact. An example of such a reformer is the Gliding-Arc Plasmatron device from Drexel University [19], which has a total volume of less than 1-liter and is capable of producing up to 20kW of syngas from heavy hydrocarbons such as diesel. Such a compact

design is again important for vehicular-based on-board reforming systems and portable auxiliary power units [71].

1.7.5 Possibility of Combining Desulfurization and Reforming

Another advantage of the plasma catalytic effect in fuel conversion systems is the possibility of combining syngas production and desulfurization in one process. When sulfur-containing fuels are reformed into syngas, the sulfur is typically converted into hydrogen sulfide (H_2S) gas, which can then react with active sites on metal catalyst surfaces causing solid sulfur to bind with the catalyst and deactivate it. Non-thermal plasma has the capability to dissociate H_2S with low energy input (1.2 eV/mol) and create solid sulfur and H_2 as products [72-73]. In addition, some researchers have investigated the effectiveness of non-thermal plasma in converting H_2S within syngas streams with varying degrees of success [74].

1.8 Plasma Reforming of C_1-C_6 Hydrocarbons

Plasma-assisted conversion of light, gaseous hydrocarbons has been widely investigated and the research areas have focused on pyrolysis, steam or CO_2 (dry) reforming, and partial oxidation (POX) to synthesis gas. Conversion of methane has drawn the most attention due to its high content within abundant natural gas sources and also the large database of kinetic information that describes the details of methane combustion and partial oxidation reactions, which some researchers have utilized for modeling and simulation of plasma-assisted conversion [75-76]. In this section, the most relevant results related to plasma-assisted conversion will be presented. The focus will be on results which provide the lowest plasma energy cost with good conversion, such as those from microwave and gliding arc plasma systems, which are among the best.

1.8.1 Non-thermal plasma-assisted partial oxidation of methane

Many non-thermal atmospheric pressure plasmas have been used to investigate methane partial oxidation, such as microwave discharges [67, 77-78], pulsed corona [79-80], and gliding arc [11, 58, 60]. Gliding arc plasmas are ideal for conversion of hydrocarbons because of their proven non-equilibrium effects [81] and relative high power density, which is desirable for high-productivity industrial systems. In addition, gliding arc plasmas have demonstrated some of the highest yields and energy efficiencies of all plasma fuel conversion systems thus far [9]. Kalra et. al. [11] investigated methane conversion using a gliding arc in tornado (GAT) system where a rotating gliding arc discharge was elongated to a fixed length between two ring electrodes inside a vortex chamber. This configuration included an internal heat exchanger to provide heat recuperation and allowed for preheating of reactants to temperatures around 700K. Experimental results for conversion efficiency are shown in figure 8, where approximately 85% conversion of methane was observed at an O/C ratio of 1.3. A kinetic model was developed to simulate the expected methane conversions with and without plasma, which are shown as the solid and dotted lines, respectively in figure 8. The experimental results of plasma-assisted conversion matched reasonably well with model predictions and were higher than the predicted conversion by thermal energy alone.

The electrical energy cost to produce syngas was approximately 0.09 kWh/m^3, which is a small fraction (3%) of the total chemical power of the system. In addition, there was no soot formation observed in the range of O/C ratios investigated when the plasma discharge was present; however, soot formation was observed in trials without the presence of the plasma. The gliding arc discharge in this system stimulates the partial oxidation process kinetically by acting as a catalyst.

Additional work on methane partial oxidation using microwave plasma discharges was performed by Babaritskii et. al. with the goal of separating the effect of thermal heating from the plasma energy input for stimulating methane conversion [77]. In these trials, a continuous, atmospheric-pressure microwave discharge (2.45 GHz, power: 0.5-3 kW) was used to generate the non-equilibrium plasma, and thermal energy was varied by controlling the pre-heat temperatures of the fuel/air mixture and the O/C ratio. The results in figure 9 show that when plasma power (ε_{dish}) is kept constant at 1.7 J/cm^3 (curve 1) and 3 J/cm^3 (curve 2) there is an increase in conversion (α^*) with increasing thermal energy input (reflected in increasing ε_{tot}). However, a larger rate of conversion occurs when thermal energy is kept constant at 1.7 J/cm^3 and plasma power is varied, which is apparent by the steeper slope of curve 3.

These results demonstrate that the effect of non-thermal plasma in stimulating partial oxidation processes is greater than the effect of adding the equivalent amount of thermal energy alone. The reported conversion in these results is low (~60%) compared to results obtained in gliding arc systems (~85%); however, this experiment highlights that the plasma catalytic effect is not necessarily a result of plasma-induced thermal deposition of energy into the reaction. Better reforming results using microwave plasmas were obtained by Rusanov et. al. who demonstrated methane conversions of 70% and 100% at plasma energy consumptions of 0.25 and 0.5 eV/molecule, respectively [82]. They attributed these results to plasma-induced initiation of chain processes. Further investigations are needed to elucidate the detailed mechanisms of the plasma catalytic effect in plasma-assisted partial oxidation systems.

1.8.2 Non-Thermal Plasma-Assisted Steam-Reforming of Methane

Plasma-assisted conversion of hydrocarbons with water vapor is a method that holds great promise because it can be organized effectively and has the potential to produce very high hydrogen selectivity and yields [62]. The methane steam-reforming process is endothermic and it

requires thermal energy input of approximately 2.2 eV/molecule to produce syngas at a ratio of H_2:CO of 3:1 under thermodynamic equilibrium conditions [16]. Deminsky et. al. [78] described results of methane steam reforming using a pulsed microwave plasma (9 GHz frequency, up to 100kW power per pulse, pulse frequency of 1 kHz, and pulse duration 0.3-1 μs) with reactant preheating from 500-570°C and CH_4:H_2O ratios of 1:1 and 1:2. With plasma energy input of approximately 5% of the total thermal energy of the process, methane conversion increased from 10% to 16%. Results showing the increase in conversion with and without plasma are shown in Figure 10.Total conversion in this case was low (only 16% H_2 in exhaust), but the presence of plasma boosts conversion and decreases energy costs by 30-60%, corresponding to a specific energy cost of approximately 2.1 eV/molecule H_2 produced [62].

Sekine et. al. investigated steam-methane reforming at a steam/carbon ratio of 1 using a pulsed spark discharge (30kV, 0-10mA, pulse frequency 0-300 Hz) [83]. The experiments were performed at low reaction temperatures of 393K, which are significantly lower than typical catalytic reforming systems (800K). The results indicated that the maximum methane conversion achieved was only 55%; however, selectivity to hydrogen was high (85%) and a high H_2/CO ratio of 4 was observed. There were some small amounts of C_2 hydrocarbons present, with acetylene predominant, but it was discovered that the selectivity to compounds other than hydrogen can be controlled by changing the partial pressure of steam. The energy cost to produce hydrogen was reported to be 2.7-3 eV/molecule at the highest conversion levels.

1.8.3 Non-Thermal Plasma-Assisted Carbon Dioxide (Dry) Reforming of Methane

The process of methane conversion to syngas using carbon dioxide can provide the possibility to utilize a major greenhouse gas pollutant and provide for better carbon resource management. This is especially desirable if the syngas produced by CO_2 is not burned but used for chemical synthesis processes. Similar to steam reforming, CO_2 (dry) reforming of methane is

an endothermic process that requires a slightly higher energy input of 2.6 eV/molecule. Many types of non-thermal plasmas have been investigated using this process: DBD [84-87]; pulsed corona [88]; and gliding arc [89-91]. The plasma catalysis effect for this process was best demonstrated by Mutaf-Yardimci et. al. when they investigated the effect of preheating on conversion both with and without a pulsed corona discharge. Hydrogen generation nearly doubled when the discharge was switched on (from 3.8% to 7.2% in exhaust), and power consumption of the discharge was less than 5% of the required reaction enthalpy. These results are attributed to a plasma-induced chain mechanism involving methanol and formaldehyde thermal decomposition for methane-carbon dioxide mixtures [88].

1.8.4 Non-thermal Plasma-Assisted Pyrolysis of Methane

Pyrolysis is an important fuel conversion scheme for acetylene production and is involved in the process of methane decomposition into hydrogen and solid carbon. Thermal arc plasmas have been used in the industrial production of acetylene, ethylene, and hydrogen for more than 50 years in a process also termed electric cracking, and the mechanisms by which this occurs are well known. The thermal plasma arcs used in pyrolysis can have power levels as high as 10 megawatts with arc lengths reaching as long as one meter [16]. Givotov et al. investigated microwave plasma-assisted pyrolysis of ethane to hydrogen gas and solid carbon (soot) with zero CO_2 emissions. The pulsed microwave discharge was operated at a frequency of 9 GHz with average power of 30-100 W, pulse duration 0.3-1 μs, pulse frequency of 1 kHz, and power per pulse near 100 kW [66]. It was found that the addition of plasma energy caused a decrease in the reaction temperature, and it is believed that a fraction of the input plasma energy (<20%) is spent in catalytic stimulation of the reaction.

1.9 Plasma Reforming of Liquid Hydrocarbons

Non-thermal plasmas have been used in a variety of transportation applications related to the conversion of refined liquid hydrocarbon fuels, such as gasoline, diesel, and JP-8. There are four major applications where plasma systems have been specifically developed for use onboard vehicles, including development of vehicular auxiliary power units that convert fuel-to-electricity using plasma reformers combined with fuel cells [92-93], hydrogen-enriched combustion for improved engine performance and reduced toxic emissions [94-95], plasma after-treatment and reduction of exhaust pollutants such as nitrogen oxides (NO_X) and solid particulates [96-99], and regeneration of NO_X absorbers and diesel particulate filters [100-102]. Plasma reformers, in general, have several advantages over catalytic systems that make then attractive for the automotive industry including near instantaneous start-up time, no pre-heating requirements, and small and compact design.

Plasma researchers face several challenges when reforming liquid hydrocarbon fuels such as diesel, because they contain a mixture of variable-length hydrocarbon chains and include some fractions of polycyclic aromatic compounds. Reforming aromatic compounds can be difficult due to the multiple kinetic pathways that can lead to solid carbon and soot formation. Many plasma researchers, however, have reported no soot or solid carbon formation even in regimes in which it is thermodynamically favorable [19, 58]. It is believed that plasma is acting to oxidize carbon-forming precursor molecules and thus soot and coke formation is avoided.

Another challenge for the plasma reforming community is to find ways to improve hydrogen selectivity. Many of the plasma reforming results presented in the literature show good conversion of fuel to syngas products, but hydrogen selectivity is lower than equilibrium predictions because a portion of the hydrogen is either oxidized to H_2O or preserved in the form of light hydrocarbons (LHCs). Oxidation of H_2 is inevitable even in fuel-rich conditions, such as

partial oxidation, because of the oxidative nature of plasma, which is due in part to the multiple oxidative radicals that it produces and the fast rate of the H_2-O_2 reaction. When hydrogen selectivity is decreased because of the production of light hydrocarbons (LHCs), this is typically the result of some amount of fuel pyrolysis that may have occurred in the vicinity of the plasma discharge - an effect which is more prevalent in higher temperature plasmas, such as gliding arc. The fact that the LHCs are preserved in the exhaust also points to incomplete reforming that is most likely caused by heat losses in the post plasma treatment zone or insufficient residence time to allow the reactions to complete. Such problems are related to system optimization and can be avoided. The LHCs preserved in the product stream are mostly comprised of methane in the range of a few percent of the absolute volume concentration, with smaller amounts of ethylene, acetylene, and ethane (usually less than 1-2 percent). Although the concentrations of the light hydrocarbons are typically low, in some cases they can account for as much as 40% of the heating value of the syngas product stream [19]. Nevertheless, the presence of the LHCs may not a pose a problem when the syngas stream is being fed to solid oxide fuel cells (SOFCs), especially when methane is the major component. SOFCs can reform methane internally even at high concentrations (up to 25% of the molar concentration) [103]. Additionally, methane in the syngas product stream was also shown to be beneficial to the thermal management characteristics of a solid oxide fuel cell because it can be endothermically reformed in the high temperatures of the anode side of the fuel cell, where abundant H_2O is present.

A large amount of research on liquid hydrocarbon reforming has been performed using gliding arc and microwave plasmas, which have demonstrated the best results thus far. Therefore the focus of this section will be to describe the major results from plasma-assisted conversion from these discharges.

1.9.1 Plasma-Assisted Partial Oxidation of Diesel Fuel and its Surrogates into Synthesis Gas

Some of the best conversion results for POX of diesel fuel to syngas have been obtained with vortex-based gliding arc plasma reformers. Bromberg et al. achieved good conversion of atomized liquid diesel in a vortex based gliding arc plasmatron at high flow rates (fuel flow rates up to 2 g/s) without the use of a catalyst [104]. Atomized fuel was injected into the reactor in the axial direction with a curtain of air that flowed along the walls to prevent the fuel droplets from making contact, thus preventing conditions for pyrolysis. A series of vortex nozzles generated a swirling flow that pushed and elongated the gliding arc discharge and provided good mixing of the reactants with the discharge. The plasmatron reformer has the capability to operate in a wide dynamic range while using limited electrical power of 200W. At an O/C ratio of 1.1, diesel fuel flow rate of 0.8 g/s and plasma power of 250W, the energy conversion efficiency was approximately 70%. The gas composition of the exhaust is shown in Table 1. An opacity meter was also used to detect the presence of soot, and none was observed under these conditions. However, some light hydrocarbons were produced and included equal parts of CH_4 and C_2H_4.

Table 3. Exhaust gas composition from the gliding arc plasmatron for partial oxidation of diesel fuel [104].

Concentration (volume %)	
H_2	8.2
O_2	1.4
N_2	68.7
CH_4	2.6
CO	14.3
CO_2	4.7
C_2H_4	2.4
C_2H_2	0.0

1.9.2 Plasma-Assisted Steam-Oxidative Reforming (SOR) of Various Hydrocarbons Fuels into Synthesis Gas

In steam-oxidative reforming, also known as auto-thermal reforming, both partial oxidation and steam reforming processes are combined and air and H_2O are used together as fuel oxidizers. The advantage of steam-oxidative reforming is found in the energy balance of the process, where it is possible to achieve thermo-neutral conditions with a zero net enthalpy change ($\Delta H=0$) in the process due to equal contributions between exothermic and endothermic reactions. It is also possible to achieve increased hydrogen yields and improved hydrogen selectivity under SOR conditions because syngas can be derived from the oxidizers themselves (i.e. H_2 from H_2O).

Paulmier et al. used a steam-oxidative reforming scheme to convert gasoline into syngas with a flat gliding arc reformer that contained two sets of electrodes that could provide two independent plasma discharges [93]. This system was also capable of operating at elevated pressures (up to 300 kPa) and at temperatures up to 773K. Experiments were performed near auto-thermal reforming conditions: H_2O/C ratio: 2.5, variable air ratio: 0.1-0.4. The results showed a maximum output composition of syngas at atmospheric pressure of H_2: 7% and CO: 4% with an additional large amount of CH_4: 9%. Reforming improved at higher pressures (250 kPa) where a maximum efficiency of 27% was achieved at an air ratio of 0.4, H_2O/C ratio of 2.5, inlet temperature of 773K, and fuel power of 10kW. It should be noted that while increasing pressure caused an increase in conversion, it also lengthened the delay between extinction/ignition cycles of the gliding arc discharge. Gliding arc discharges are auto-oscillating and they normally extinguish and re-ignite periodically; higher pressures make breakdown more difficult and can increase the delay between breakdowns making large gaps where there is no discharge. The low conversion efficiency observed in these experiments was most likely a result of both the increased discharge extinction time and the flat geometry of the discharge, which is known to have poor mixing with reactants.

The experimental results of plasma-assisted liquid hydrocarbon conversion show good conversion, in general, especially those using transitional (warm) non-equilibrium plasma discharges like gliding arc [9]. One possible reason for the improved reforming with gliding arc plasmas compared to DBDs or corona discharges, is because the higher translational gas temperatures accelerate the kinetics of the reforming reactions while the plasma radicals act simultaneously to reduce energy barriers and prevent unwanted by-product (soot) formation. This hypothesis has not been proven however, and some researchers believe that low-current transitional arcs like gliding arc contribute energy through gas heating alone with no catalytic effects from plasma active species [75]. Further work is needed to elucidate the plasma catalysis effect in plasma-assisted reforming systems and understand the underlying mechanisms so that future fuel conversion systems may be improved and optimized.

1.10 Combined plasma-catalytic reforming of hydrocarbons fuels into hydrogen-rich synthesis gas

There is a distinction between reforming hydrocarbon fuels using plasma independently for its own catalytic properties, which is referred to as *plasma catalysis*, and reforming using the *plasma-catalytic* approach that combines plasma with traditional metal catalysts [16]. Investigations involving the plasma-catalytic approach have grown significantly over the past decade and the results have demonstrated a positive synergistic effect, with improved reforming results that are often better than the results produced by either technology alone. Researchers have applied the plasma-catalytic approach for hydrocarbon reforming using various schemes that include CO_2 (dry) reforming [105-106], steam reforming [107-108], partial oxidation reforming [109-112], and non-oxidative reforming [53, 113]. Both plasma and traditional catalyst technologies have their own drawbacks with regard to hydrocarbon conversion, namely energy

spent on gas heating in plasmas can be expensive and energy inefficient and catalysts have flow restrictions due to their high density and deactivation problems from sulfur and soot formation that can occur on their surfaces. However, combining these technologies into plasma-catalytic hybrid reactors can work to eliminate the weaknesses of both technologies by providing increased conversion at lower reaction temperatures, avoiding soot and unwanted byproduct formation, and improving energy costs and efficiency.

Plasma-catalytic reforming systems are most commonly arranged in either a single-stage and two-stage configuration [114]. In the single stage configuration, the plasma and catalyst regions can completely or partially overlap and the plasma discharge is ignited within the catalyst bed or on electrodes that are coated with catalyst material. The single stage configuration is somewhat more complex because the overlapping catalyst and plasma discharge are known to have strong interactions which can affect the properties of both. For instance, the electrical conductivity and the sharp edges of pelletized metal catalyst material can affect the reduced electric field of the plasma thereby altering the types and concentrations of the active species it produces [114]. In addition, the behavior of the catalyst can be influenced by plasma-induced surface heating [110] and possibly by other unknown effects caused by current flowing across the catalyst surface. The plasma and catalyst regions are separated in the two-stage configuration, with plasma placed upstream from the catalyst bed to provide pre-processing or downstream for post-processing of the catalyst-treated effluent. Pre-processing of reactants is more commonly used and has also yielded the best results [114] in terms of conversion because it is believed that the plasma can excite hydrocarbon molecules in such a way that they are more easily converted by the catalyst material. Regardless of their differences, researchers have shown that both the single-stage and two-stage plasma-catalytic systems are capable of providing improved reforming with greater results compared to either plasma or catalyst alone.

1.10.1 Plasma-catalytic two-stage configuration for hydrocarbon reforming

Sobacchi et al. used a two-stage plasma-catalytic reformer to compare the effects of pre-processing and post-processing for the steam-oxidative reforming of isooctane (trimethylpentane, C_8H_{18}) into synthesis gas [112]. In this system, a pulsed corona discharge was developed using a wire-into-cylinder coaxial electrode configuration and combined with a separate catalyst bed reformer in such a way that it could be placed either upstream (pre-processing) or downstream (post-processing) from the catalyst. The plasma-catalytic system was placed inside a tube furnace in order to control the catalyst bed temperature, which was varied from 630-800°C. The catalyst used in these trials was specially developed by Argonne National Laboratory, and the details of its composition were not provided. The system was operated using a simulated air mixture of 50% O_2-50% N_2, which was held constant at an air-to-fuel O/C ratio of approximately 1. Steam was introduced at an H_2O/C ratio of 1.1 and the fuel flow rate was low (0.04 ml/min) with a heating value of 22W. Figure 11 shows a comparison of hydrogen yields between pre-processing, post-processing, and the pure catalyst case. It is clear that at low temperatures (near 640°C), hydrogen yields increased nearly 2.5 times for both the plasma pre- and post-processed cases compared to the pure catalyst case. Despite the increase in yield, the plasma-catalytic system cannot obtain maximum hydrogen yields (denoted by the straight dashed line in Figure 11) at these low temperatures; however, the authors noted that a significant fraction of isooctane remains unconverted in this regime. In addition, some heavy organic acids produced by partial oxidation were detected in the exhaust. The maximum H_2 yield occurred at higher reaction temperatures, near 800°C, where the synergistic effect between plasma and catalyst seems to wane and become indistinguishable from the pure catalyst case. Figure 11 also shows that the pre-processed reactant stream had slightly better conversion and product yields over the post-processed stream. The authors observed slight changes in power input to the corona discharge between the pre- and post-processed cases, which can occur because of the dissimilar reactant

compositions, and a slight pressure increase located upstream of the catalyst bed caused by the dense packing of the catalyst material. The authors attribute the improved reforming in the plasma pre-processed case to plasma stimulation of the kinetically-suppressed and slower initial stages of isooctane oxidation which allows the catalyst to act more effectively on the intermediate oxidized components and ultimately move the reforming reaction along further. The plasma power was kept below 8 W in all trials and was varied slightly to examine its effect on hydrogen yield. It was found that increasing plasma power had little positive effect on conversion of isooctane to hydrogen and eventually caused a decrease in hydrogen yield. Experiments were performed intermittently for more than 100 hours and the catalyst showed stable performance throughout with no signs of deactivation or plugging. The results presented here show that low power non-thermal plasma combined with metal catalyst has a positive synergistic effect that promotes greater fuel conversion and higher hydrogen yields at low overall reaction temperatures.

1.10.2 Plasma-catalytic single-stage configuration for hydrocarbon reforming

A single stage setup using a dielectric barrier discharge (DBD) plasma-catalytic hybrid reactor for methane steam-reforming was demonstrated by Nozaki et al. [115]. A strong synergistic effect between plasma and catalyst was observed in the temperature range between 400-600°C, with almost no effect observed below 200°C. Figure 12 shows the methane conversion curve as a function of temperature for three cases: DBD only, Ni/SiO_2 catalyst only, and DBD + Ni/SiO_2. The results show that the methane conversion curve is shifted 200°C towards the low-temperature region for the case of DBD + Ni/SiO_2, which exceeds the expected conversion at equilibrium (dashed line). At higher reaction temperatures (approaching 700°C) the plasma-catalytic effect seems to diminish and conversion approaches the equilibrium and catalyst only case. Energy cost and energy efficiency were reported to be 134 MJ/kg H2 and 69%, respectively. The authors noted that while conversion was higher than equilibrium in the

low temperature case, product selectivity mainly followed the equilibrium predictions. The authors suggest that the reason for higher than predicted conversion of methane may be the result of plasma-induced electron impact excitation, which can further induce vibrational excitation of methane. Vibrationally excited methane is known to have a sticking probability of one to two orders of magnitude higher than ground state methane, thus promoting dissociative chemisorptions on catalyst surfaces [116].

The plasma-catalytic synergistic effect has shown promise in its ability to promote greater conversion and product yields than stand-alone plasma or catalyst technologies. Single-stage systems have demonstrated better reforming results thus far, but determining which configuration is best for reforming is not possible at this time. Studies of plasma-catalytic systems are still in progress and a comprehensive comparison between single-stage or two-stage systems is not yet available. In general, the consensus among researchers seems to be that plasma is effective at increasing the internal energy of reactants and specifically stimulating vibrational excitation which can be effectively utilized in thermal catalysis reactions. More research is needed to identify the roles of plasma and catalysts in combined systems and to investigate the detailed kinetic mechanisms responsible for the synergy that provides improved conversion and product selectivity.

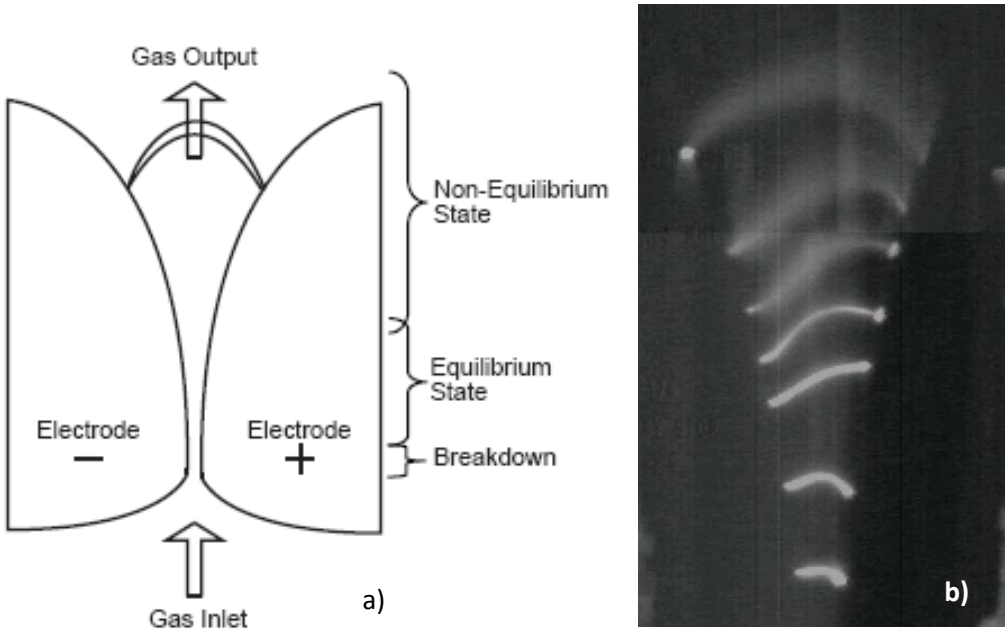

Figure 1. Schematic of the planar Gliding Arc (a); An image of several snapshots of the discharge at various lengths along the diverging electrode (b).

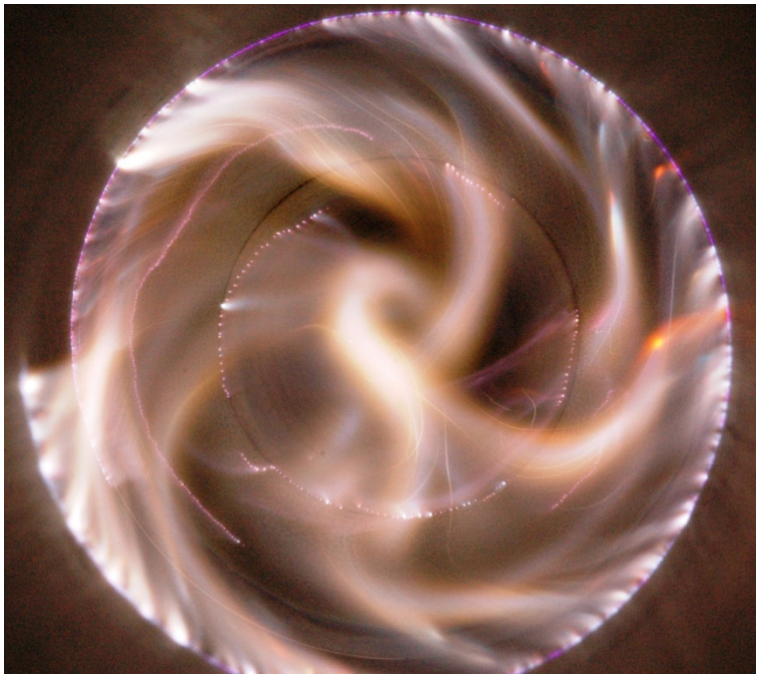

Figure 2. Gliding arc plasma discharge in reverse vortex flow configuration (top view).

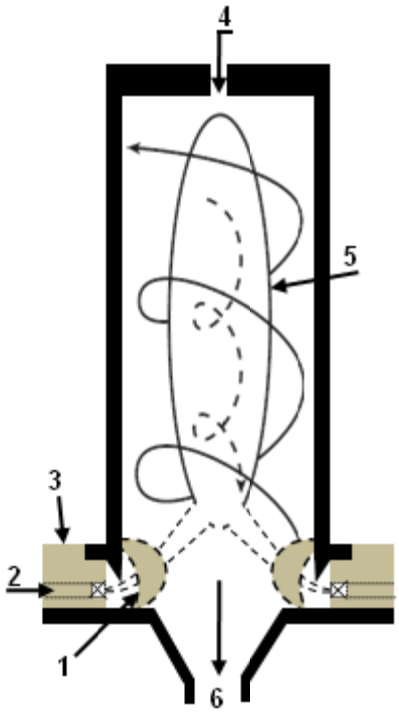

Figure 3. Schematic of a vortex-based gliding arc reactor. 1) plasma discharge; 2) Pre-mixed fuel and air tangential jets; 3) Ceramic dielectric; 4) Additional air input port (optional); 5) Vortex-stabilized flame; 6) Exhaust nozzle.

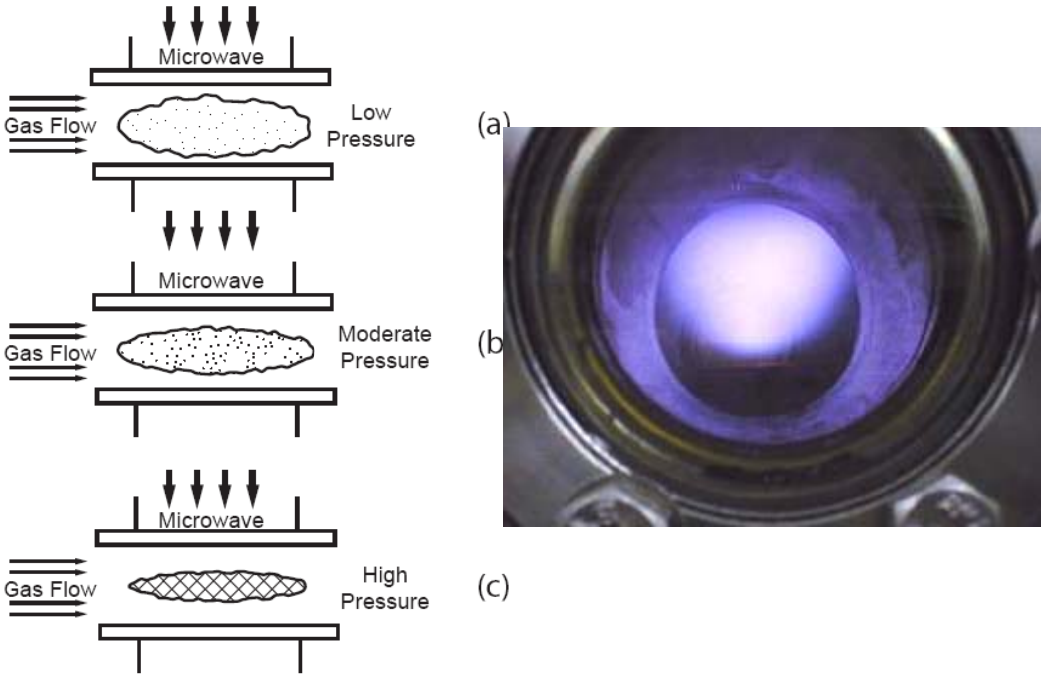

Figure 4. Image of a microwave plasma. Configurations include low pressure (a), moderate pressure (b), and high pressure (c). Photograph (right) shows a low pressure microwave discharge.

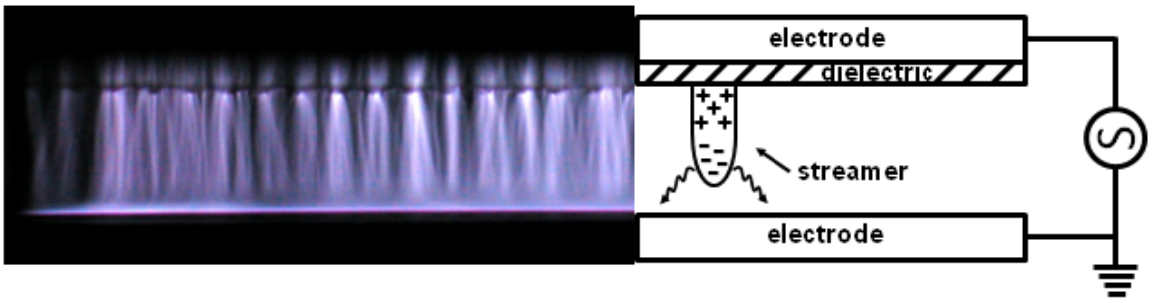

Figure 5. Dielectric Barrier Discharge Plasma in a planar configuration.

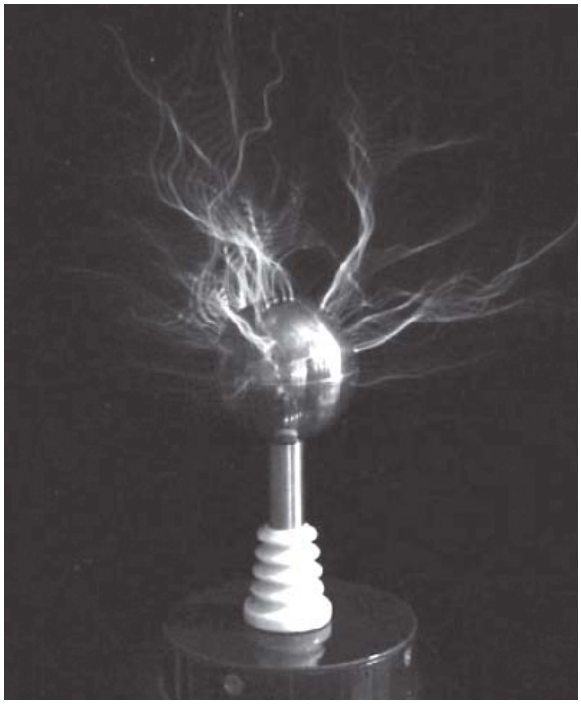

Figure 6. Image of a corona plasma discharge.

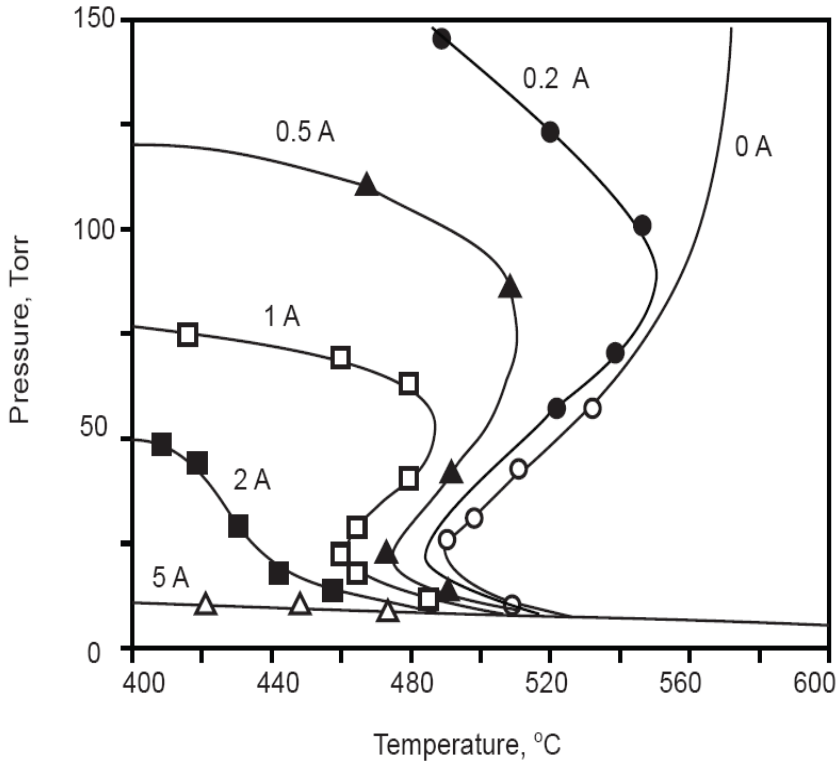

Figure 7. Demonstration of the effect of plasma in lowering the autoignition temperature of a H2-O2 mixture. The "0A" curve corresponds to the conventional limit (no plasma).

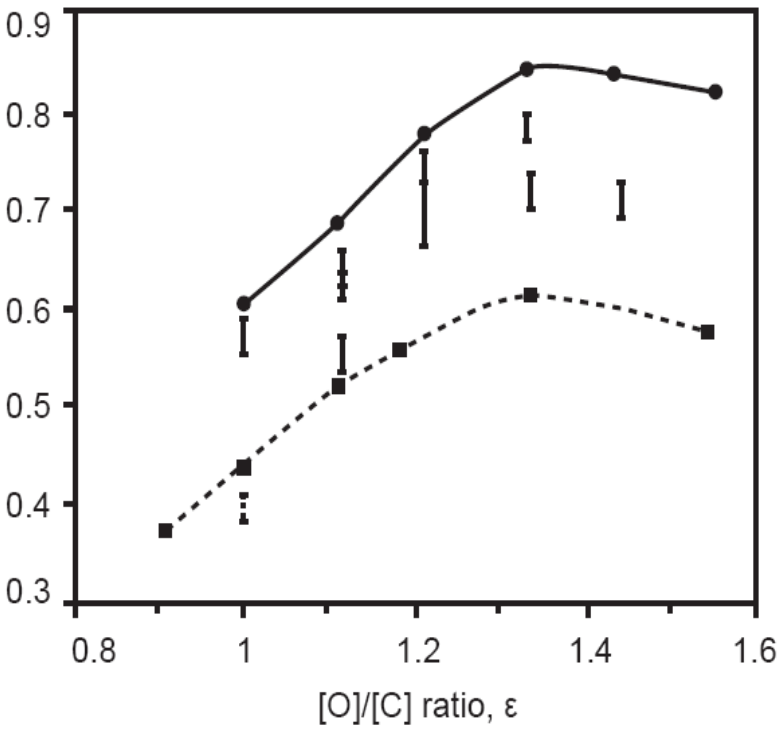

Figure 8. Methane conversion for the Gliding Arc in Tornado (GAT) system. Kinetic simulation results w/ plasma (solid line with dots); plasma experimental results (solid bars); kinetic simulation w/o plasma (dotted line); and results w/o plasma (dotted bar).

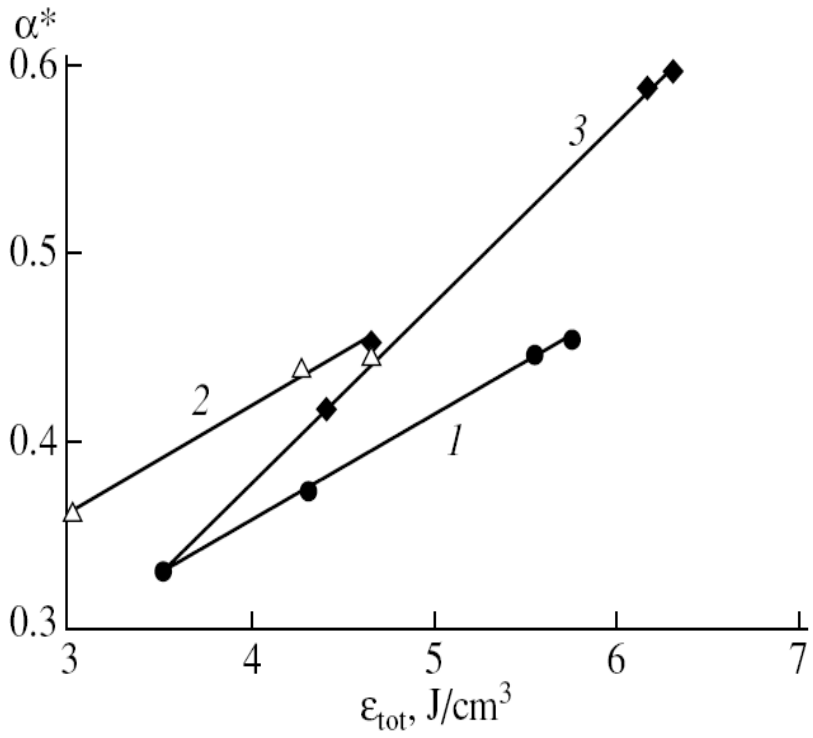

Figure 9. Relative conversion of methane into synthesis gas as a function of the total specific energy input in a coaxial microwave plasmatron. Variation in thermal energy input at (1) ε_{dish} = 1.7 J/cm^3 = const, (2) ε_{dish} = 3 J/cm^3 = const, and (3) change in the discharge energy input at $\varepsilon_{thermal}$ = 1.7 J/cm^3 = const.

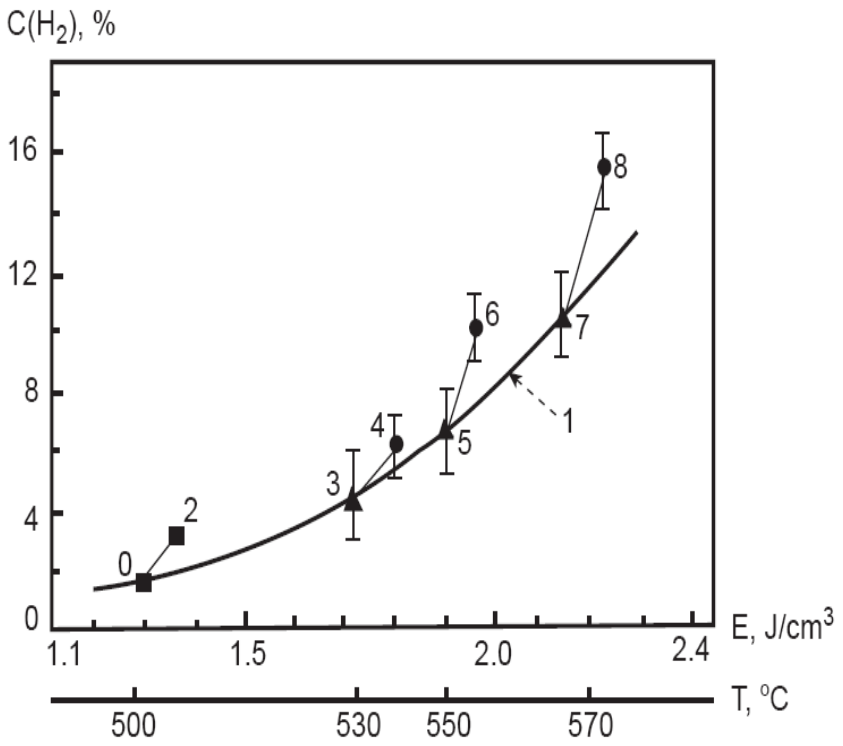

Figure 10. Hydrogen concentration (%) as a function of specific energy input (J/cm3) for microwave plasma-assisted methane-steam reforming. Curve 1 represents reforming with thermal energy input only (no plasma); Points 2, 4, 6, and 8 represent experimental results with microwave plasma discharge.

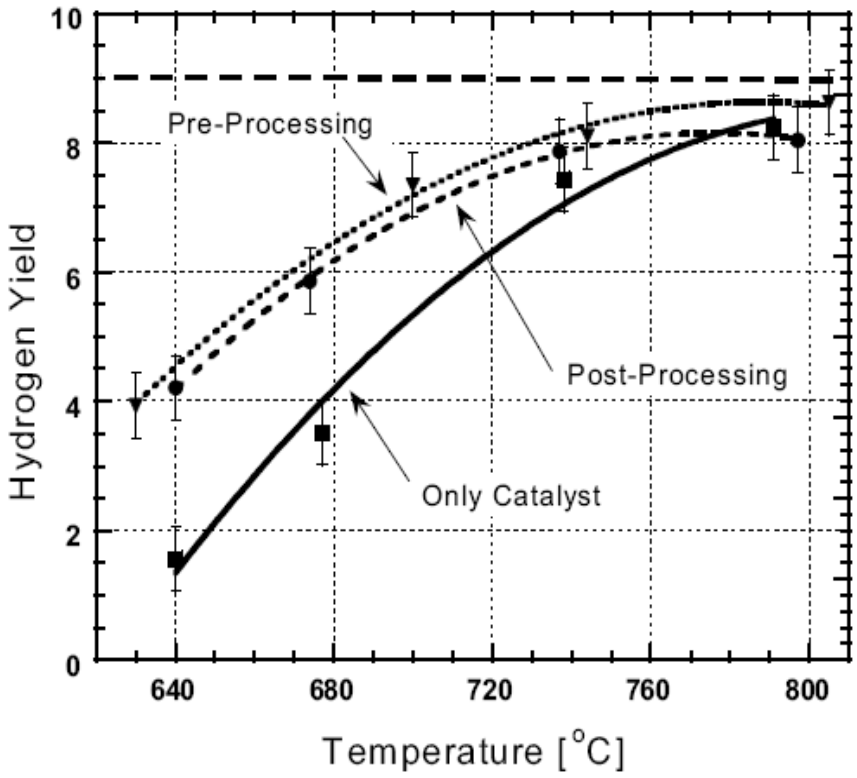

Figure 11. Hydrogen yield as a function of Temperature for system configurations that include: plasma pre-processing, post-processing, and catalyst only. The maximum possible H_2 yield from isooctane is represented by the straight dashed line.

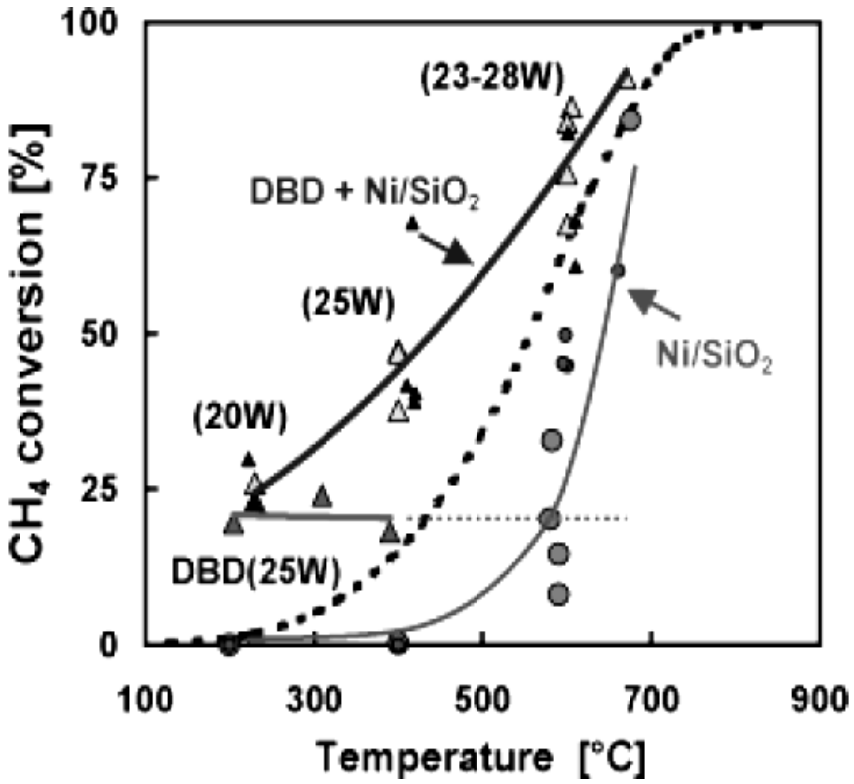

Figure 12. Methane conversion versus temperature is shown for four separate cases: DBD plasma only, Ni/SiO2 catalyst only, combined DBD + Ni/SO2, and Equilibrium methane conversion (dashed line).

2. Design, Testing, and Evaluation of Gliding Arc Plasma Reformers for Partial Oxidation of n-Tetradecane and Diesel Fuel to Synthesis Gas

2.1 Introduction

This chapter describes the design, evaluation, and testing of a new type of gliding arc plasma reformer that is based on a reverse vortex flow configuration and was designed for the specific purpose of reforming heavy hydrocarbon fuels such as n-Tetradecane and commercial-grade low-sulfur Diesel fuel into synthesis gas. As previously described, vortex-based gliding arc reformers have shown considerable promise as being among the most efficient plasma reformers due to their high level of mixing and contact of the reactant stream with the plasma discharge itself. This new reverse vortex flow gliding arc (RVF-GA) reformer will be introduced along with design details, experimental results, and a comparison of those results with the predicted results from thermodynamic equilibrium simulations. In addition, a second reactor known as the Gliding Arc Plasmatron (GA-Plasmatron) device was used to investigate syngas conversion using a slightly different forward-vortex mixing scheme. The reforming results from this device will be presented and compared against the results from the RVF-GA system. Specifically, a comparison of the performance of each device is made with regard to the hydrogen yield, energy conversion efficiency, and specific energy requirements.

2.2 Materials and Methods

2.2.1 General System Scheme

The plasma reformers are connected to a larger system with several important components for pre-heating fuel and air and post-treatment gas analysis. A schematic of the overall system is shown in Figure 13. A fuel evaporation system was constructed from stainless

steel tubing coils that were heated by temperature controlled resistive heating elements. Both reactors were connected to a heat exchanger to condense water vapor and cool exhaust gases before sampling. Gas sampling always occurred at steady state temperature conditions and the syringe method was used, sometimes in conjunction with a particulate filter to remove any solid contaminants such as soot or coke. Mass flow controllers were used to control and monitor flows and a fuel pump was used to deliver liquid fuel to the fuel vaporization system. Two different DC power supplies were used to generate the plasma: BRC 10000 Universal Voltronics combined with an external ballast resistor box, and a custom-made power supply (Quinta, Ltd.) that uses the reactive capacitance resistance to control current.

2.2.2 Gas Chromatography and Detection of Products

A dry-basis analysis of the gas composition was made using a Gas Chromatograph (Agilent 3000 Micro-GC) using the thermal conductivity detection method. Two separate columns were used; the Agilent HP-PLOT Molsieve column for detection of H_2, CO, CH_4, O_2 and N_2; and the Agilent GS-GasPro column for detection of CO, CO_2, N_2, CH_4, C_2H_2, C_2H_4, C_2H_6. The atomic mass balances for carbon, hydrogen, nitrogen, and oxygen were used to provide for an estimate of the conversion of tetradecane and the production of H_2O in the product stream. As nitrogen is inert in this system, it is used as a linking substance to calculate the total exhaust flow rate of products and subsequently the molar flow rate of each substance detected by the GC. In regimes where no visible soot was formed in the exhaust, the atomic carbon balance provided a means to qualitatively estimate the physical conversion of fuel to products. It was not possible to quantify unreacted tetradecane because the GC used in these trials did not have the ability to detect higher hydrocarbons above C_2. Condensed water vapor could also not be directly measured; however, estimations of H_2O produced during each experiment were made based on oxygen mass balance of the system. The mass flow rate of known oxygen that was input into the

system (as air) was compared to the sum of the oxygen that was contained in the detectable product stream as indicated by the GC (CO, CO_2, and O_2). The difference between these values ($O_{2in} - O_{2out}$) was assumed to be in the form of H_2O, since there is little chance that the oxygen could have formed other species, including oxygenated hydrocarbon species. The following equation demonstrates the estimated H_2O in the product stream.

$$Residual\ H_2O\ \left(\frac{g}{min}\right) = \ O_{in} - \sum_{out} O_{CO} + O_{CO2} + O_2\ \left(\frac{g}{min}\right) \tag{2-1}$$

The oxygen mass balance, when compared to the hydrogen balance, was typically close to 1:2 for O:H for most experiments.

2.2.3 Plasma power supplies

As many as three different power supplies were used to conduct fuel reforming experiments in both gliding arc reformers. A direct current (DC) power supply (BRC 10000 Universal Voltronics) connected to a ballast resistor box, and two custom DC power supplies (manufactured by Quinta, Ltd.) were used to generate the plasma and the high voltage electrode acted as the negative polarity cathode. The power supplies were capable of delivering 10 kV open circuit voltage and a maximum current of 400 mA. During reforming experiments on both systems, the average voltage of the discharge was approximately 1 kV and average current was fixed at approximately 250 mA. Average power was kept constant in all trials at a value of approximately 250 W, which is about 3.5 percent of the lower heating value of the tetradecane flow (also kept constant at a flow rate of 0.15 g/s). It should be noted that there was no detectable difference in reforming results when using these various power supplies.

2.3 Concept and design of the Reverse Vortex Gliding Arc Reformer

The first generation reverse vortex gliding arc (RVF-GA) reformer reactor was developed by Kalra et. al. at Drexel University for the partial oxidation (POX) of methane to syngas [12]. The system contained movable electrodes and quartz reactor walls for observation of the discharge during reforming experiments (see figure 14). The system successfully demonstrated the concept of transitional plasma-assisted reforming and the results are among the best of those reported in the literature as of today for POX of methane with non-thermal plasma [9]. The system, however, had several design issues that severely limited its capability, which included poor temperature stability of the movable electrode system, which ultimately warped and interfered with discharge elongation and stability. Also, the quartz reactor walls were not sealable and caused leaking of product gases and the flexibility and range of the system was limited as it was strictly designed to work with gaseous fuels in a narrow flow regime. Shortly after the conclusion of this work, another interesting application of this technology was developed and called for the creation of a plasma reformer that could convert heavy hydrocarbon fuels, such as Diesel, to syngas with the ultimate goal of producing electricity on-board vehicles. The plasma reformer would be combined with a solid-oxide fuel cell and could potentially have a fuel-to-electricity conversion efficiency of nearly 45%. This transportation-related application was supported by the U.S. Department of Energy and eventually spurred the interest of the U.S. Army. Hence, a RVF-GA plasma reformer was developed as a laboratory-scale prototype for reforming Diesel (initially n-tetradecane) and JP-8 fuels, for use on-board long-haul trucks and military vehicles such as tanks.

2.3.1 The Concept of Reverse Vortex Flow

The RVF-GA reactor, as its name implies, uses a reverse vortex flow scheme that has an outer swirling rotation along with a low pressure area at its center, which is very similar to a

natural tornado. The advantage of using RVF inside a chemical reactor is the high degree of mixing and contact of the reactant stream with the plasma discharge. The vortex flow pushes the plasma arc and elongates it while simultaneously the reactants (fuel and air) interact with the discharge allowing plasma heat and active species to initiate partial oxidation of the fuel. RVF is also similar to forward vortex flow, which the distinction being in the size of the exhaust diaphragm and the location of the swirl-generating jets. In a RVF device, the diameter of the exhaust diaphragm is much smaller than the internal diameter of the vortex chamber and this acts as a barrier that causes vortex flow to reverse direction and flow backwards into the cylindrical vessel. In addition, the swirl jets in a RVF device are located on the same plane as the exhaust diaphragm. Figure 15 shows the axial and rotational streamlines of flow inside a reverse vortex flow chamber as well as a photograph that visualizes an ink stream acting under the influence of the rotating flow. Another advantage of the RVF scheme is a thermal insulation effect that keeps reaction heat focused in the center of the chamber, as cold incoming air circulates near the internal vessel walls. Investigations into the thermal efficiency of reverse vortex flow demonstrated the low heat losses near the reactor walls in [117-118].

2.3.2 System Design Constraints for the RVF-GA Reformer

The RVF-GA reformer was designed according to specifications designated by the National Energy Technology Laboratory (NETL) under the U.S. Department of Energy, who provided partial funding for the project. NETL dictated reactant flow rate ranges for fuel and air, and certain safety restrictions including a pressure vessel shell capable of containing an explosion, coaxially shielded high voltage lines, and optical windows for observation of the plasma discharge. A report containing calculations of pressure vessel safety is included in Appendix A. Additional design constraints included size restrictions on the diameter (to be no

larger than 3 inches), requirements for a built-in heat exchanger to recuperate heat for pre-heating of the reactants, and an internal fuel vaporization system.

2.3.3 RVF-GA Reactor Design Scheme

A schematic of the RVF-GA reactor is shown in Figure 16. Heat from the exhaust pipe (1) is exchanged with incoming air (2) to temperatures up to 600C. The preheated air flows into a mixing chamber (3) where it is combined with vaporized fuel and steam (steam line was optional, not shown in Figure 16). The fuel and water injected into the mixing chamber originated from stainless steel vaporization coils (4), which were heated with an external resistance heater (not shown). The temperature and O/C ratio of the premixed reactants in the mixing chamber was carefully monitored to minimize the possibility of ignition outside of the reaction zone. It was discovered during testing that the O/C ratio of the reactants in the pre-mixing chamber cannot exceed 1.1 or fuel ignition can occur resulting in coking due to the high-temperature oxygen deficient environment. Because of this limitation, an axial air input port (5) was added to the top of the reaction vessel to allow for more air to be introduced into the reaction zone, thus allowing investigation of a slightly wider range of O/C ratios. A dielectric ring made from boron nitride (6) separates the high voltage electrode (7) and the grounded exhaust nozzle (8). The premixed reactants enter the cylindrical reaction zone through tangential jets that were machined within the dielectric ring. The gliding arc discharge (9) is initiated at the pointed tip of the high voltage electrode located just in front of the tangential swirl jets. This allows the incoming reactant stream to have maximum interaction with the plasma discharge and also to be the driving force which causes discharge rotation and elongation. The reaction vessel has internal volume of approximately 0.4 L (inner diameter of 4.3 cm) and there is a relatively small post-plasma treatment volume, which is essentially a 0.5 inch diameter stainless steel exhaust tube that is approximately 30 inches in length. The dotted arrows in figure 16 show the stream-lines of flow

on the axial plane (10). A quartz tube lining (11) was inserted into the reactor to protect the grounded outer pressure shell (12) from arcing due to the high voltage electrode which is in very close proximity. Quartz windows (13) were installed in the both the top flange and the top of the high voltage reaction vessel in order to view the stability of the discharge and observe the plasma/flame interaction. A special high voltage feed-through (14) was developed that allows the high voltage line to pass through grounded pressure shell while still maintaining pressure in the system.

2.4 Thermodynamic Analysis of Partial Oxidation of n-Tetradecane

Thermodynamic equilibrium simulations were performed (using HSC Chemistry, version 6.0) in order to understand the maximum theoretical energy conversion efficiency and syngas yields for the partial oxidation of n-Tetradecane. Figure 17 shows the predicted energy conversion efficiency versus O/C ratio for POX of n-tetradecane. The simulations were performed at the adiabatic flame temperature for each corresponding O/C ratio with a reactant pre-heat temperature of 400C. The maximum energy conversion efficiency from figure 17 is approximately 87%, which occurs at the stoichiometric POX point (O/C ratio = 1) where there is exactly enough oxygen to oxidize all fuel carbon to carbon monoxide and hydrogen. This system cannot reach 100% energy conversion efficiency because the POX reaction is exothermic and therefore some energy is lost during the conversion process from n-Tetradecane to syngas. The solid and dashed lines in Figure 17 show the energy conversion efficiency for two cases: the production of H_2 + CO + light hydrocarbons (dashed line), and H_2 and CO only (solid line). There is very little difference between these two cases until low O/C ratios near 0.5, where methane formation is predicted to occur. The solid black dots in Figure 17 indicate solid carbon (coke, soot) formation, which is thermodynamically favorable at O/C ratios < 1. In addition, the amount of carbon formed steadily increases with decreasing oxygen. Figure 18 shows a slightly

different case where solid carbon is not included as a product, therefore even at conditions where solid carbon formation is thermodynamically favorable (figure 17) it is not allowed to form. As a result of this slight change in allowable products, the unreacted carbon at O/C ratios < 1 in Figure 18 is preserved in the form of light hydrocarbons (mostly methane).

2.5 Experimental investigation of Partial Oxidation of n-Tetradecane using the RVF-GA Reformer

This section describes the experimental results for the POX of n-Tetradecane with the RVF-GA reformer. The main parameters investigated included: the effect of the oxygen-to-carbon (O/C) ratio on the hydrogen and carbon monoxide yields and the energy conversion efficiency; the effect of increasing plasma power on the hydrogen yield; and the effect of 5% unsaturated hydrocarbon additives (methylnaphthalene) on reforming and syngas yields. When the RVF-GA reactor was initially designed, the devised test plan called for variation of the O/C ratio between 0.8-1.5; however later it was discovered that the system has a limited range of O/C ratio variance between 0.8 and 1.1. The system becomes unstable at O/C ratios greater than 1.1 due to overheating that can occur in the air-fuel premixing chamber. As per the original design of the reactor, air and fuel are pre-heated and mixed to promote a more uniform conversion and the reactor recuperates heat from the exhaust stream. There is no way to control the amount of heat given to the premixing zone and at O/C ratios greater than 1.1, the fuel/air mixture can ignite in the premixing chamber causing coking and soot formation in the region where the high voltage and grounded electrodes meet. The carbon-rich soot can create a path for the plasma to arc to ground, much like a short circuit, outside of the reaction vessel. Such conditions require an immediate shutdown of the system to protect the power supply from overloading and to prevent damage to the ceramic dielectric ring and metal electrodes.

2.5.1 Effect of Increasing O/C Ratio on the H_2 and CO Yields

The conversion of evaporated n-tetradecane to the syn gas products of hydrogen and carbon monoxide as a function of the O/C ratio is shown in Figure 19. The solid and dashed lines in figure 19 show the expected yields at thermodynamic equilibrium and were calculated at the adiabatic flame temperature at each corresponding O/C ratio with a preheat temperature of 400C. The experimental yields show a slight linearly increasing trend of with the O/C ratio, which follows the general trend of the equilibrium simulation. The experimental yields are less than what can be expected from thermodynamics under adiabatic conditions; however, there is a significant fraction of light hydrocarbons (HCs) in the product stream amounting to as much as 11% (by volume) of the total exhaust at O/C ratios less than one.

2.5.2 Effect of Increasing O/C ratio on Energy Conversion Efficiency

Figure 20 shows the experimental values of the energy conversion efficiency as a function of the O/C ratio. The energy conversion efficiency, previously defined in section 1.5.4, compares the ratio of the lower heating value (LHV) of n-Tetradecane fuel to the syngas products and is a measure of how well the energy value of the fuel was transformed into useful syngas products. The solid and dashed lines on Figure 20 show the predicted thermodynamic equilibrium energy conversion efficiency for two cases: H_2, CO, and light HCs; and H_2 and CO only. The thermodynamic equilibrium energy conversion values were calculated using the product compositions at the adiabatic flame temperature at each O/C ratio. The simulation follows the conditions described in section 2.4 where solid carbon formation was not allowed in the product stream. As a result, the formation of light HCs becomes thermodynamically favorable at O/C ratios < 1. The experimental energy conversion points for H_2 and CO only are much lower than the equilibrium predictions; however, when the additional fractions of light hydrocarbons are included, the trends are nearly identical. This points to a kinetic limitation in

the system where too short residence time may have prevented the light hydrocarbons from fully converting to syngas (H2 and CO only). In addition, the experimental results suggest that the plasma may be acting to prevent soot formation because, although solid carbon is a thermodynamically favorable product at low O/C ratios (from figure 17), experimentally the carbon is preserved in the form of light hydrocarbons.

2.5.3 Effect of Increasing Plasma Power on H_2 Yield

The effect of increasing plasma power on the hydrogen yield was investigated for various O/C ratios. Figure 21 shows that increased plasma power generates a greater yield of H_2 (& CO, not shown). The reason for higher syngas yields with greater power is because as power increases, current increases, and so does the local gas temperatures within the discharge. High gas temperatures are kinetically favorable to accelerating partial oxidation reactions and facilitate further completion of conversion reactions within the residence time of the system. As previously described, partial oxidation often occurs in a two-stage process: a portion of the fuel is combusted and releases heat, CO_2, and H_2O; the second stage is the endothermic conversion of fuel with steam and CO_2 released in the first stage. The additional heat from the increased plasma power can promote and support these slower second stage reactions. It is important that the plasma power is limited to only a fraction of the total chemical power of the system (less than 5%) in order for plasma to be competitive as an economically viable catalyst. In these trials, the total chemical power of the system is approximately 6.3 kW, the plasma power range of 100-400W is equivalent to 1.5-6.3% of the total power of the system.

2.5.4 Effect of Aromatic Compound Additives on Syngas Yields

In these trials, a mixture of 95% n-Tetradecane and 5% Methylnaphthalene (by wt.) were reformed under POX conditions in the plasma reformer reactor. Unsaturated polyaromatic

compounds, such as methylnaphthalene, are typically present in commercial fuels like Diesel and it was included as a fuel constituent in these trials to evaluate plasma-assisted reforming with a more realistic composition of fuel. Aromatic compounds have double-bonded partial carbon ring structures that make reforming more challenging due to the additional energy needed to destroy these rigidly bonded carbon structures. Also, aromatic compounds are prone to coking during reforming, especially at higher temperatures, due to the multiple kinetic pathways that favor condensation of their carbon structure. Figure 22 shows the H_2 & CO yields versus O/C ratio for the Tetradecane only trials and the Tetradecane/Methylnaphthalene mixture. Both H_2 and CO yields are lower in the mixed fuel trials and the increasing O/C ratio does not increase yields by much. Figures 23 and 24 show the absolute composition (mol %) of the products for partial oxidation of 100% n-Tetradecane and 95% n-Tetradecane with 5% methylnaphthalene, respectively. In the trials with the aromatic compounds (figure 24), there tended to be less light hydrocarbons in the product stream and slightly higher amounts of CO_2 and H_2O. This indicates incomplete conversion of the fuel: the additional CO_2 and H_2O are present because they did not have enough residence time (or energy) to endothermically react with the aromatic compounds in the fuel during the second stage of partial oxidation. Furthermore, the carbon balance in the aromatic compound trials tended to be worse; as much as 12% of the carbon introduced as fuel into the system remained unaccounted for in the detectable product stream, which is further proof of incomplete fuel conversion. Soot production was not measured in these trials; however, very little, if any, soot was visually observed in the exhaust stream.

2.6 Concept and Design of the Gliding Arc Plasmatron Reformer

The Gliding Arc Plasmatron (GA-Plasmatron) device is a vortex-based fuel reformer that can convert both vaporized and liquid hydrocarbon fuels into syngas. The GA-Plasmatron uses a forward-vortex flow scheme and is much smaller and compact as compared to the RVF-GA

reformer. The GA-Plasmatron does not have a pre-mixing chamber for fuel and air, instead it has a fuel atomization nozzle built into the device that can introduce fuel axially within the reaction chamber. The GA-Plasmatron was optimized to work in cold start-up mode and heat recuperation from the exhaust products was not included in the design of the system. The GA-Plasmatron was originally designed by Rabinovich et. al [104], but has since been modified and optimized at Drexel University.

There are two sets of experiments described in this section; one in which fuel was vaporized and pre-mixed with pre-heated air external to the reformer (fuel atomization nozzle not utilized); and experiments where spray-liquid fuel was introduced into the GA-Plasmatron device via an atomization nozzle and mixed with ambient temperature air (and plasma) within the reaction chamber. The results of the vaporized fuel experiments are described in the context of comparing the performance between the GA-Plasmatron and the RVF-GA reformer.

2.6.1 Reactor Design Scheme for the GA-Plasmatron Device

A schematic of the GA-Plasmatron is shown in Figure 25. The GA-Plasmatron consists of two main pieces: a small compact plasma head unit which contains swirl-generating jets (1) that create vortex flow and a high voltage electrode (with inner diameter of approximately 2.2 cm) (2) that is separated from the ground by a Macor© dielectric ring (3); and a post-plasma treatment zone (4) that is surrounded by a layer of inert ceramic thermal insulation (5). Air is injected through the tangential jets, which are placed near a small gap (~3 mm) where the plasma discharge (6) is ignited. The fuel atomization nozzle (7), when utilized, requires a small amount of axial flow to assist in atomization process. The cross-sectional streamlines of flow on the axial plane (8) are indicated in figure 25 and there is a slight amount of reverse flow inside the vortex chamber, which was verified through computational fluid dynamic simulations [119].

2.7 Evaluation and Comparison of the Partial Oxidation of evaporated n-Tetradecane for the RVF-GA and GA-Plasmatron Reformers

Efforts were made to evaluate the performance of the GA-Plasmatron device and compare its performance to the RVF-GA reformer, given the inherent similarities of these systems. The experimental conditions for partial oxidation reforming of n-Tetradecane reported in the following sections were exactly the same as the conditions used in trials with the RVF-GA reformer. In addition, each reactor has a similar total residence time in the range of approximately 0.16-0.19 seconds. The total residence time considers the volumes of both the plasma reaction zone and the post plasma zone, which is provided to allow for completion of secondary reactions.

2.7.1 Comparison of the H_2 and CO yields as a function of the O/C ratio for the RVF-GA and GA-Plasmatron Reformers

Figure 26 shows the H_2 and CO yields as a function of the O/C ratio for both the GA-Plasmatron and RVF-GA reformers. A comparison of the experimental yields from both reformers shows that they nearly identical when operated under the same experimental conditions. As shown in Figure 26, there is a slight linearly increasing trend of yields with increasing O/C ratios. The experimental results follow the trends of the predicted yields at thermodynamic equilibrium, which are indicated by the solid and dashed lines in Figure 26; with the exception that they do not reach a maximum at the O/C ratio of 1. Instead, the experimental yields continue to increase with the O/C ratio. The thermodynamic equilibrium simulation maximum yields occur at the O/C ratio of 1 because this is the stoichiometric partial oxidation point, where there is exactly enough oxygen to allow for complete conversion of the fuel to syngas. The experimental system does not follow this trend exactly, however, because of kinetic limitations within the system. These kinetic limitations include too short residence time or heat losses downstream of the reaction zone that prematurely quench the partial oxidation reactions.

The experimental yields continue to increase above the O/C ratio of 1 and this is due to the excess heat released at higher O/C ratios which accelerates the POX reactions and allows the reactions to progress further in the limited residence time of the system. At progressively higher O/C ratios (greater than 1), this effect should diminish as there will be enough oxygen to combust the fuel and oxidize the syngas further into H_2O and CO_2.

2.7.2 Comparison of the Energy Conversion Efficiency as a Function of the O/C Ratio for the RVF-GA and GA-Plasmatron Reformers

Figure 27 shows the energy conversion efficiency as a function of the O/C ratio for both the RVF-GA and GA-Plasmatron reformers. The solid and dashed lines in Figure 27 show the predicted energy conversion efficiency for two cases: H_2 and CO only (dashed); H_2, CO, and residual light HCs (solid). The solid line also shows the expected energy conversion efficiency when solid carbon is not included as a product, even though it is thermodynamically favorable to be produced. The experimental energy efficiency points are again nearly identical between both reformers, and they also follow the predicted trend at equilibrium. The energy efficiency for the production of H_2 and CO only is significantly less than the equilibrium predictions, however when the light hydrocarbons are included, the experimental and predicted efficiencies match very well. The results here suggest that the plasma may be acting as a soot suppressant. Solid carbon is typically a thermodynamically favorable product (see figure 17); however, instead there is a large fraction of light hydrocarbons preserved in the product stream and this is in very good agreement with simulations that do not allow solid carbon to form as a product.

2.7.3 Experimentally Measured Absolute Composition of Products as a Function of the O/C Ratio for Both the RVF-GA and GA-Plasmatron Reformers

Both the experimental and equilibrium product compositions of H_2, CO, CO_2, and light HCs are shown in Figure 28. The experimental light HCs, shown in Figure 28 as a lumped category, include mostly CH_4 and some C_2H_4; however smaller amounts of C_2H_2 and C_2H_6 are present in some cases in quantities of less than 2% over the range of O/C ratios investigated. H_2O content in the exhaust stream was estimated through the atomic hydrogen balance as was the ‘‘unreacted” carbon, which is assumed to be in the form of C_3 + higher hydrocarbons. The carbon balance at O/C ratios ≥ 1 indicates that all of the initial fuel was reacted and corroborates the fact that very little, if any, soot was observed in the exhaust stream. In addition, we did not observe wax or tar formation. The equilibrium simulation results presented in Figure 28 (solid lines) shows an expected sharp increase in H_2 that reaches a maximum at the O/C ratio of one and this directly correlates with the decreasing concentration of light hydrocarbons. The light HCs from the simulation are mostly comprised of CH_4 with less than 1% of other HCs present. It is apparent that overall trends for experimental composition are similar to the anticipated compositions at equilibrium; however they are all slightly shifted such that H_2O and CO_2 exist at much lower O/C ratios and the light hydrocarbons species are preserved even at relatively high O/C ratios (up to 1.6).

The deviation of the experimental product composition from thermodynamic equilibrium points to a kinetic limitation within the system, in particular, the well-known two-stage process for partial oxidation [29-30] may not have had sufficient time or energy to complete. The two-stage partial oxidation process begins with an initial rapid oxidation phase where all free oxygen is consumed to produce mainly H_2O and CO (and some CO_2 at lower temperatures) [31-32], and then a second much slower endothermic reforming stage follows where mostly H_2O and some CO_2 react with residual hydrocarbons to further produce syn-gas. Evidence of the stage one rapid

oxidation phase is shown in Figure 28 where H_2O and CO_2 were produced even at O/C ratios < 1, which is below the stoichiometric limit where not enough oxygen is present to even complete partial oxidation.

2.7.4 Evaluation of the H_2O Content of the Product Stream

It is possible to estimate the extent to which the secondary endothermic reforming phase occurred in our system by comparing the calculated amount of H_2O that was produced at the end of the rapid oxidation phase with the experimentally estimated amount H_2O present in the exhaust stream. Figure 29 shows a comparison between the expected levels of H_2O after the rapid oxidation phase and at thermodynamic equilibrium, and the experimentally estimated H_2O from both plasma reformer systems. One could conclude from Figure 29 that approximately 50% of the secondary reforming stage was completed under the experimental conditions of both plasma-assisted reformer systems. It is possible that the secondary reforming stage did not reach completion because of heat losses in the post-plasma treatment zone or too limited residence time.

2.7.5 Partial Oxidation of n-Tetradecane With and Without Gliding Arc Plasma

In order to determine the influence of the gliding arc discharge on partial oxidation, an interesting effect was observed when the plasma discharge was switched off during reforming. During this investigation period, the temperature of the reactor remained constant for a period of time not exceeding 15 minutes, after which time, the temperature decreased due to heat losses and the reaction began to diminish. The composition of products changed slightly when the discharge was turned off with a marked decrease in H_2, CO, and light hydrocarbons, and a slight increase in H_2O and CO_2. The temperature in the exhaust also increased slightly in the case without the plasma discharge. Figure 30 shows the product composition and temperature variance for the

cases of 'plasma on' and 'plasma off.' One explanation of this effect could be that the active species provided by the plasma were acting to lower the energy barriers for the reactions to proceed, thus requiring a lower reaction temperature to produce syngas. These results are not conclusive, and there is an alternate explanation for these results whereby the plasma may have acted as the reaction flame-holder that allowed fuel and air to immediately react once introduced into the system. Faster initiation of partial oxidation would allow for slightly longer residence time in the heated reaction zone. This would allow for further completion of the second-stage endothermic reforming process causing lower H_2O and CO_2 levels in the exhaust, and the production of more syngas. Furthermore, without the plasma discharge, the exothermic POX reaction may have been initiated on the hot internal reactor walls (located further downstream from the plasma ignition point) and caused higher temperatures to be recorded in the exhaust stream. These results are an interesting observation of the effect with and without plasma, but they cannot conclusively explain the plasma catalysis effect. More research is needed to elucidate the role of plasma active species and separate thermal and non-thermal effects due to the presence of the plasma discharge.

2.7.6 Effect of Increasing O/C Ratio of the H_2 Yield using spray liquid versus vaporized n-Tetradecane

There is a marked increase in the measured hydrogen yields when using vaporized fuel versus spray liquid fuel in the GA-Plasmatron device. Figure 31 shows H_2 yields of nearly 40% at O/C ratio =1 as compared to 20-30% yields in the liquid fuel case. This result is expected since vaporized fuel has higher sensible enthalpy with which it can assist in the initiation the partial oxidation reaction. In addition, there was a wider variance of yield values in the case of liquid fuel. This was because the fuel atomization system is not optimized and can cause fuel droplets to impact the interior (high-temperature) walls of the reactor. This leads to conditions for fuel pyrolysis and significant coking can occur.

2.7.7 Effect of Increasing O/C ratio on Energy Conversion Efficiency using sprayed liquid n-Tetradecane versus Diesel Fuel

Figure 32 shows energy conversion efficiency as a function of the O/C ratio for both spray liquid and vaporized n-Tetradecane fuel. The results follow a similar trend to the hydrogen yields where energy conversion efficiency is higher for the case of vaporized fuel. There is however, a greater fraction of light hydrocarbons present in the product stream for the liquid fuel case (9% absolute concentration) versus the 7% in the vaporized fuel case. The higher production of the light hydrocarbons in the liquid fuel case was mostly due to the additional production of ethylene with ratios of CH_4:C_2H_4:C_2H_2 as 2:1:1.2 and 2:2:1.2 for the cases of vaporized and liquid fuel, respectively.

2.7.8 Comparison of the specific energy requirement for RVF-GA, GA-Plasmatron, and Thermal POX systems

Figure 33 shows a comparison of the specific energy requirements to produce syngas for the RVF-GA, GA-Plasmatron, and a thermal POX reformer described in [120]. The RVF-GA reformer has the lowest specific energy requirement for the production of H_2 and this was due to the feature of its own internal heat recuperation. The RVF-GA reformer is able to preheat fuel and air using its own the exhaust heat (to temperatures up to 500C), whereas, both the GA-Plasmatron and the Thermal POX reformers are required to use an external heat source for vaporization. Two sets of reforming data are shown for the GA-Plasmatron reactor, which include vaporized and liquid n-Tetradecane. The specific energy cost for the vaporized fuel case was lower than the spray liquid fuel case (even though the liquid fuel case required no preheating). The reason for this discrepancy is because reforming using ambient temperature liquid fuel and air generated less syngas and therefore, when compared to the electrical energy cost from the plasma discharge, the energy requirement was greater (i.e. the same amount of power generated less syngas). The thermal POX reformer used vaporized diesel (to 400C) with

additional temperature added to the system (up to 900C) to allow reforming to occur. The results presented here show that plasma-assisted reformers are competitive to thermal reformers in terms of the specific energy requirement to generate syngas.

2.8 Conclusions for Gliding Arc Plasma-Assisted Partial Oxidation of n-Tetradecane

In this chapter, the development and testing of two vortex-based gliding arc plasma reformers was described in the context of experiments pertaining to the partial oxidation of n-Tetradecane fuel to syngas products. The goal of this research is to create advanced fuel reforming technologies to generate syngas as fuel to support electrical power generation through solid oxide fuel cells (SOFCs). Gliding arc plasma-assisted reformers have several advantages that are well suited for these goals, which include fast start time, stable operation with a wide variety of heavy hydrocarbons fuels, and low electrical energy consumption (2–5% of total chemical energy of the system). This is especially important when considering transportation-related applications where syngas is required to be generated on-board vehicles.

Several important parameters were investigated that include the effect of increasing O/C ratios and plasma power, and polyaromatic compound additives. The effect of these parameters was evaluated against the hydrogen and carbon monoxide yields, the energy conversion efficiency, and the specific energy requirement to generate syngas for both systems. The experimental results were also compared against the predicted yields and efficiencies expected if the system were to reach thermodynamic equilibrium conditions. This is especially true in the case when solid carbon formation was not included as a product in the thermodynamic simulations, even though it is a thermodynamically favorable product. This suggests that the plasma may be acting as a soot suppressant; however, further work is needed to elucidate this effect.

The performance of these gliding arc plasma fuel conversion systems has showed great promise in terms of efficient conversion of heavy hydrocarbons fuels, such as n-Tetradecane, to syngas products. Despite the fact that there was a significant fraction light hydrocarbons in the syngas product stream, this should not hinder the performance of a SOFC, however, because the majority of these light hydrocarbons are comprised of methane. Researchers have shown that residual methane in the syngas product stream (up to 25% molar concentration) is actually beneficial to the thermal management characteristics of a solid oxide fuel cell [103]. This is because methane can be reformed in the high temperatures of the anode side of the fuel cell, where abundant H_2O is present. The endothermic methane-steam reforming reaction can balance the exothermic oxidation of hydrogen that occurs as the fuel cell produces electricity (as H_2 reacts with oxygen ions transported across the electrolyte membrane to form H_2O).

Overall, the experimental results show that both the RVF-GA and GA-Plasmatron reformers achieved partial oxidation of heavy hydrocarbons to syn-gas with approximately 50% efficiency with formation of an additional fraction of nearly 40% of light hydrocarbons in the product stream. When the light hydrocarbons are included in the energy-mass balance with syn-gas, the energy conversion efficiency of both systems can be as high as 80–90%, which is very close to the thermodynamic equilibrium energy efficiency for conversion. Further work is needed to optimize these systems to minimize heat losses in the post-plasma treatment zone and increase residence time in the vicinity of the plasma discharge itself. Such modifications should improve syn-gas selectivity and yields. Furthermore, when considering that the residual light hydrocarbons, which are comprised of mostly methane, can be fully converted within a SOFC, the energy conversion efficiency can then be increased from 50% to approximately 83%. Complete conversion (tetradecane-to-electricity) using the plasma reformers combined with a solid oxide fuel cell (with 50% maximum efficiency) would be then as high as 42%.

Even though the exact mechanisms of the plasma catalysis effect for partial oxidation are unknown at this time, there is some experimental evidence that gliding arc plasma is acting catalytically within the system. Fundamental research on the exact kinetic mechanisms of the plasma active species is needed as well as identification of the influence of these species on accelerating the reaction rates for partial oxidation.

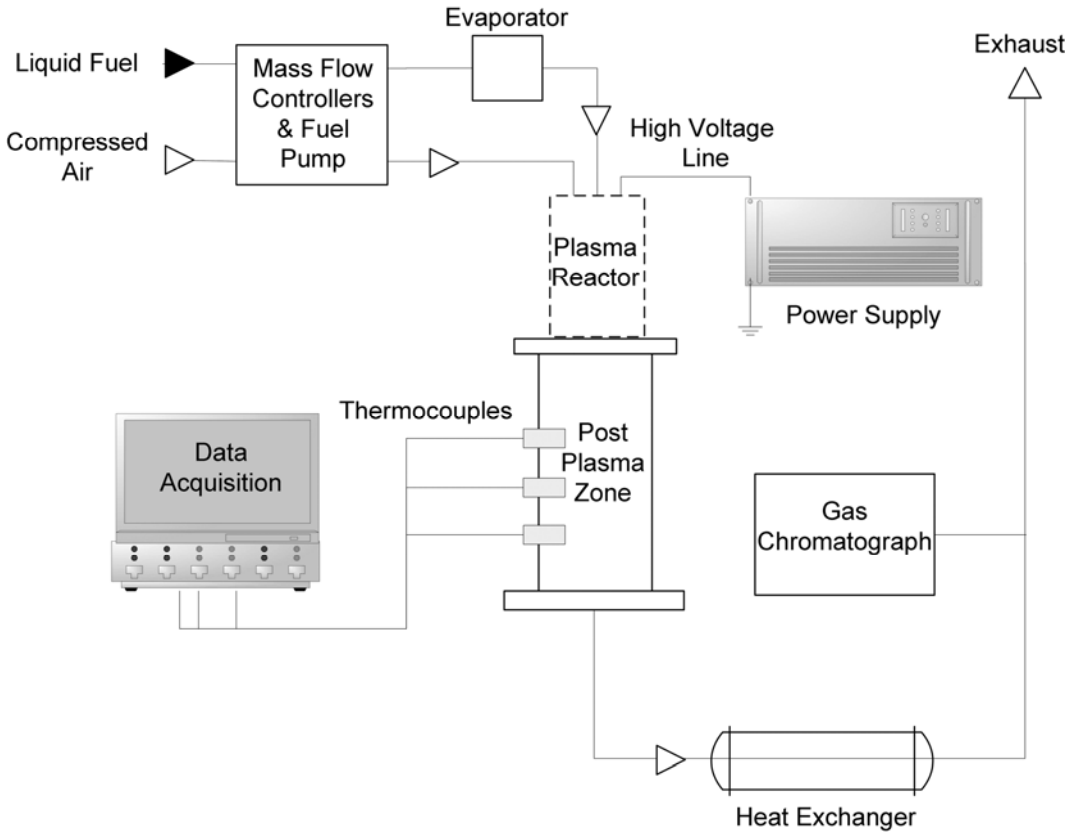

Figure 13. General system scheme showing components that are external to the RVF-GA plasma reformer.

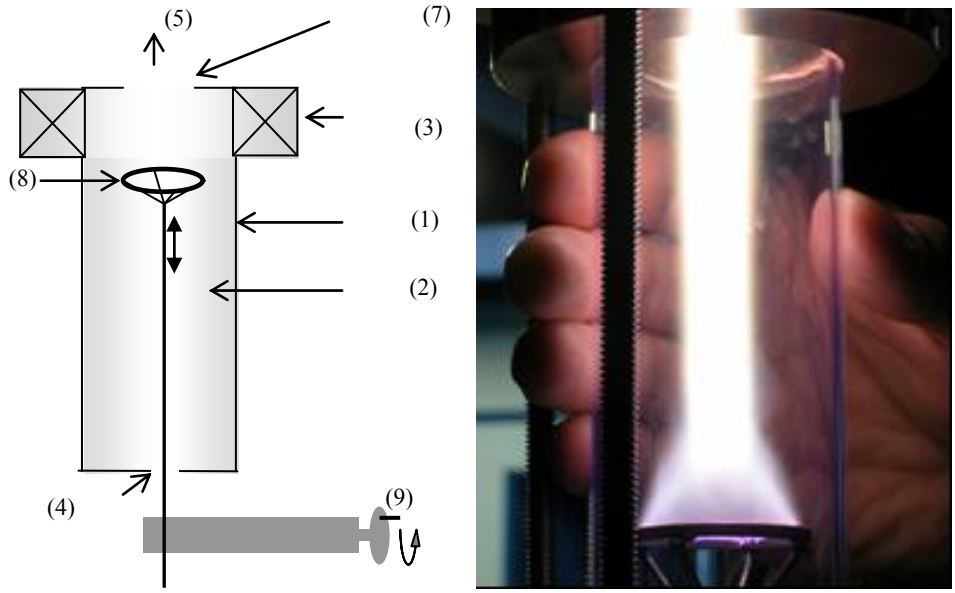

Figure 14. A schematic of the gliding arc plasma reformer for conversion of methane to syngas (left) [11]. A photograph of the rotating plasma discharge which is suspended between a ring electrode and a grounded flange [121].

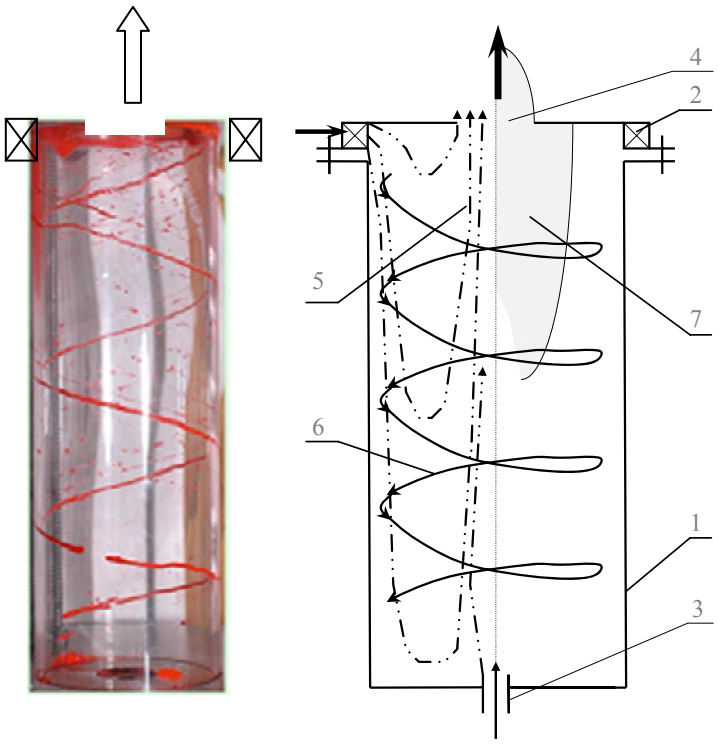

Figure 15. Photograph depicting rotating flow inside a reverse vortex flow chamber (left) [12]. Schematic of the axial and rotational streamlines of reverse vortex flow [11].

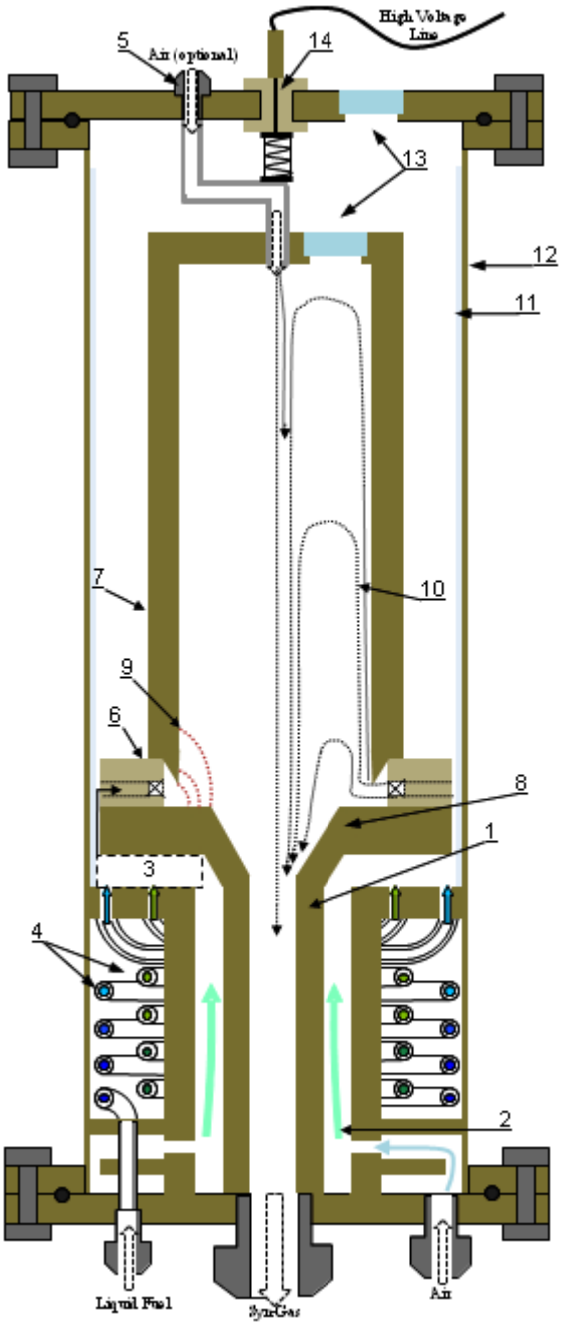

Figure 16. Schematic of the RVF-GA reactor.

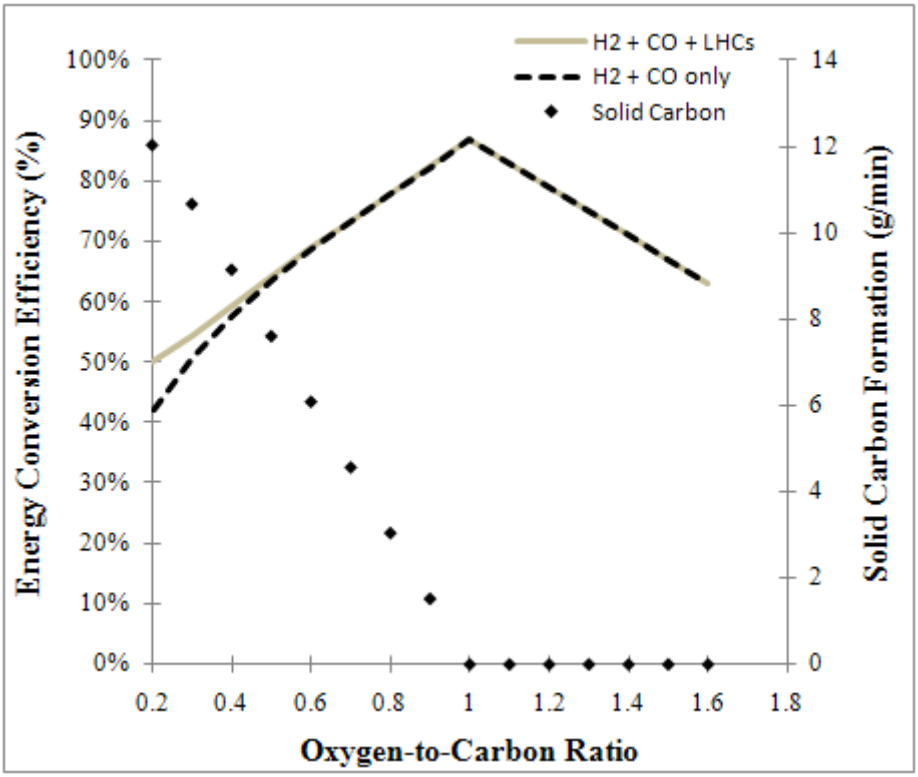

Figure 17. Thermodynamic equilibrium simulation predictions for the energy conversion efficiency of the partial oxidation of n-tetradecane versus the oxygen-to-carbon ratio. Solid line represents energy efficiency of syngas plus residual light hydrocarbons (LHCs) which are mostly comprised of methane. The dashed line corresponds to the conversion efficiency of syngas (H_2 & CO) only. The black dots represent the mass flow rate (g/min) of solid carbon formation region, which begins just below the O/C ratio of 1.

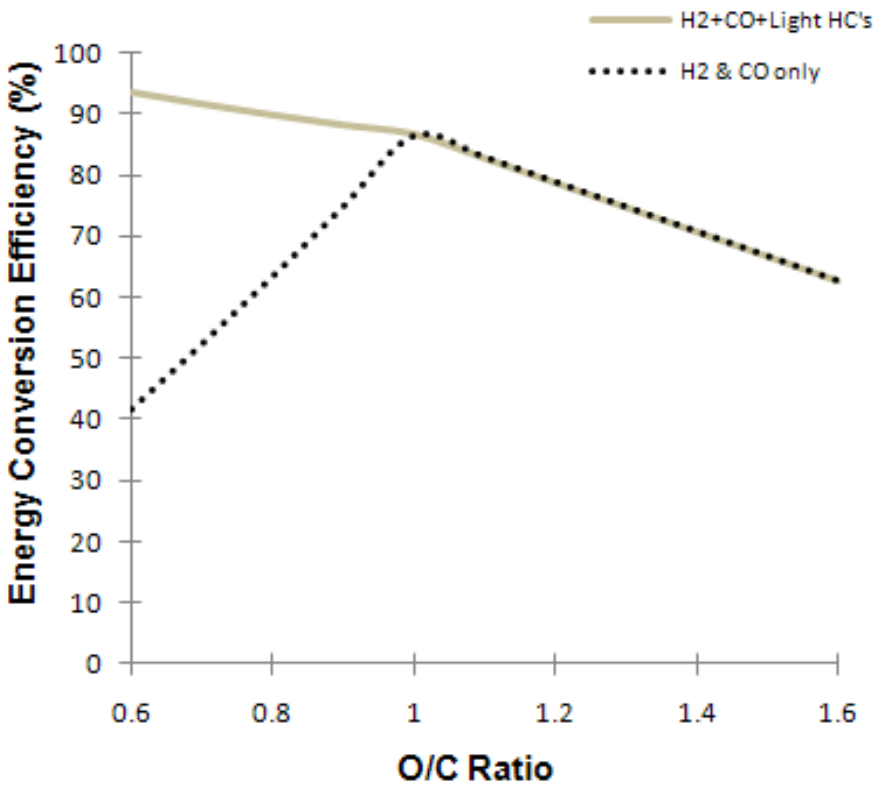

Figure 18. Thermodynamic equilibrium energy conversion efficiency of the partial oxidation of n-tetradecane versus the oxygen-to-carbon ratio without solid carbon formation. The solid line represents energy efficiency of syngas plus residual light hydrocarbons (LHCs) in the case where solid carbon is not allowed to form. The dashed line corresponds to the conversion efficiency of syngas (H_2 & CO) only.

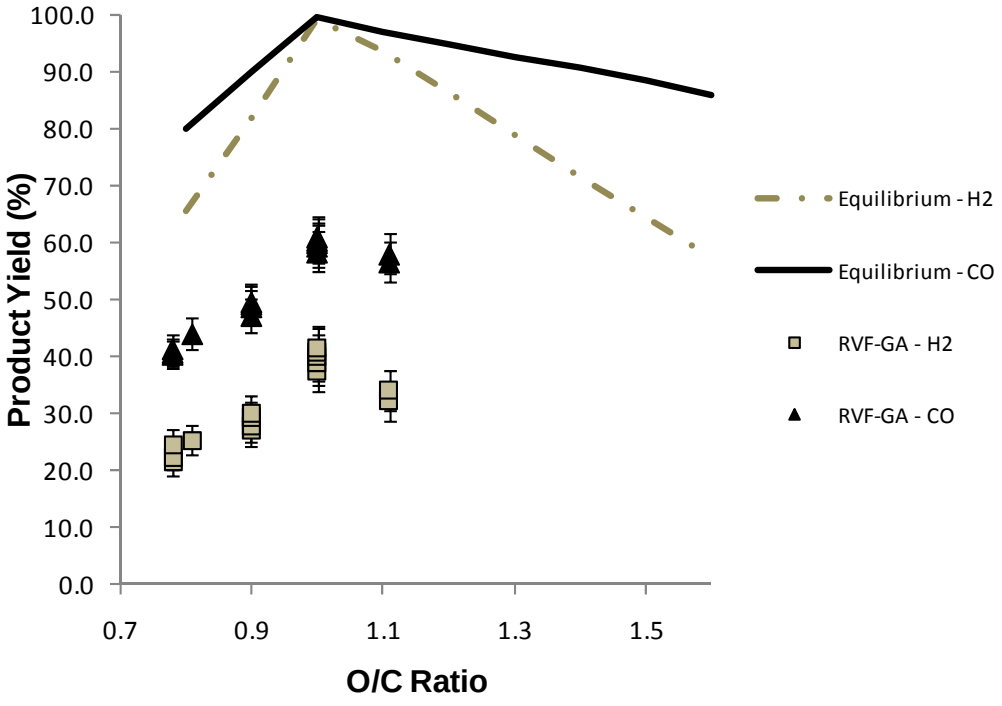

Figure 19. Hydrogen and Carbon monoxide yields as a function of the O/C ratio for the RVF-GA reformer. The solid and dashed lines show the predicted yields at thermodynamic equilibrium.

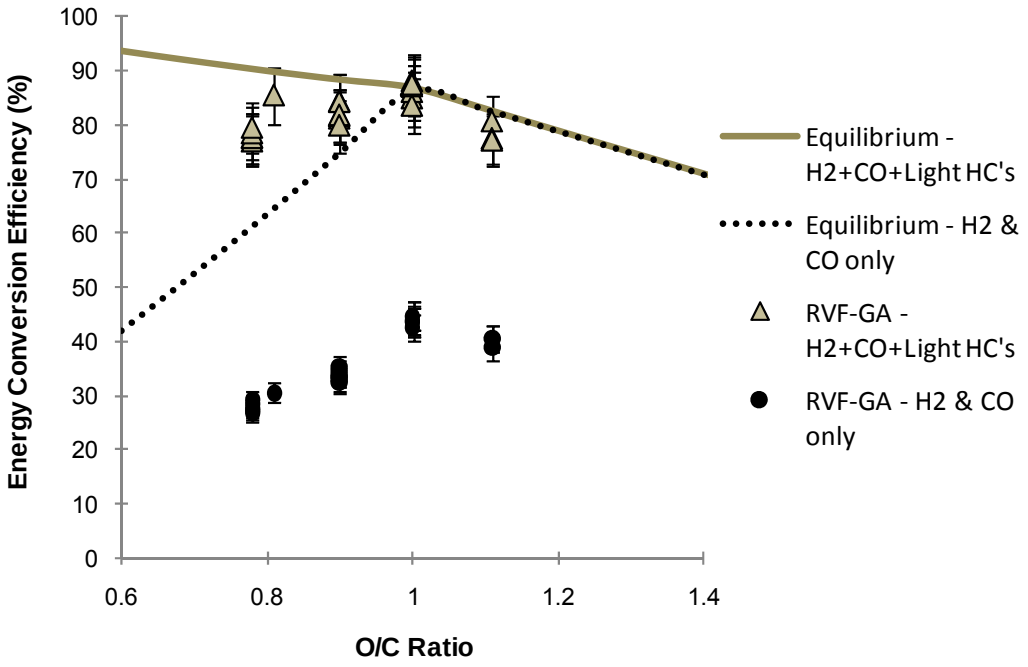

Figure 20. Energy conversion efficiency as a function of the O/C ratio for the RVF-GA reformer. The solid and dashed lines show anticipated conversion efficiency based on thermodynamic equilibrium predictions for the case of H_2 + CO + light hydrocarbons and H_2 + CO only.

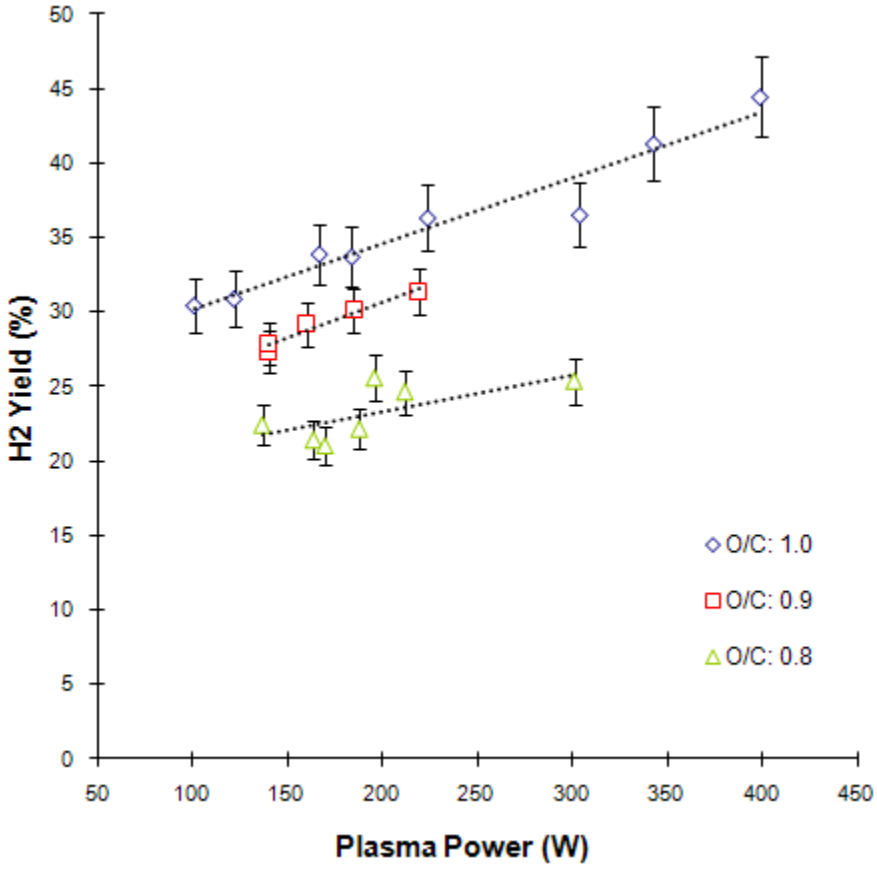

Figure 21. Dependence of the hydrogen yield on plasma power for various cases of the O/C ratio (0.8, 0.9, 1.0).

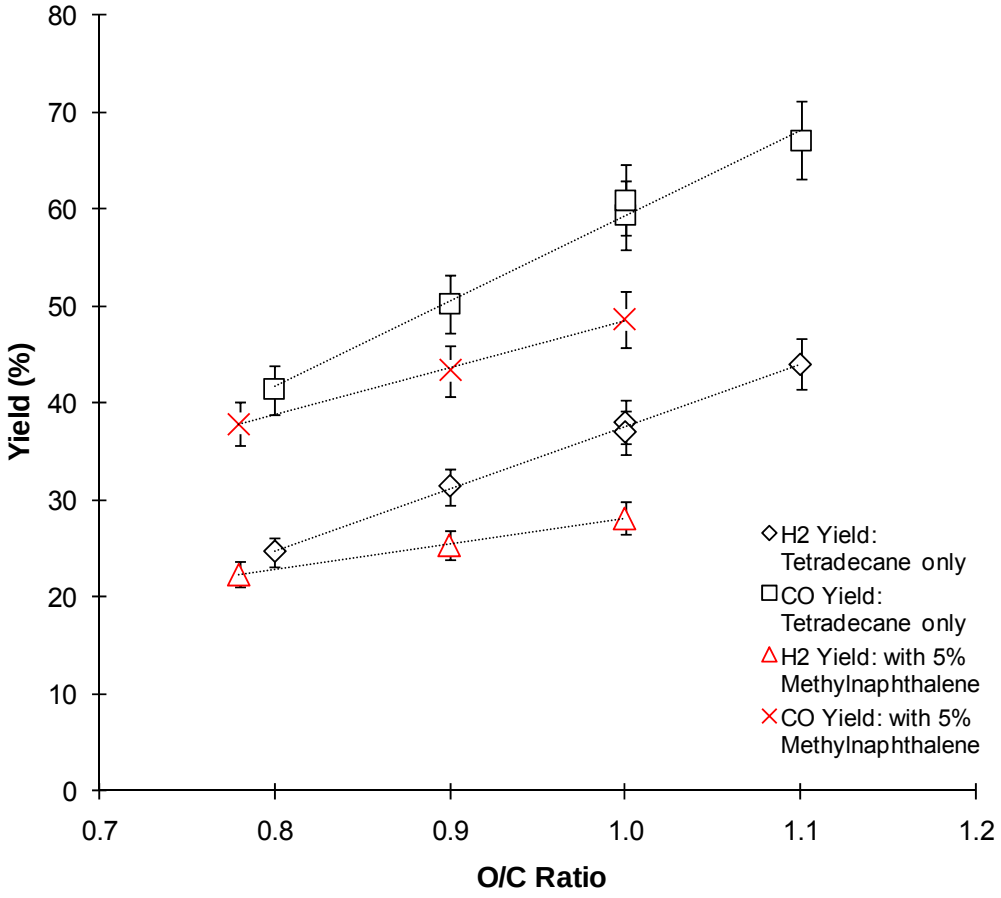

Figure 22. Comparison of the hydrogen and carbon monoxide yields versus the O/C ratio for 100% n-Tetradecane and 95% n-Tetradecane plus 5% Methylnaphthalene.

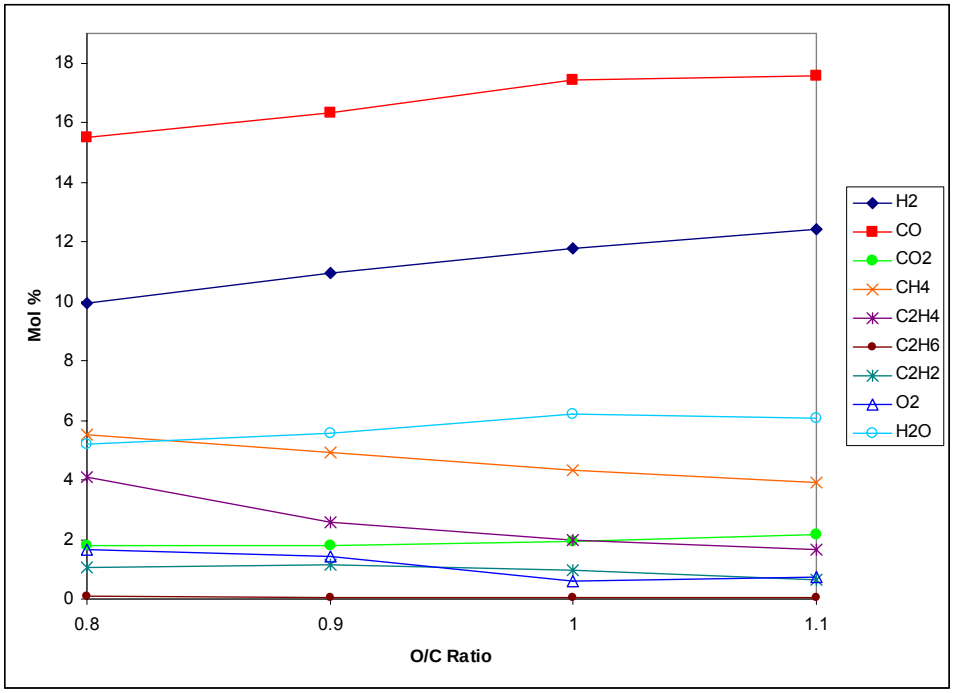

Figure 23. Absolute composition of products on a wet basis for partial oxidation of 100% n-Tetradecane in the RVF-GA reformer.

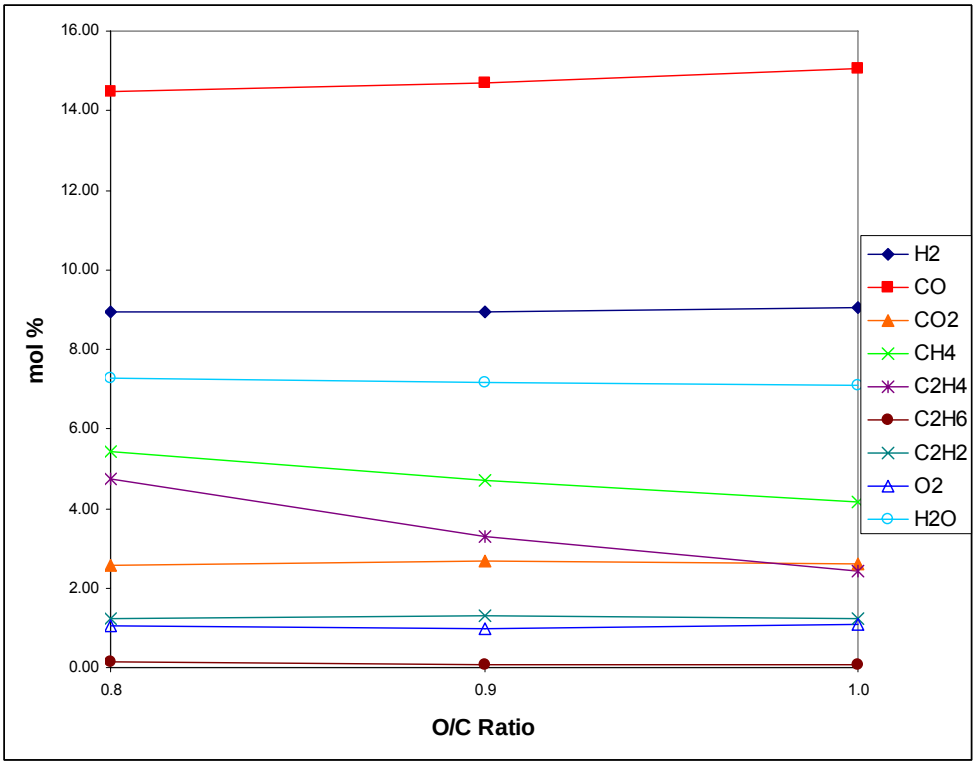

Figure 24. Absolute composition of products on a wet basis for partial oxidation of 95% n-Tetradecane/5% Methlynapthalene fuel mixture in the RVF-GA reformer.

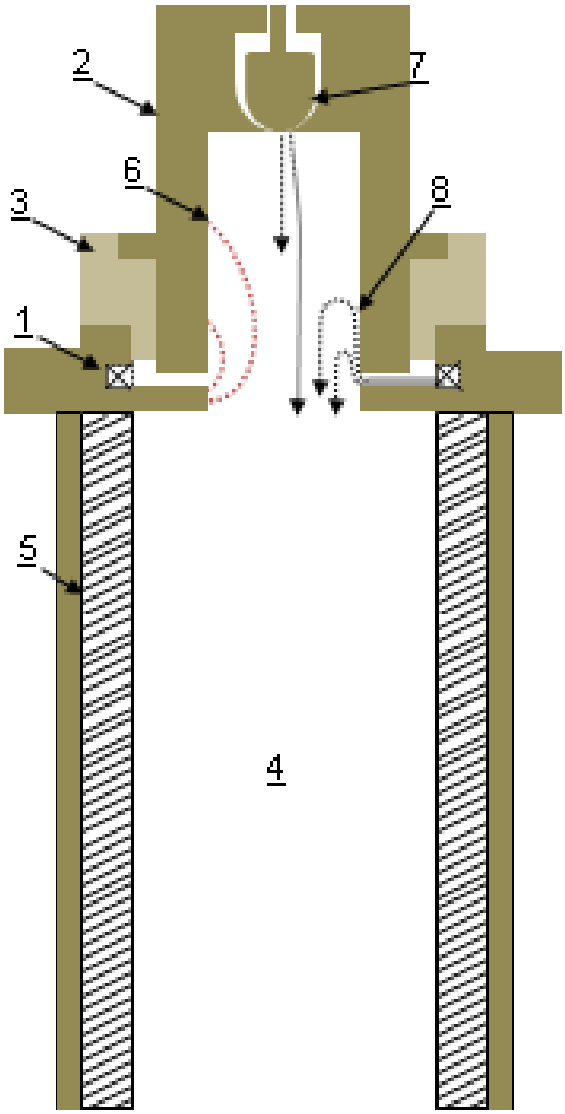

Figure 25. Schematic of the GA-Plasmatron reformer.

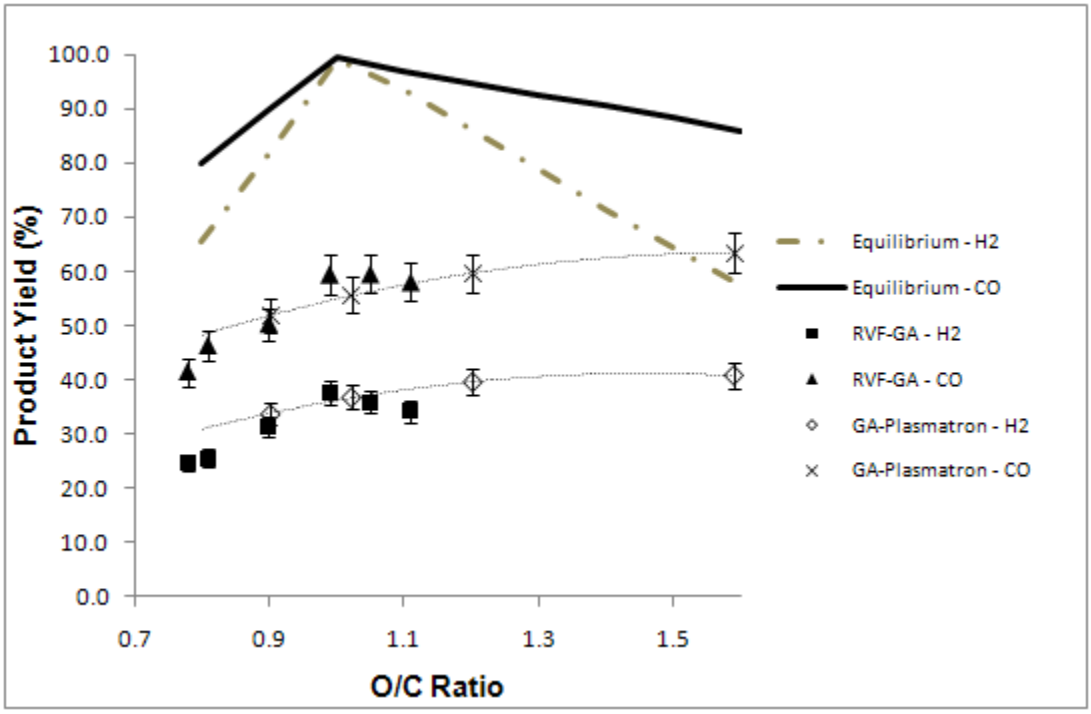

Figure 26. Comparison of the hydrogen and carbon monoxide yields as a function of the O/C ratio for the RVF-GA and GA-Plasmatron reformers. The solid and dashed lines represent the syngas yields as predicted from thermodynamic equilibrium simulations.

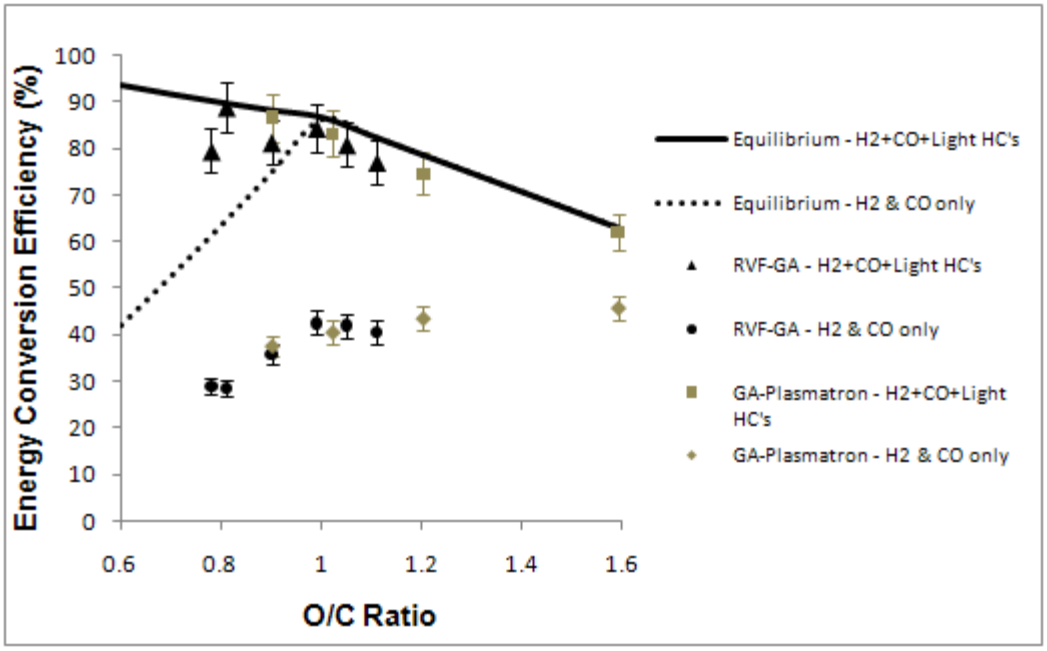

Figure 27. Comparison of the energy conversion efficiency as a function of the O/C ratio for the RVF-GA and GA-Plasmatron reformers. The solid and dashed lines represent the expected energy conversion efficiency as predicted from thermodynamic equilibrium simulations.

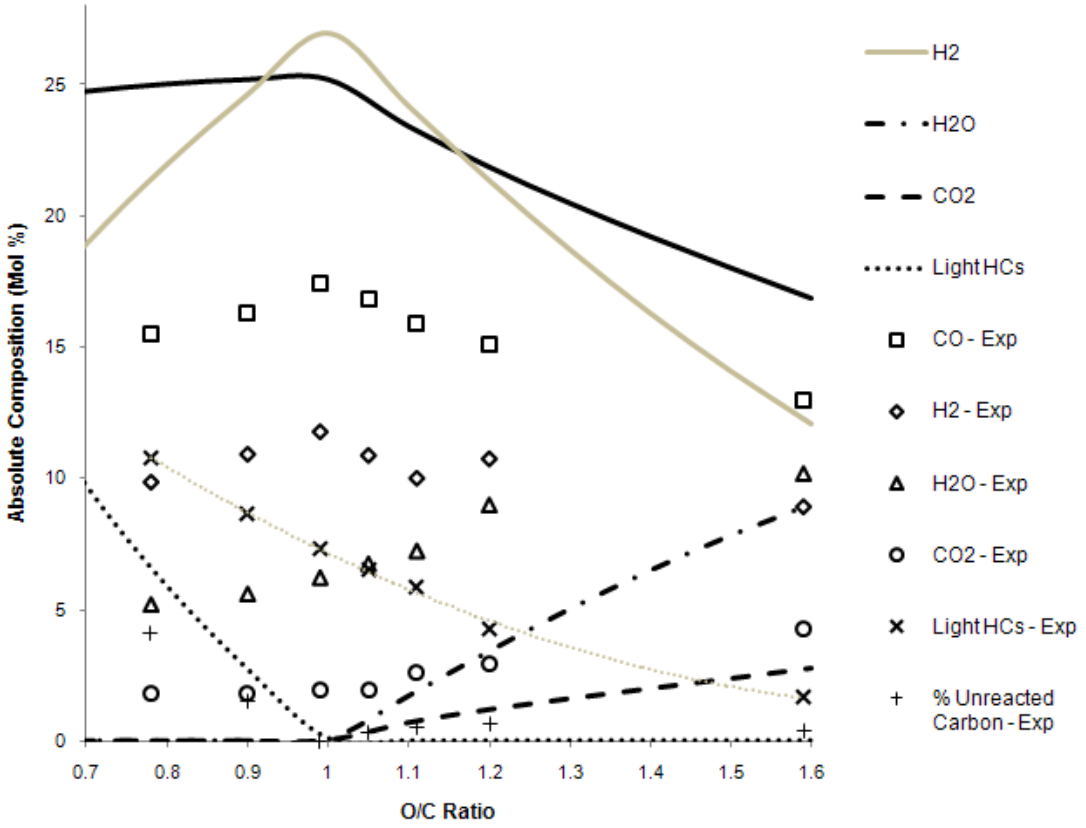

Figure 28. Experimentally measured absolute composition of products as a function of the O/C ratio for both the RVF-GA and GA-Plasmatron reformers.

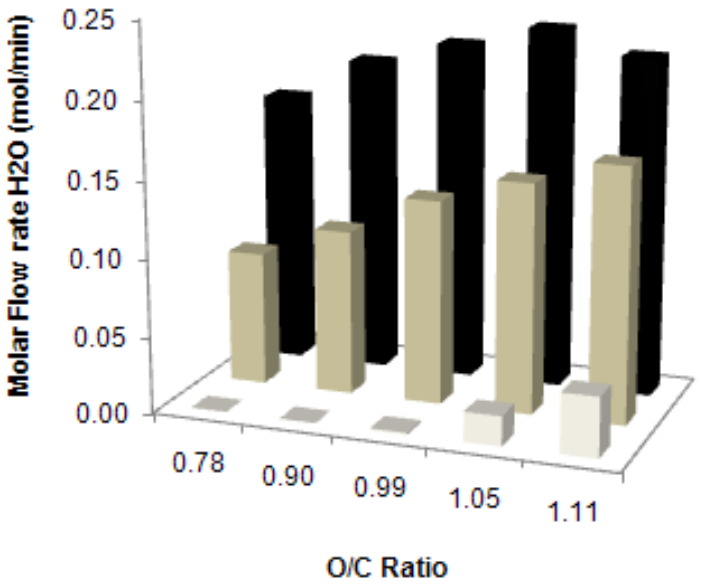

Figure 29. Comparison of the H2O content of the product stream: expected value for the end of the rapid oxidation phase (black), experimental estimations (grey), and thermodynamic equilibrium (white).

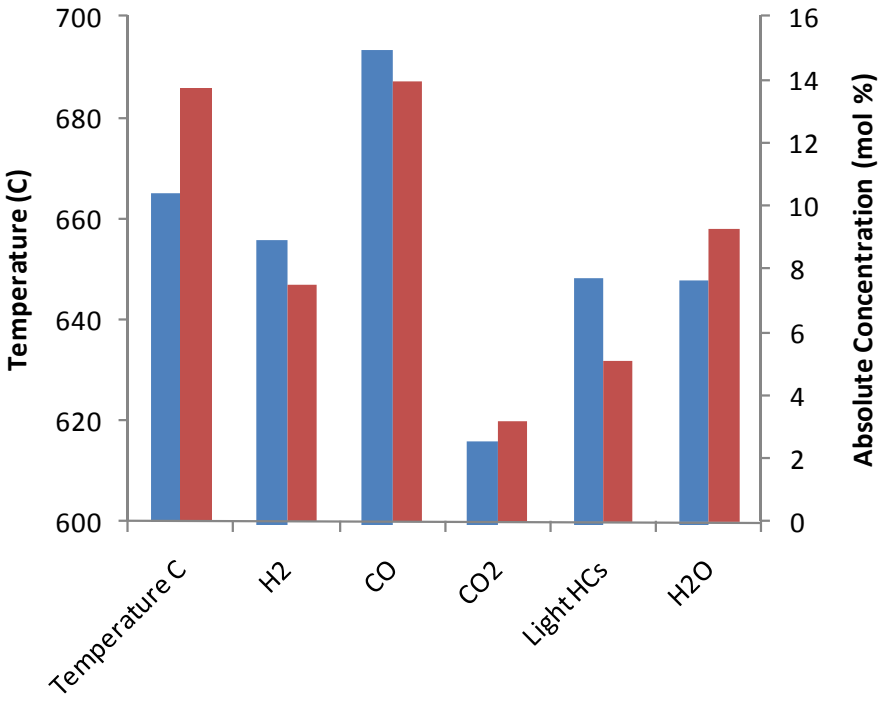

Figure 30. Comparison of product compositions and temperatures for partial oxidation of n-Tetradecane both with and without gliding arc plasma.

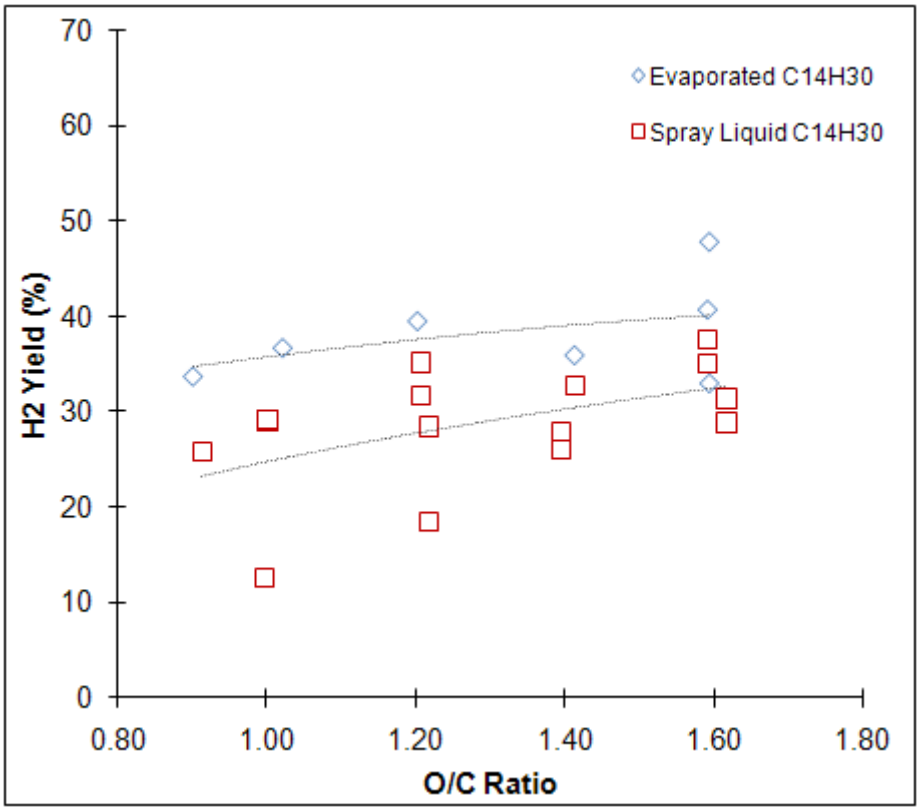

Figure 31. Hydrogen yield versus O/C ratio for the cases of evaportated and spray liquid n-Tetradecane.

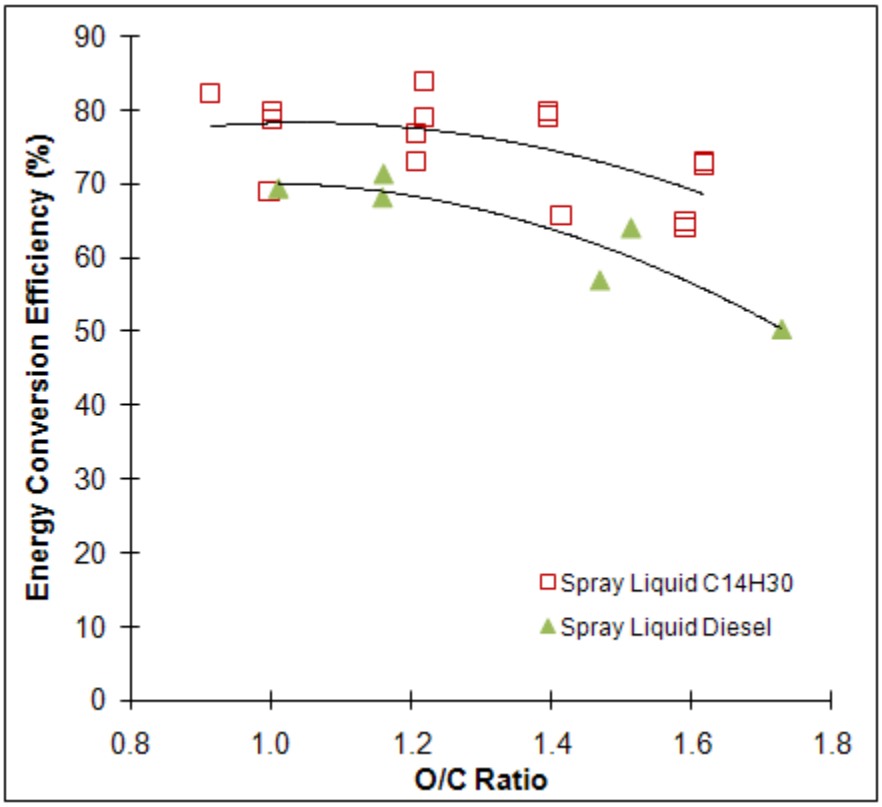

Figure 32. Energy conversion efficiency versus O/C ratio for the cases of spray liquid n-Tetradecane and Diesel fuel.

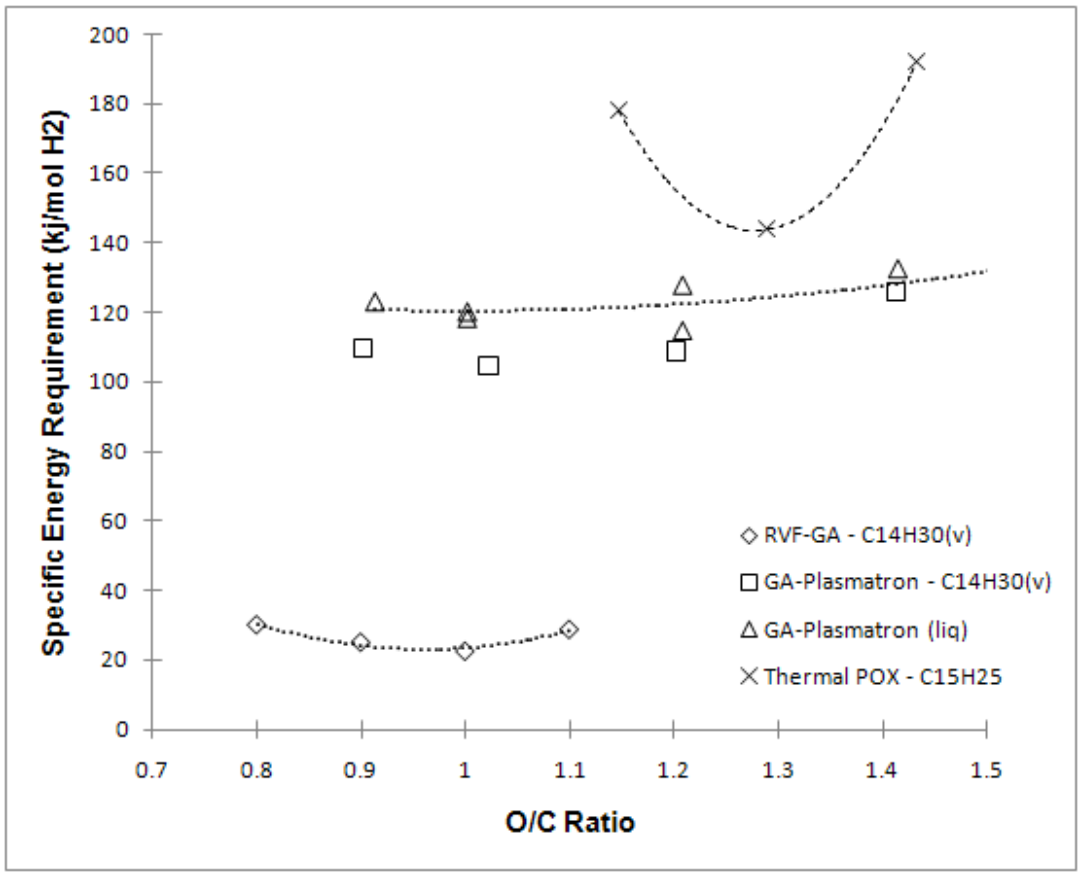

Figure 33. Comparison of the specific energy requirement as a function of the O/C ratio for the RVF-GA, GA-Plasmatron, and a Thermal POX reactor.

Chapter 3. Design, Testing, and Evaluation a Gliding Arc Plasma Reformer for Autothermal reforming of Diesel and JP-8 Fuels to Synthesis Gas for Auxiliary Power Unit

3.1 Introduction

In this chapter, a modified version of the Gliding Arc Plasmatron (GA-Plasmatron) was developed to reform Diesel and JP-8 fuels into synthesis gas using the oxidative steam reforming regime, which is also known as autothermal reforming. Autothermal reforming is a more energy efficient reforming regime than partial oxidation because the process is thermo-neutral, that is, it balances exothermic oxidation reactions with endothermic steam and CO_2 reforming thus creating a zero net enthalpy change of the process ($\Delta H=0$). It is also possible to achieve increased hydrogen yields and improved hydrogen selectivity under oxidative steam reforming conditions because syngas can be derived from the oxidizers themselves (i.e. H_2 from H_2O). The GA-Plasmatron that was specially developed for this application was combined with a desulfurization system and a solid oxide fuel cell (SOFC) to create a novel non-thermal plasma auxiliary power unit for military tanks (under funding from the U.S. Army through TARDEC) [71]. As stated earlier, non-thermal plasma reforming technology is well-suited for vehicular on-board reforming because the systems are typically compact, are capable of working with high-sulfur fuels (JP-8 can have up to 3000 ppm), and have a near instantaneous start-up time. In this system, the GA-Plasmatron reformer is capable of incorporating high temperature SOFC anode tail gas exhaust into the reactant stream. The flow diagram in Figure 34 shows the components of the system along with the compositions of the reactant and product streams. The system is designed to support a 10 kWe SOFC and contains two plasma reformers that can process up to 16 kWth of fuel each (approximately 32 kWth total). Each component of the non-thermal plasma auxiliary power unit system was developed and tested separately. The design of the GA-Plasmatron

reformer, evaluation of its performance, and a discussion of the results will be included in the following sections of this chapter.

3.2 Process Flow Diagram for the Non-Thermal Plasma Auxiliary Power Unit

Figure 35 shows the process flow diagram for the non-thermal plasma auxiliary power unit. The highlighted lines represent the portion of the system that was replicated at Drexel University and used to evaluate the modified GA-Plasmatron reformer. The input streams into the plasma reformer include stream B1 (air), stream A (Diesel), and Stream F, which represents variable amounts of the SOFC anode tail gas that was tested in three increments (3%, 6%, and 10%). The optimum amount of EGR (10%) was chosen based on the maximum predicted thermodynamic energy conversion efficiency at the autothermal point. The autothermal point is located where the difference in the stream enthalpies for reactants (in) and products (out) approaches zero ($\Delta H=0$). To balance the energy requirements of the process, the calculation requires additional thermal energy from the SOFC exhaust (assumed to be 850C). Table 4 shows the specifications of each process flow stream in terms of mass flow rates, compositions, and temperatures. The remaining two increments of EGR (3%, 6%) were included in this investigation because even though the thermodynamic predictions show the optimum EGR as 10% of the SOFC exhaust, kinetic limitations of real-world systems (heat losses, residence time limitations) often dominate experimental processes. Lower amounts of EGR allow for a longer residence time of treatment in the heated zone of the reactor.

Table 4. Non-thermal plasma auxiliary power unit SOFC exhaust gas recycle (EGR) components for 3, 6, and 10 percent of total SOFC exhaust.

EGR components	**Concentrations of EGR (mol%)**	**EGR flow input (SLPM)**		
		3%	**6%**	**10%**
H_2	5.7%	2.61	5.23	8.71
H_2O	34.5%	15.82	31.63	52.72
CO	6.8%	3.12	6.24	10.39
CO_2	36.3%	16.64	33.28	55.47
N_2	16.7%	7.66	15.31	25.52
Total:	100.0%	45.85	91.69	152.82

Figure 36 shows a design image of the auxiliary power unit. The system was designed to house two plasma reformers within M-shaped enclosures that reside on either side of the SOFC. This design was chosen to maximize heat transfer between the SOFC and plasma reformers. Figure 37 (top) shows the thermally insulated box that was fabricated to house the SOFC and plasma reformers. The specifications imposed on the design of system required that the system volume not exceed 150L. Figure 37 (bottom) shows the actual M-shaped enclosures with a heat exchanger located between them. *Note: it was later decided by TARDEC not to include the SOFC for initial trials, therefore a heat exchanger was added to simulate heat transfer from the SOFC.*

3.3 Materials and Methods

The materials and methods employed in this chapter are very similar to the methodology described in chapter 2. The modified GA-Plasmatron reactor was connected to a heat exchanger to condense water vapor and cool exhaust gases before sampling. Gas sampling always occurred at steady state temperature conditions and the syringe method was used, sometimes in

conjunction with a particulate filter to remove any solid contaminants such as soot or coke. A dry-basis analysis of the gas composition was made using a Gas Chromatograph (Agilent 3000 Micro-GC) using the thermal conductivity detection method. Two separate columns were used; the Agilent HP-PLOT Molsieve column for detection of H_2, CO, CH_4, O_2 and N_2; and the Agilent GS-GasPro column for detection of CO, CO_2, N_2, CH_4, C_2H_2, C_2H_4, C_2H_6.

The SOFC anode tail gas was created in the laboratory and was preheated to temperatures near 850°C (near to the normal operating temperature of most SOFCs). The simulated anode tail gas mixture, which was comparable in composition to a real SOFC exhaust, contained a mixture of the following components: 36.3% CO_2, 34.5% H_2O, 5.7% H_2, 6.8% CO, 16.7% N_2. The SOFC exhaust gas recycle (EGR) amounts were varied between 3%, 6%, and 10% of the total exhaust flow from a typical 10 kW fuel cell. In addition, some amount of air was also used during reforming and was preheated to temperatures less than 200°C. Reforming experiments using both diesel fuel and JP-8 were performed and the fuels were vaporized using a custom-made wall-heated coiled-tube vaporizer. The fuel flow rates were kept constant for each trial at 0.3 g/s for 3% and 6% EGR trials; however, lower fuel flow rates of 0.15 g/s and 0.1 g/s were used during the 10% EGR trials.

Most of the experimental trials utilized commercial-grade low-sulfur diesel fuel; however some data points using JP-8 fuel were obtained during testing of the integrated system (see section 3.7). The energy conversion efficiency definition, previously defined in section 1.5.5, was slightly modified here to account for the additional amount of H_2 and CO coming from the exhaust gas recycle stream of the SOFC. The residual H_2 and CO were considered to be an additional source of fuel and were accounted for in the following equation:

$$Moified\ Energy\ Conversion\ Efficiency\ (\%) = \frac{LHV_{products} \times 100}{LHV_{fuel} + \left(LHV_{H_2} + LHV_{CO}\right)_{EGR}} \quad (3\text{-}1)$$

3.4 Concept and Design of the Modified GA-Plasmatron Device

A schematic of the modified GA-Plasmatron device is shown in Figure 38. The plasma discharge is initiated in a 3mm gap (1) between the high voltage electrode (4) and the grounded exhaust flange which contains the tangential jets (3) that generating the swirling vortex flow. The SOFC exhaust gas recycle is pre-mixed with fuel and injected into the system through a side port (2) and is ultimately the flow that pushes and elongates the plasma discharge. The high voltage electrode is shielded from the outer grounded reactor shell with a glass-filled teflon plug (6) that is rated to withstand temperatures as high as 300C. An air cooling port (5) was added to the grounded flange that contains the teflon dielectric plug to prevent overheating. The modified GA-Plasmatron device houses a fuel atomization nozzle (10) and liquid fuel can be introduced through (8). A small amount of air is needed to properly atomize fuel and is introduced though the port located at (9). In addition, another small amount of air is introduced through port (7) and flowed along the inner wall of the high voltage electrode to keep the atomized droplets from making contact with the wall and thus reducing the possibility for pyrolysis. The modified GA-Plasmatron device is relatively small and compact and has an overall length of 8 inches. A photograph of the device is shown in Figure 39.

3.4.1 Experimental Laboratory Setup

Figure 40 shows the experimental setup that was developed to evaluate the performance of the modified GA-Plasmatron reformer. The system includes a tube furnace (2) which was used to simulate the heat transfer between the plasma reformer and the solid oxide fuel cell and to

preheat the SOFC recycle gases; exhaust pipe with built-in heat exchanger (3); mass flow controllers (4); control station with labview (5); plasma power supply (6); and fuel pump (7).

3.5 Thermodynamic Analysis of the Oxidative Steam Reforming of n-Tetradecane using Variable Exhaust Gas Recirculation from a SOFC

In the following section, thermodynamic equilibrium simulations were performed to replicate the conditions of experiments. The predicted energy conversion efficiency was used to compare the performance of the system against what is considered possible from the standpoint of the laws of energy conservation. The simulation assumes ideal and somewhat unrealistic conditions (adiabatic, infinite residence time, etc.); however, it shows the theoretical maximum possible energy conversion efficiency attainable given the experimental conditions.

Thermodynamic equilibrium simulations of the system were initially performed using HSC Chemistry, version 6.0, and the anticipated energy conversion efficiencies were found for two cases: production of syngas only (H_2 and CO), and syngas plus LHCs, which are mostly comprised of methane. Figures 41 and 42 show the equilibrium energy conversion efficiencies for syngas plus LHCs (H_2, CO, and LHCs) and syngas only (H_2 and CO) as a function of increasing air-to-fuel oxygen to carbon (O/C) ratio, respectively. These figures also include increasing amounts of SOFC EGR in increments of 0, 3, 6, and 10 percent, where zero percent EGR is analogous to the partial oxidation case. As evidenced by figures 41 and 42, the peaks of maximum energy conversion efficiency increase with increasing amounts of SOFC EGR. This may seem intuitive because as EGR increases, so does the concentration of H_2O and CO_2 which are replacing air as the primary oxidizer. Increasing the EGR shifts the system closer to the steam reforming regime where additional hydrogen is produced, thus causing the increase in the energy conversion efficiency. But if this trend were to continue with ever-increasing amounts of EGR, the energy balance shifts away from the thermo-neutral point ($\Delta H=0$) to the endothermic steam

reforming regime ($\Delta H>0$). This is not possible given the limited amount of heat available in the overall system. The solid black dots on Figures 41 and 42 mark the onset of solid carbon formation which continues at lower O/C ratios where pyrolysis is predicted to occur.

3.6 Evaluation of the Performance of the Oxidative Steam Reforming of Diesel Fuel using the Modified GA-Plasmatron Reformer

The experimental modified energy conversion efficiency as a function of the air-to-fuel O/C ratio is shown in Figure 43 for two cases: 3% and 6% EGR. The dashed lines in Figure 43 show the predicted thermodynamic equilibrium efficiencies for EGR amounts of 3% and 6%. The energy conversion efficiency for the 3% EGR case (~60%) was almost twice higher than the 6% case (~30%). The general trend of the experimental data points follows the thermodynamic equilibrium predictions with the peaks of the curves shifted to higher O/C ratios. The deviation of the efficiencies from equilibrium is most likely a result of kinetic limitations within the system. As the EGR increases, so do the volumetric flow rates of reactants within the system. As a consequence, the residence time of treatment decreases, and the kinetically slower endothermic fuel reforming reactions may not have enough time to reach completion. In addition, there are heat losses in the post-plasma reaction zone which could act to quench the reforming reactions prematurely. Trials with longer residence time were investigated, which was achieved by scaling back all reactant flow rates proportionally. Figure 44 shows the 10% EGR case with two flow rates that were scaled lower by 50% ($\dot{m_{fuel}} = 0.15 g/s$) and 70% ($\dot{m_{fuel}} = 0.1 g/s$). As as result, the conversion efficiency results were greatly improved as was the estimated H_2O consumption, which is demonstrated in Figure 45. The experimentally estimated H_2O consumption in Figure 45 is shown for 3 cases: 3%, 6%, and 10% EGR with the 10% case having flow rates scaled to 50% of those shown in Table 4. The H_2O consumption trends are similar to the predicted consumption at thermodynamic equilibrium, which is represented by the solid and dashed lines. Negative consumption is analogous to production of H_2O and this occurs

at increasing O/C ratios as expected. CO_2 consumption (not shown) was almost negligible and this result is expected given that H_2O consumption was low and the endothermic H_2O reforming reaction requires 0.5 eV/mol less energy than conversion with CO_2.

3.7 Evaluation of the Performance of the Oxidative Steam Reforming of JP-8 Fuel using the Modified GA-Plasmatron Reformer

A brief trial to evaluate the performance of the GA-Plasmatron when using low sulfur JP-8 as fuel was investigated when the reactor was integrated into the overall auxiliary power unit system at Ceramatec Inc's headquarters. The conditions of this trial were slightly different as there was only CO_2 and H_2O used in the simulated EGR stream. Also, Ceramatec's integrated system has a post-plasma treatment zone with a volume that is double that of the system used at Drexel, thus the residence time of treatment is also doubled. Figure 46 shows the experimental energy conversion efficiency of JP-8 using 6% EGR for the cases of H_2 + CO + light hydrocarbons (mostly methane) and H_2 + CO only. The results are much improved over the 6% EGR trials using Diesel fuel (Figure 43) however they are still below the thermodynamic predicted maximum efficiency. Heat losses were not estimated, however they are expected to be greater due to the larger metal capacity (thermal mass) of the heated zone (see figure 37). Further improvements to minimize heat losses in the post plasma treatment zone should greatly improve conversion efficiency.

3.8 Conclusions

The results presented in the previous section described the development and testing of a novel. advanced auxiliary power unit that incorporated a gliding arc plasma reformer with a solid oxide fuel cell. Variable amounts of exhaust gases from the SOFC were recycled back into the plasma reformer in an effort to reach the energy-efficient autothermal reforming regime in which the net enthalpy change of the process is zero. The presence of SOFC exhaust gases improved

energy conversion efficiency; however, higher volumetric amounts of EGR caused a reduction in conversion. This result was attributed to a kinetic limitation in the system in which higher recycle gas flow reduced residence time for reaction completion. Upon scaling back flow rates of all reactants, thus increasing residence time, the energy conversion efficiency improved further, reaching as high as 80%.

The integration of plasma fuel reformers within auxiliary power units for vehicles is in the early stage of development and the results look promising. Before the syngas reformate from plasma reformers can be integrated with an actual solid oxide fuel cell, some improvement is needed to reduce C_2 hydrocarbons that have been reported in the product streams. The concentrations of these light hydrocarbons is low (1-2% in absolute concentration), but compounds such as acetylene and ethylene are known to cause degradation in the performance of the SOFC. Future efforts to optimize plasma fuel conversion systems may reduce these unconverted hydrocarbons and improve syngas yields, thereby eliminating this problem.

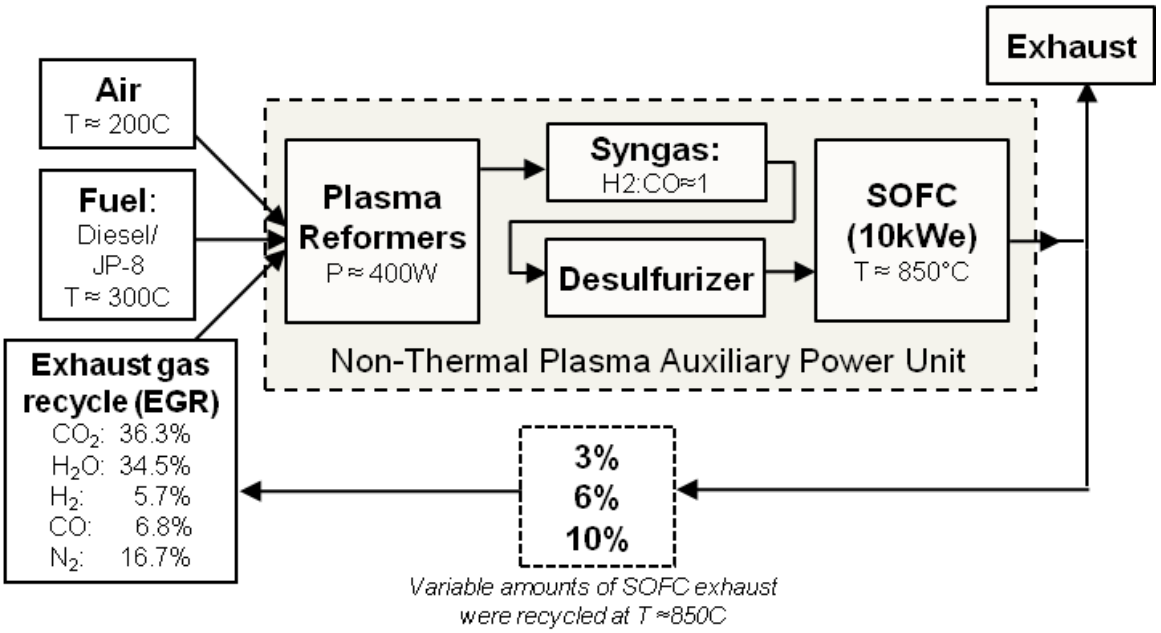

Figure 34. A scheme of the major components of a non-thermal plasma auxiliary power unit. This system was operated in steam-oxidative reforming mode and a variable portion of the SOFC exhaust was recycled back into the reformer to provide H_2O and CO_2.

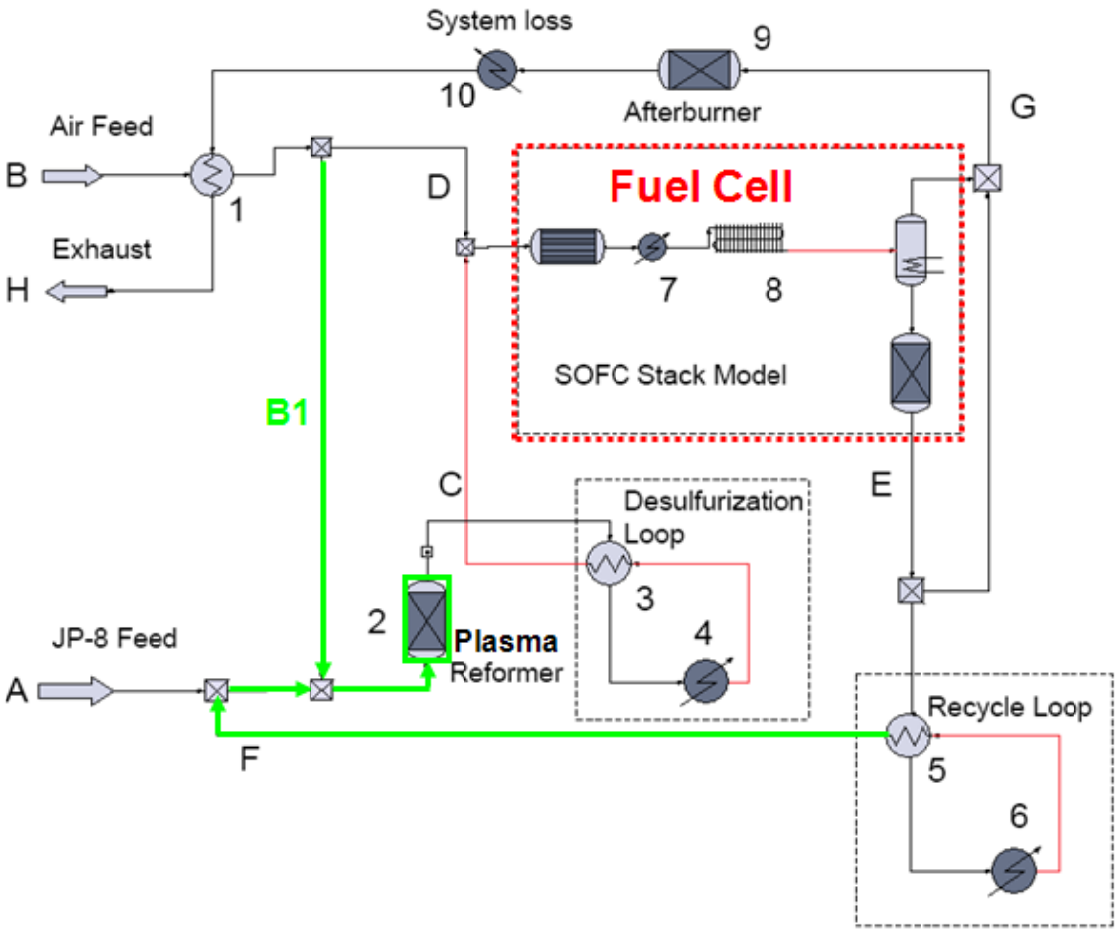

Figure 35. Process flow diagram for the non-thermal plasma auxiliary power unit system.

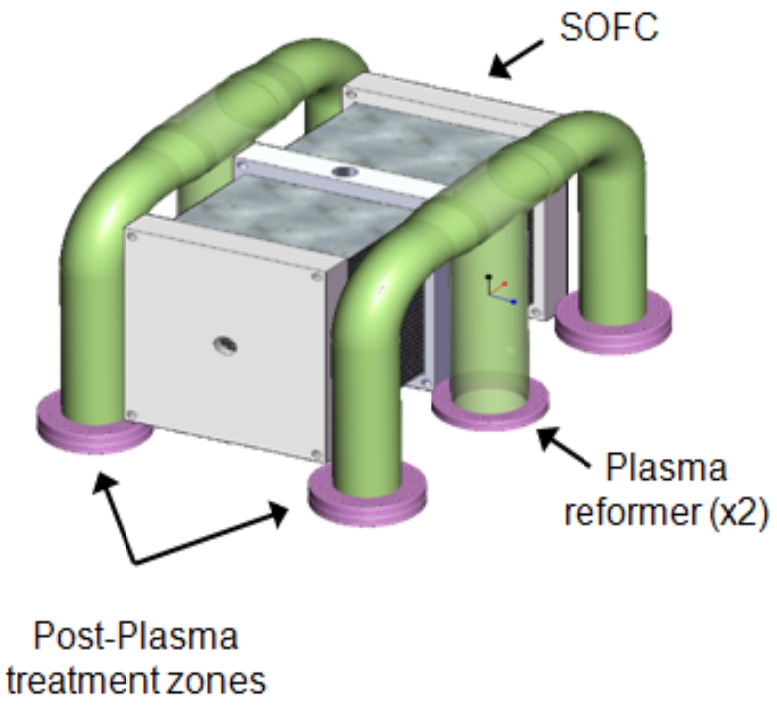

Figure 36. Design image of the internal portions of the plasma auxiliary power unit. The system contains a solid oxide fuel cell with two M-shaped reactor enclosures that house the plasma reformers.

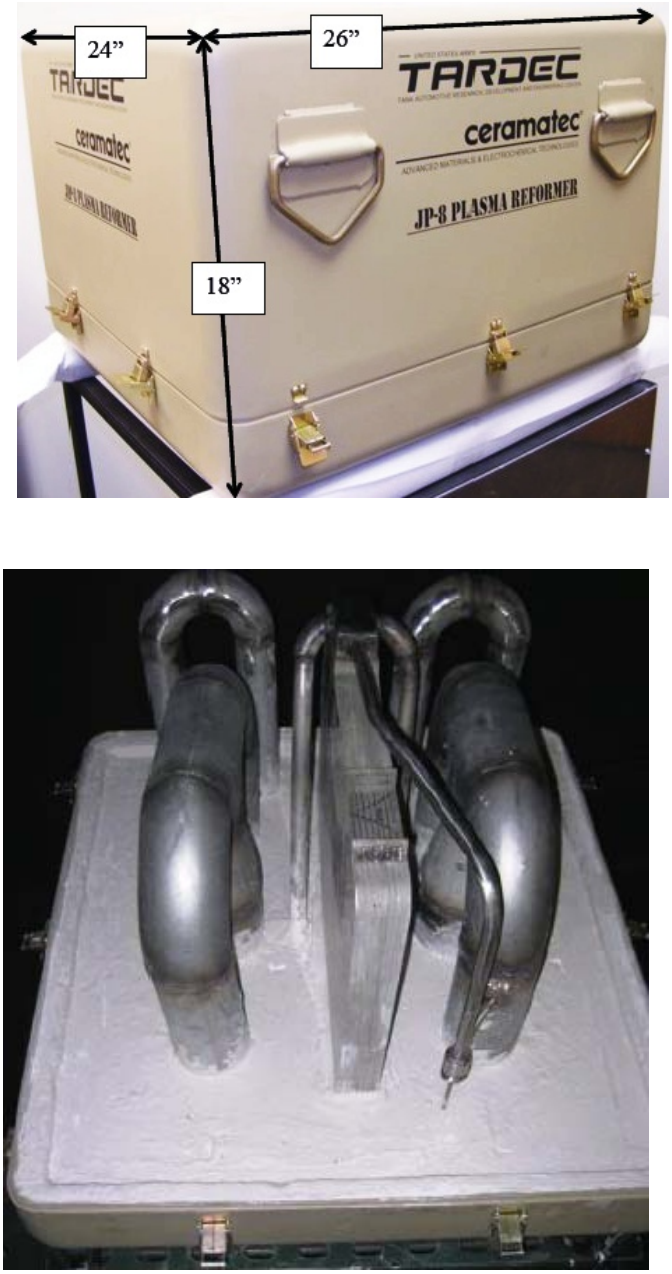

Figure 37. Photographs of the auxiliary power unit box that was constructed to house the two plasma reformers (top). An image of the internal M-shaped reactor enclosures (bottom).

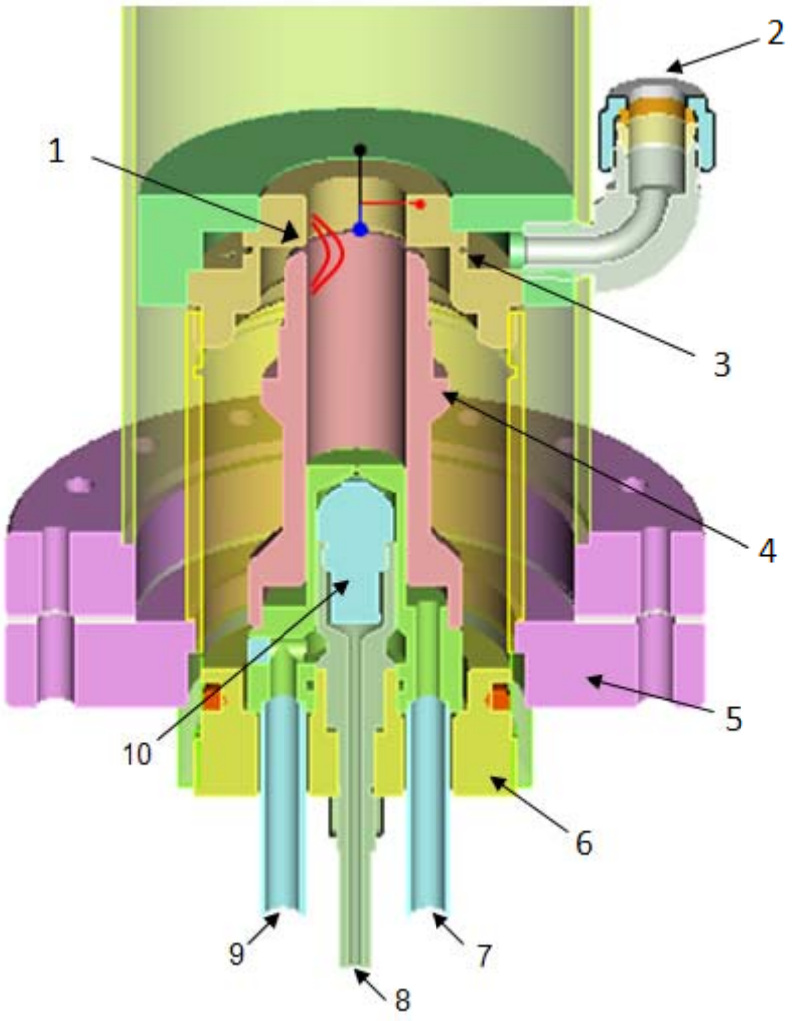

Figure 38. Schematic of the GA-Plasmatron reformer.

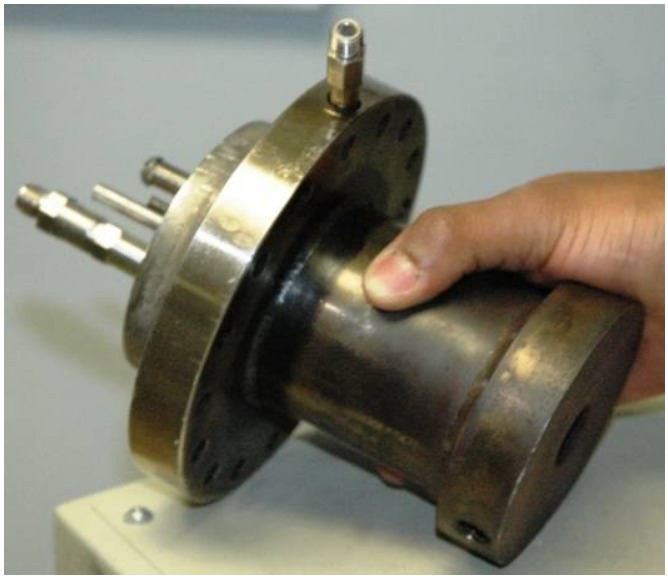

Figure 39. Photograph of the GA-Plasmatron device.

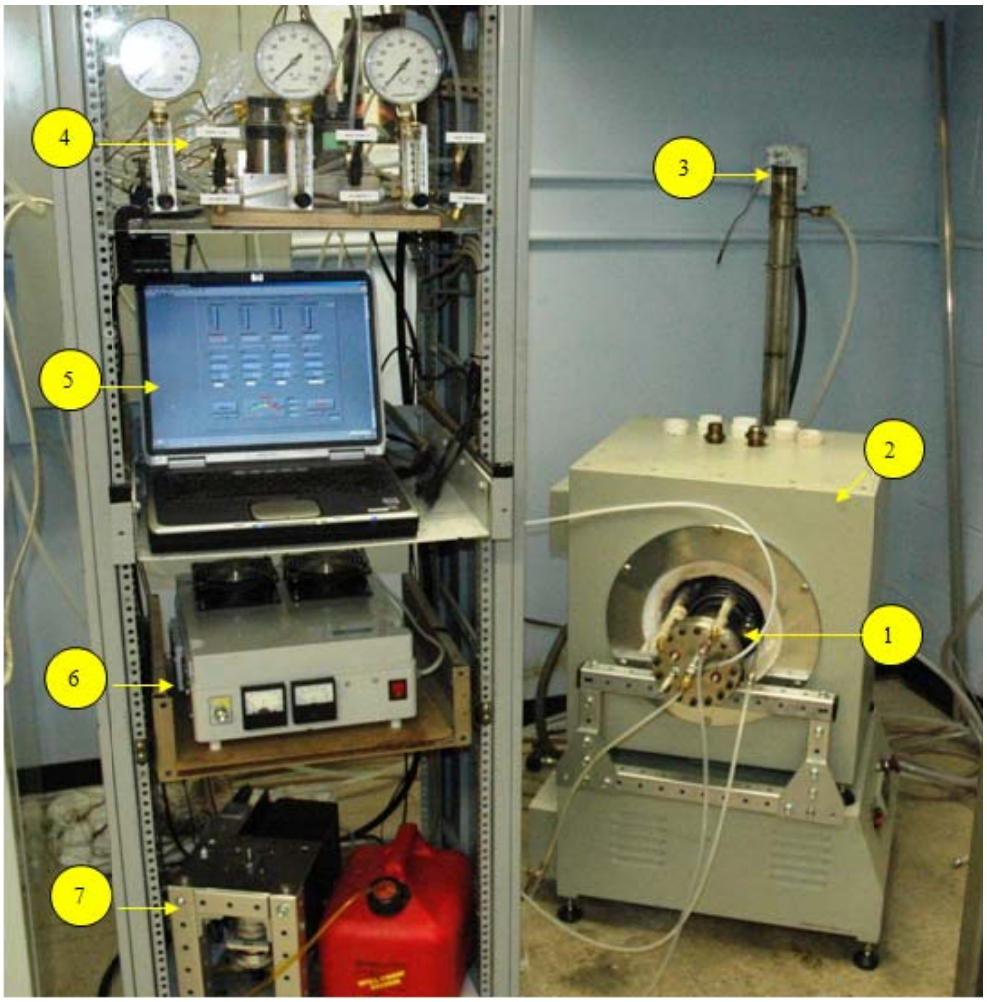

Figure 40. Photograph of the experimental setup used to evaluate the modified GA-Plasmatron reformer. 1) Gliding arc reformer, 2) Tube furnace, 3) Exhaust with built-in heat exchanger, 4) Mass flow controllers, 5) Control station with Labview, 6) Plasma power supply, 7) Fuel pump.

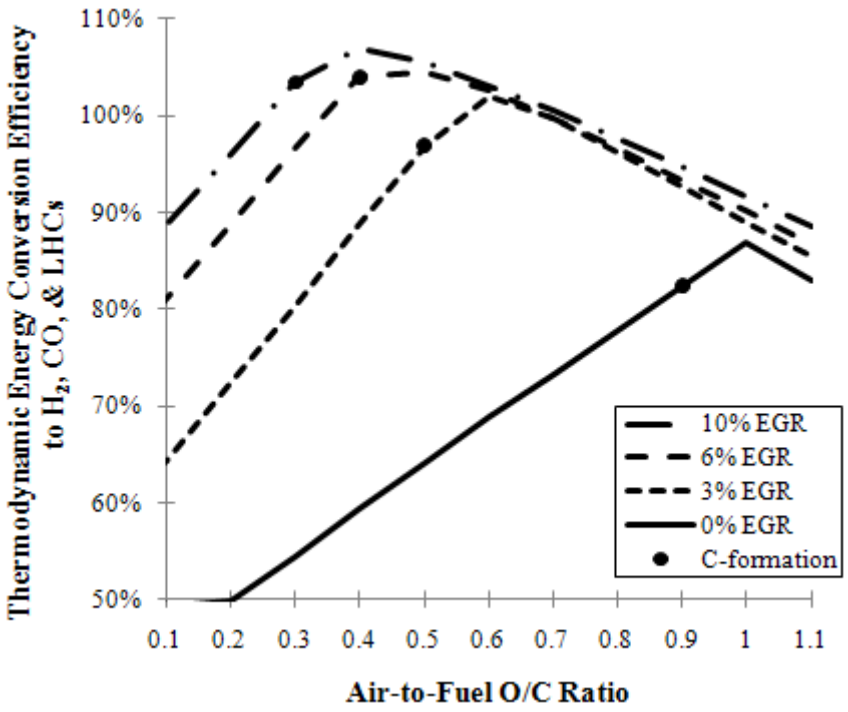

Figure 41. Thermodynamic equilibrium energy conversion efficiency versus the air-to-fuel O/C ratio for production of H2, CO, and light hydrocarbons (LHCs). Also included are several cases of increasing exhaust gas recycle (EGR) from a solid oxide fuel cell with zero EGR being analogous to partial oxidation. The black dots represent the onset of the carbon formation region, which continues (to the left) towards lower O/C ratios.

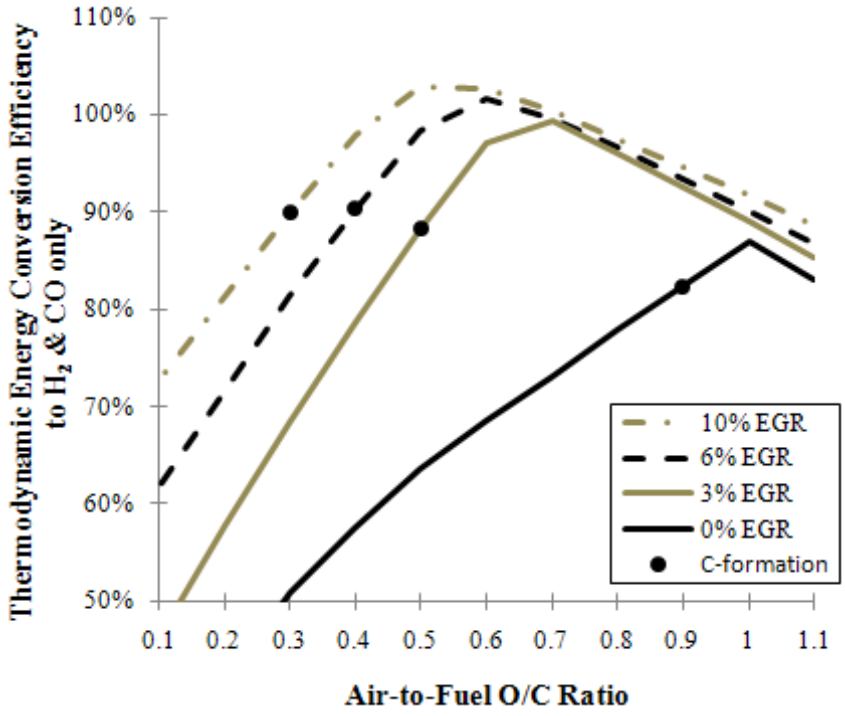

Figure 42. Thermodynamic equilibrium energy conversion efficiency versus the air-to-fuel O/C ratio for production of H2, CO, and light hydrocarbons (LHCs). Also included are several cases of increasing exhaust gas recycle (EGR) from a solid oxide fuel cell with zero EGR being analogous to partial oxidation. The black dots represent the onset of the pyrolysis and carbon formation region.

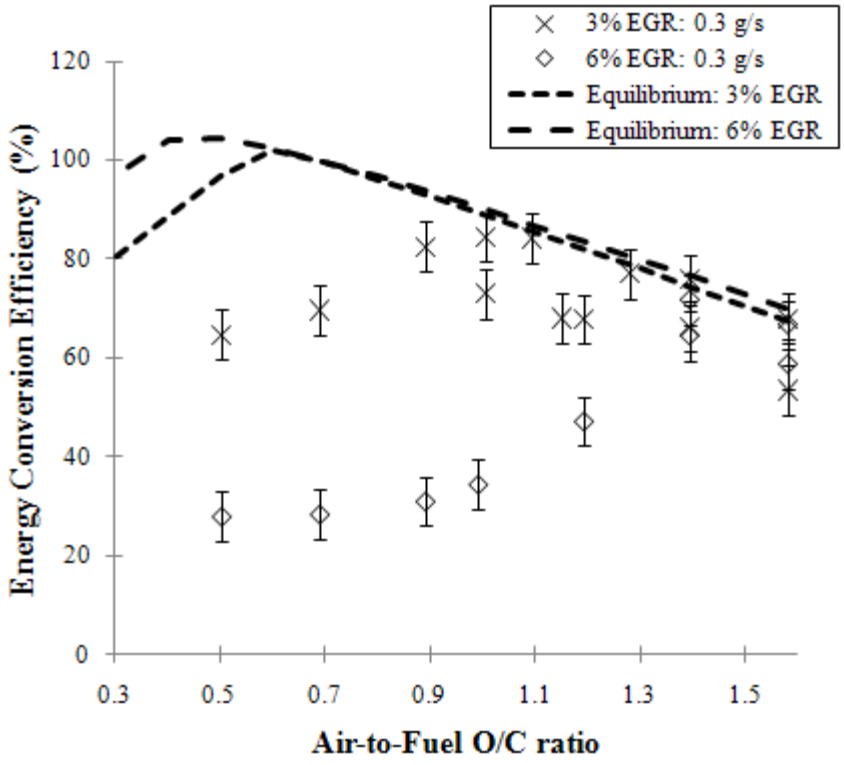

Figure 43. Energy conversion efficiency versus the air-to-fuel O/C ratio for production of H2, CO, and light hydrocarbons (LHCs). The points show experimental data from gliding arc assisted reforming of Diesel fuel at a fuel flow rate of 0.3 g/s. The solid and dashed lines depict the predicted thermodynamic energy efficiencies. Also included are several cases of increasing exhaust gas recycle (EGR) from a solid oxide fuel cell.

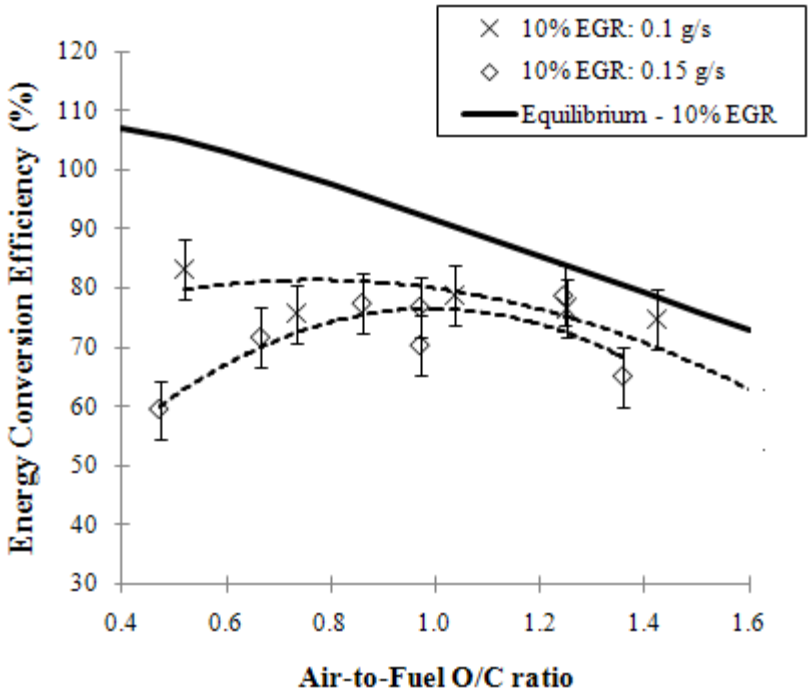

Figure 44. Energy conversion efficiency versus the air-to-fuel O/C ratio for production of H2, CO, and light hydrocarbons (LHCs). The points show experimental data from gliding arc assisted reforming of Diesel fuel at fuel flow rates of 0.15 g/s and 0.1 g/s, where all reactant flow were reduced by 50% and 70%, respectively. Higher conversion efficiency is achieved at lower flow rates, which indicates that longer residence time is beneficial. The solid line depicts the predicted thermodynamic energy efficiency under the experimental conditions (10% EGR).

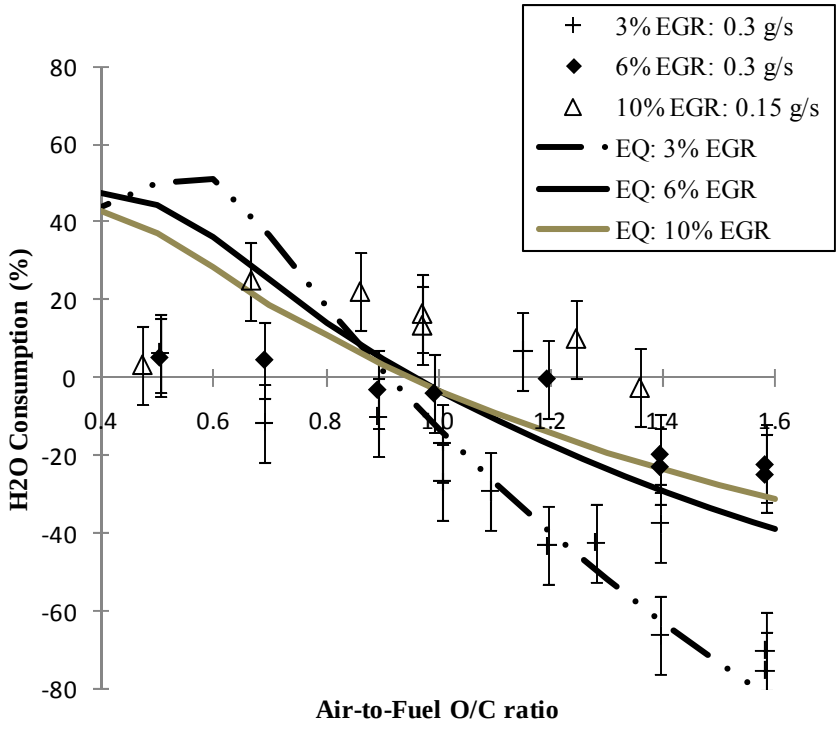

Figure 45. H_2O Consumption versus the air-to-fuel O/C ratio for the plasma-assisted steam-oxidative reformer. Several cases of variable SOFC exhaust gas recycle (EGR) were investigated using Diesel fuel. For the case of 10% EGR shown here, the flow rates of all reactants were reduced by 50% thereby increasing the residence time of treatment. The solid and dashed lines represent expected H_2O consumption at thermodynamic equilibrium (EQ). Negative H_2O consumption is analogous to H_2O production.

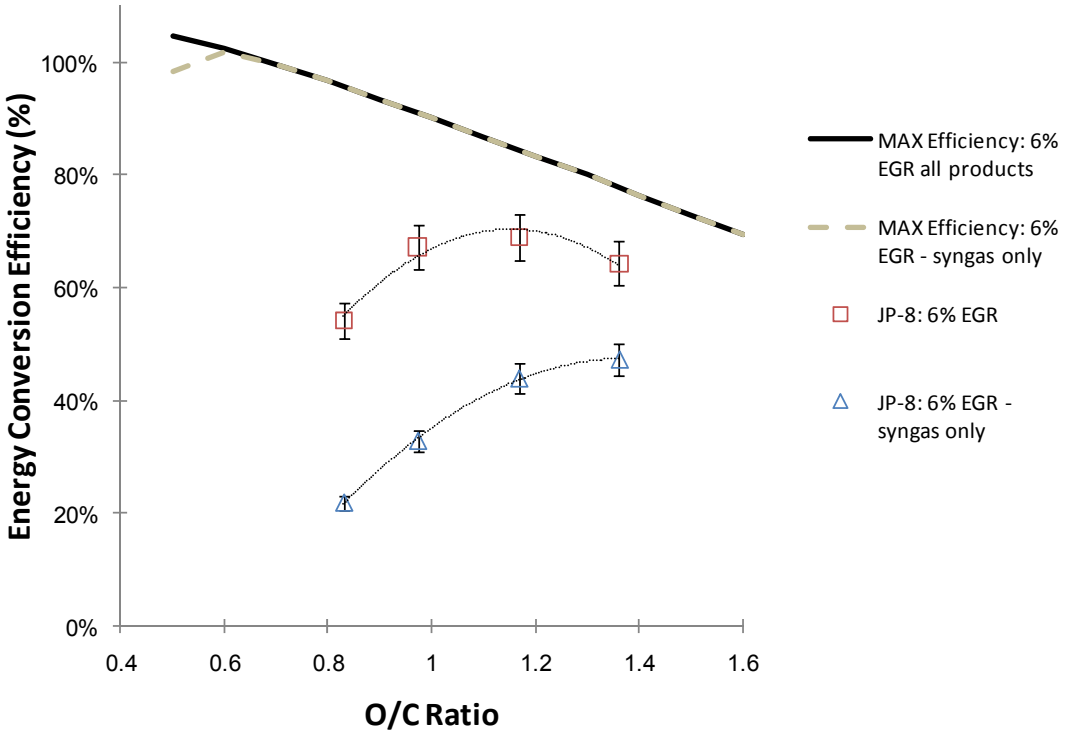

Figure 46. Energy conversion efficiency versus O/C ratio for the autothermal reforming of JP-8.

4. Characterization of Gliding Arc Plasmas

4.1 Introduction

Plasmas are often characterized into one of two major regimes: thermal (quasi-equilibrium) and non-thermal (non-equilibrium). Thermal plasmas usually have a very high translational gas temperature, which is created by providing large amount of current (high number density of electrons), or operating the plasma at high pressure to allow for energy dissipation as translational heating through a high degree of electron-neutral collisions. The mechanism of ionization in thermal plasmas is called stepwise ionization and this occurs when a large number of electrons are able to electronically excite the background gas molecules (though multiple steps if necessary), which ultimately leads to ionization. A competing process, known as direct electron impact ionization, can also occur but it requires electrons with sufficiently high energy to cause ionization in one impact. An example of the reversible process of direct impact ionization and recombination is as follows:

$$A + e \leftrightarrow A^+ + e + e \tag{4-1}$$

However, when the number density of electrons in the plasma is high (due to high current or pressure), ionization occurs through a series of steps involving electronically excited states of neutral gas molecules (A) and low energy electrons:

$$A + e \leftrightarrow A^* + e \leftrightarrow A^+ + e + e \tag{4-2}$$

The rate of stepwise ionization is 10^3-10^4 times faster than direct impact ionization due to the large statistical weight of the excited species and electrons involved in the process.

Thermal plasmas are sometimes referred to as quasi-equilibrium and this refers to kinetic and chemical equilibrium and other plasma properties as being a function of the same temperature. In a perfect system, the thermal plasma would be homogeneous and the

temperatures of its species would be the same for all degrees of freedom (translation, rotational, vibrational, electronic). This is not always the case as energy losses occur near the boundaries of the discharge due to convection, conduction, or diffusion. An assumption called local thermodynamic equilibrium (LTE) is usually invoked to provide a means to ignore boundary effects and assume equilibrium in a smaller localized region. The temperature equilibrium that is achieved in thermal plasmas is not always desirable for chemical processes because energy is spent heating all components of the system, even those which may not participate in the process (translational heating of N_2 in combustion systems, for example). Furthermore, if the gas temperatures in the reaction zone are too high and the products are allowed to cool slowly, reverse reactions can proceed lowering the efficiency of the process.

Non-thermal plasmas are often referred to as non-equilibrium plasmas because energy is distributed un-equally to a smaller number of free electrons, which absorb energy from the electric field and primarily store it in vibrational excitation of diatomic neutral gas molecules. Since vibrational excitation of these molecules can be much faster than the vibrational-translational relaxation rate (also responsible for causing gas heating), the vibrational temperature of molecules in a non-thermal plasma can be much higher than the translational temperature [15]. The translation temperatures of the gas molecules of typical non-thermal plasmas are often near room temperature (T~300K) while the vibrational temperatures can exceed 3000K. The vibrationally excited species generated by non-thermal plasmas are said to be very effective at stimulating endothermic reactions [15], which is one of the main features of the plasma catalysis effect.

Gliding arc plasmas are a unique type of plasma because they span both the thermal and non-thermal plasma regimes. Gliding arc is sometimes referred to as a transitional discharge, that is, it begins as a thermal arc discharge and through the force of convective flow (or an externally

applied magnetic field) the arc elongates, cools, and transitions into a plasma with moderate gas temperatures (1000-4000K) and non-equilibrium properties (T_e = 1eV > T_{vib} = 0.5eV > T_{trans} = 0.3 eV). A plasma discharge with these properties are said to have the best of both worlds: moderate gas temperatures that are beneficial for certain chemical processes and high productivity systems; and non-equilibrium properties that allow for chemically selective processes to occur using non-thermal pathways where plasma active species act to reduce energy barriers of chemical processes. Table 5 shows some examples of typical electron and gas temperatures and other plasma parameters for thermal, non-thermal, and gliding arc (transitional plasma).

Table 5. Typical plasma parameters for thermal, non-thermal, and transitional plasmas.

Plasma Parameter	**Quasi-equilibrium Thermal Plasma**	**Transitional "Warm" Plasma**	**Non-equilibrium Non-thermal plasma**
Current	10^1-10^3 A	10^{-1}-10^0A	10^{-2}-10^0A
Voltage	10^1-10^2 V	10^2-10^3 V	10^2-10^3 V
Electron Density	10^{15}-10^{19} cm^{-3}	10^{11}-10^{12} cm^{-3}	10^9-10^{11} cm^{-3}
Gas Temperature	1-10 eV (10,000-100,000K)	0.1-0.4eV (1000-4000K)	300-600 K
Electron Temperature	1-10 eV	1-3 eV	1-10 eV
Cathode Current Density	10^4-10^7 A/cm^2	10^1-10^3 A/cm^2	10^1-10^2 A/cm^2

In this chapter, several plasma diagnostic techniques that were used to evaluate the gliding arc plasma contained in both the RVF-GA and GA-Plasmatron reactors will be introduced. The point of this diagnostic analysis is to demonstrate that the gliding arc plasma used in the experimental fuel conversion systems presented in this thesis were behaving as a transitional plasma with some degree of non-equilibrium plasma-catalytic properties. An additional complication of the diagnostic analysis is that the properties of the plasma may change when reactants are present and the system is operating at elevated temperatures. Certain techniques such as optical emission spectroscopy cannot be used to evaluate the plasma discharge

during reforming experiments because the plasma/flame interaction produces strong atomic emissions that drown out regions of the spectrum that are necessary for discharge characterization. Despite this fact, basic evidence will be presented that our gliding arc plasma has rotational gas temperatures and voltage-current (V-I) characteristics that are similar to those found in the non-equilibrium gliding arc plasmas previously studied [18, 81, 122].

4.2 Visualization of the Gliding Arc Plasma

Gliding arc plasmas have similar structural features to both thermal arc plasmas and non-thermal glow discharge plasmas. Figure 47a shows the structure of a typical glow discharge which includes cathode and anode spots, the positive column, and faraday dark space. Figure 47b and 46c show high speed images of the gliding arc plasmas for the GA-Plasmatron and RVF-GA reactors, respectively. From the high speed images, it is possible to see some similarities to the glow discharge, including the relative small size of the cathode spot and weakly luminous glow of the positive column.

4.3 Power measurement and V-I Characteristics of Gliding Arc Plasmas

The voltage and current profiles of gliding arc plasmas, as measured by oscillograms, have a characteristic "sawtooth" profile as shown in Figures 48 and 49. This occurs because as the plasma length grows due the force from the convective flow, the current decreases due to increasing resistance and voltage increases because specific power (w) per length is assumed to be constant. The relation between these parameters can be explained by Ohm's law for the initial quasi-equilibrium phase of the arc through the following relation [15]:

$$V_o = RI + \frac{wl}{I} \tag{4-3}$$

Where V_o, R, and I are the open circuit voltage, external resistance of the circuit, and the

current, respectively. The quasi-equilibrium phase of the arc evolution ends when the arc reaches a certain critical length which is defined by [81]:

$$l_{cr} = \frac{V_o^2}{4wR} \tag{4-4}$$

When the critical length is achieved, the current falls to its minimum value and voltage, electric field, and power reach their maximum values:

$$I_{crit} = \frac{V}{2R} \tag{4-5}$$

$$V_{crit} = \frac{V_o}{2} \tag{4-6}$$

$$E_{crit} = \frac{w}{I_{crit}} \tag{4-7}$$

$$W_{crit} = \frac{V_o^2}{4R} \tag{4-8}$$

Figure 50 shows the evolution of these parameters versus the column length of the plasma discharge. Beyond the critical length, heat losses from convective cooling exceed the energy supplied by the power supply and it is not possible to sustain the arc in a state of thermodynamic equilibrium [15]. However, as the discharge rapidly cools, the plasma conductivity is maintained by a high value of electron temperature ($T_e \sim 1eV$). The gliding arc discharge now enters the non-equilibrium (non-thermal) phase if the electric field is sufficiently high (current also must be below threshold value $I < 0.5A$). Because of the shift to lower gas temperatures while still maintaining a reasonably high electric field strength, the ionization mechanism changes from the thermal stepwise mechanism to the direct electron impact mechanism. The non-equilibrium phase of gliding arc is unstable, however; and the discharge will eventually extinguish, re-ignite, and the process will be repeated. Further studies on the stability of gliding arc discharges showed that it is possible to maintain the plasma discharge long after maximum power was attained, an effect previously thought impossible [17]. This effect is known as “overshooting” and the

concept was used as a basis to develop a magnetically-stabilized gliding arc plasma [18]. The magnetically stabilized gliding arc plasma has the advantage of trapping the plasma at a fixed length (in the non-equilibrium regime) and its rotation frequency was a function only of the magnetic field strength. Such systems were employed for investigating plasma-related combustion phenomena [37]; however, they are not practical for transportation systems mainly because of the issue and expense of incorporating strong magnets into the design of a compact vehicular system.

The voltage-current (V-I) characteristics of DC plasmas have been long studied and the shape of the experimental plasma V-I curves can provide basic information in order to classify the plasma regime of operation. Figure 51 shows the classic V-I curve for self-sustaining DC plasma discharges and includes the major discharge regimes [18]. There are several plasma regimes indicated on Figure 51 that include the non-thermal plasma regimes of the dark and glow discharge, the abnormal glow and the glow-to-arc regime which is where warm (transitional) plasmas exist, and the arc regime. Warm plasmas typically have a descending V-I curve, which corresponds to the transition from a non-thermal glow discharge to a thermal arc plasma. Figure 52 shows the experimentally measured V-I curves for both the GA-Plasmatron and RVF-GA reactors during partial oxidation of n-Tetradecane. Both reactors have nearly identical V-I characteristics therefore the points on Figure 52 do not distinguish between reactors. The V-I measurements were made at the various O/C ratios (0.8-1.0) and power was kept constant at 200W. Figure 53 shows additional V-I curves for the RVF-GA reformer again during POX reforming but at a constant O/C ratio of 1 and variable power from 100-400W. It is interesting that at the low power level (100W) the peak of the V-I curve falls well into the abnormal glow regime.

4.4 Spectral Diagnostics of Gliding Arc Plasmas in Air

There are several spectral diagnostic methods that are commonly employed to probe the temperatures (average energies) of the active species that are produced by plasmas. The level of these temperatures can provide a means to classify the discharge as thermal, non-thermal, or transitional. One popular method is to compare the measured and theoretical spectrums of the second positive system of N_2 ($C^3\prod_u$- $B^3\prod_g$) when operating plasma in air. The comparison of these spectra is accomplished using the SPECAIR code [123] which can provide an estimate of the rotational temperatures of the N_2 (C-B) band. For gas temperatures above 1000K, the translational and rotational energy levels are assumed to be fully excited and in temperature equilibrium [123]. Figure 54 shows an example of the curve fit used to compare the theoretical and experimentally measured spectra for the N_2 (C-B) system (at 337nm).

In order to experimentally measure the optical emission spectra (OES) for the gliding arc plasma of the GA-Plasmatron reformer, an optical focusing system was developed to block out the bright emission spots from the cathode and anode spots of the discharge. The bright light emitted from the cathode and anode spots is very intense and can drown out light emission from N_2 (C-B) bands. Figure 55 shows the experimental system developed for the OES studies. Light from the positive column was collected using a lens and transmitted back to an optical probe connected to a spectrometer. A barrier was used to block the light emitted from the cathode and anode spots. This focusing system worked relatively well, although the location of the positive column moved slightly off-center depending on the volumetric swirl flow rates. The rotational temperatures of N_2 in the gliding arc discharge was measured at several swirl flow rates (30, 50, 70, 90 SLPM) and several current levels (50, 70, 90, 110, 130 mA). Figure 56 shows a surface plot of the rotational gas temperatures for the GA-Plasmatron. The gas temperature significantly increased with decreasing swirl flow rates and this was a result of decreased convective cooling

of the discharge, thus preventing it from transitioning into the non-equilibrium state. Gas temperatures at low currents (<70mA) varied between 2000-3000K for nearly all swirl flows and increased to 3000-4000K at currents between 70-90mA. These results are consistent with the previous spectral analyses of the magnetically-stabilized gliding arc discharge [18] where a much more detailed investigation of plasma parameters revealed the existence of the warm (transitional) plasma regime.

An additional measurement was made to compare the ratio of intensities of the 2nd positive system of N_2 (λ = 337nm) with the 1st negative system of N_2^+ (λ = 391nm). The method can provide an estimation of the reduced electric field (E/n) which is the electric field strength divided by the neutral gas concentration [122]. The strength of the reduced electric field can then be correlated to the electron energy and provides an estimation of the temperature non-equilibrium of the discharge. The ratio of intensities method requires a similar measurement to the spectra obtained in Figure 54, along with integration of the intensity (area under the curve). The ratio of these areas (337/391) was entered as a parameter into a computational computer program developed by [124] to generate the values of E/n (in units of Townsend (Td)). The results from the analysis are shown in Figure 57, which shows very high values of the reduced electric field (400-600 Td) for several current values (mA) and several cases of swirl flow. These E/n values are several times greater than the typical breakdown threshold (100 Td) for DC discharges and are many times larger than the observed values of the magnetically-rotated gliding arc plasma [18]. These values of E/n were compared to Figure 58, which describes the relation of the reduced electric field to the average electron energy (eV). The average electron energies are on the level of 8-10 eV, which is near the energies typically observed during streamer initiation phenomena [125]. There are two logical explanations of these results: the high electron energy is a result of capturing emission from the streamer-head initiation phase of gliding arc breakdown; or errors in measurement of the emission spectra were propagated leading to inaccurate

integration and ratio of intensity values. It is unclear at this time whether it is possible to have captured breakdown phenomena using the current focusing method with such a rapidly oscillating gliding arc discharge. The results are interesting however, and further investigation of this phenomenon is needed.

4.5 Conclusions

The gliding arc discharge used in the RVF-GA and GA-Plasmatron reactors was driven by vortex flow, and as a result of the cylindrical geometry of each vessel, the discharge rapidly oscillated on the metal reactor walls causing a state of constant transition between the thermal and non-thermal plasma regimes. Such oscillations made optical diagnostic measurements quite challenging; however a scheme was devised to measure the average emissions from the center portion of the discharge by means of an optical focusing system. The spectral measurements showed that the rotational temperatures of N_2 were within the warm (transitional) plasma regime (1000-3000K) under certain conditions (current <70mA with vortex flow >50 SLPM). Such regimes were used during reforming of hydrocarbon fuels as previously described. Furthermore, the V-I characteristics for the gliding arc discharge used in this investigation matched very closely to those that were reported in the literature. The combination of the similarity of the V-I curves and the rotational gas temperatures is the basis on which the final conclusion that the gliding arc discharges used in this investigation was in fact non-thermal.

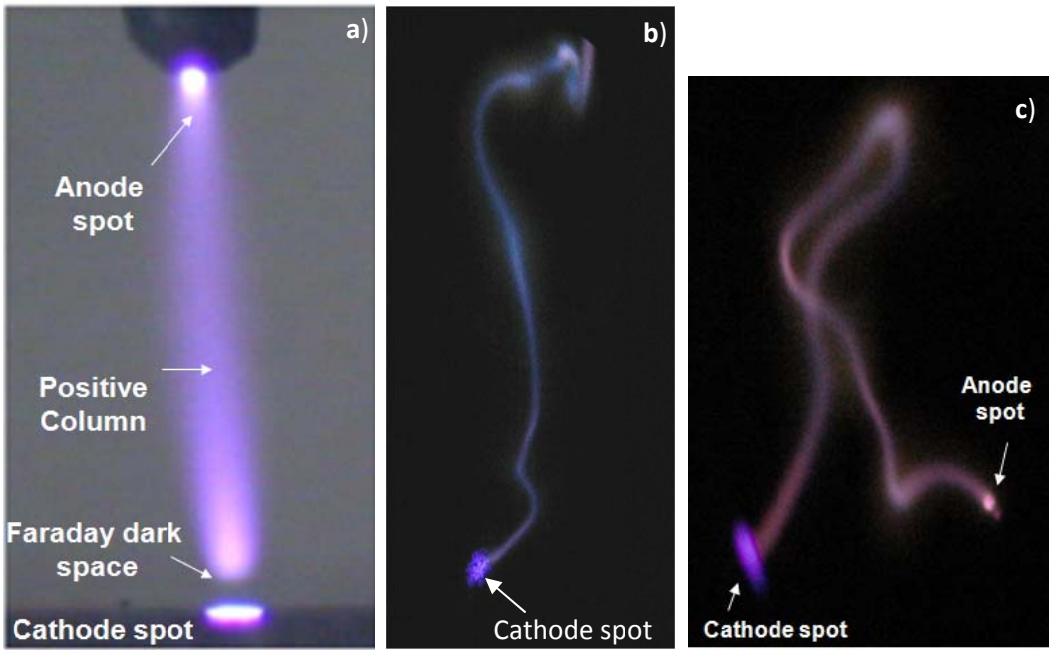

Figure 47. Structure of a typical micro glow discharge (a). High speed images of the gliding arc discharge from both the GA-Plasmatron (b) and RVF-GA reactor (c).

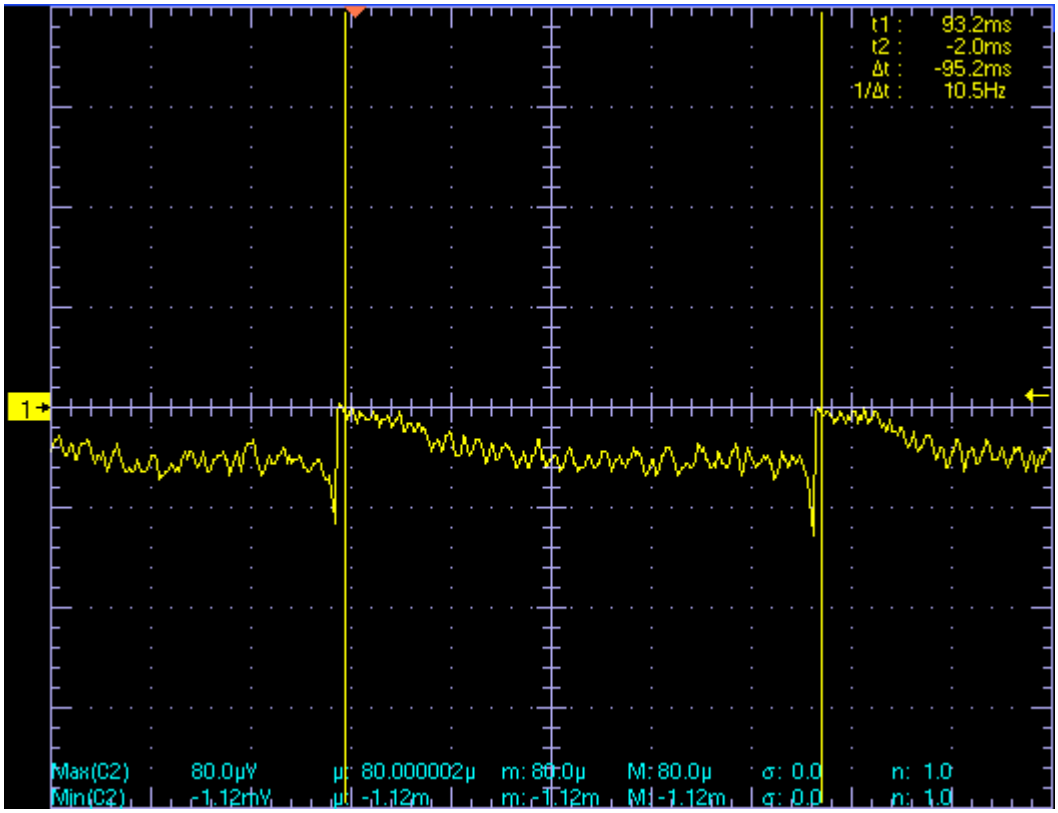

Figure 48. Typical sawtooth oscillogram profile for a gliding arc plasma discharge in room temperature air. The signal marker "1" denotes the zero voltage point.

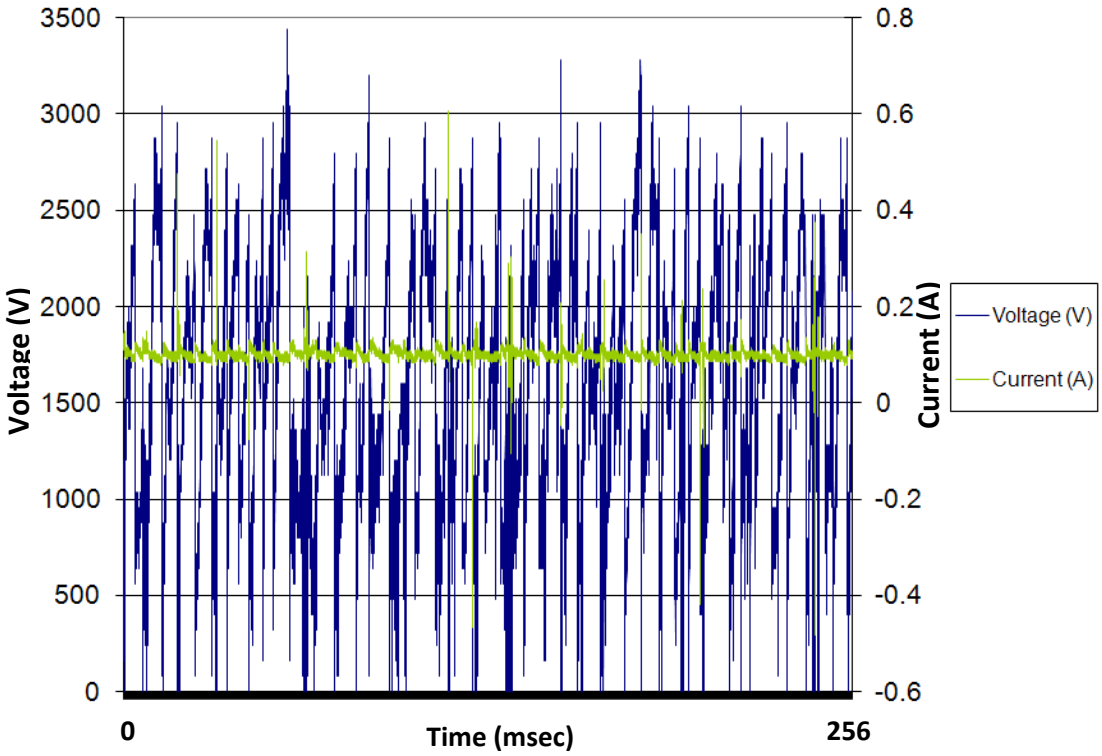

Figure 49. Oscillogram showing voltage and current profiles of the gliding arc discharge during reforming of n-Tetradecane (O/C ratio: 1). The arc breaking frequency here is enhanced during reforming to approximately 166 kHz.

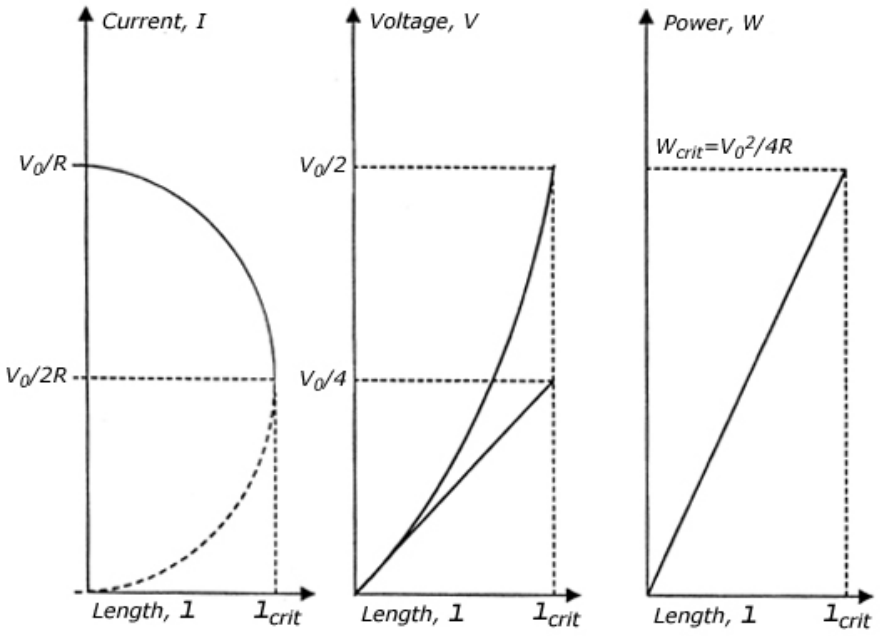

Figure 50. Dependence of arc length on current, voltage, and power for gliding arc discharges.

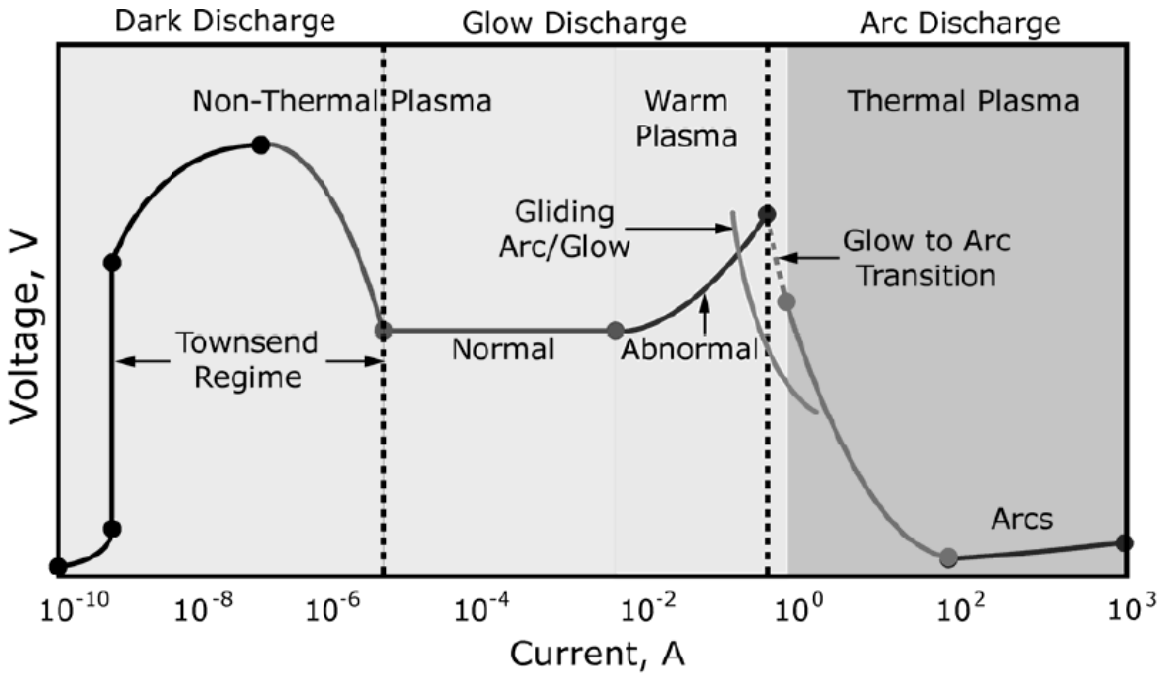

Figure 51. Voltage-current (V-I) characteristics for direct current plasmas. [18]

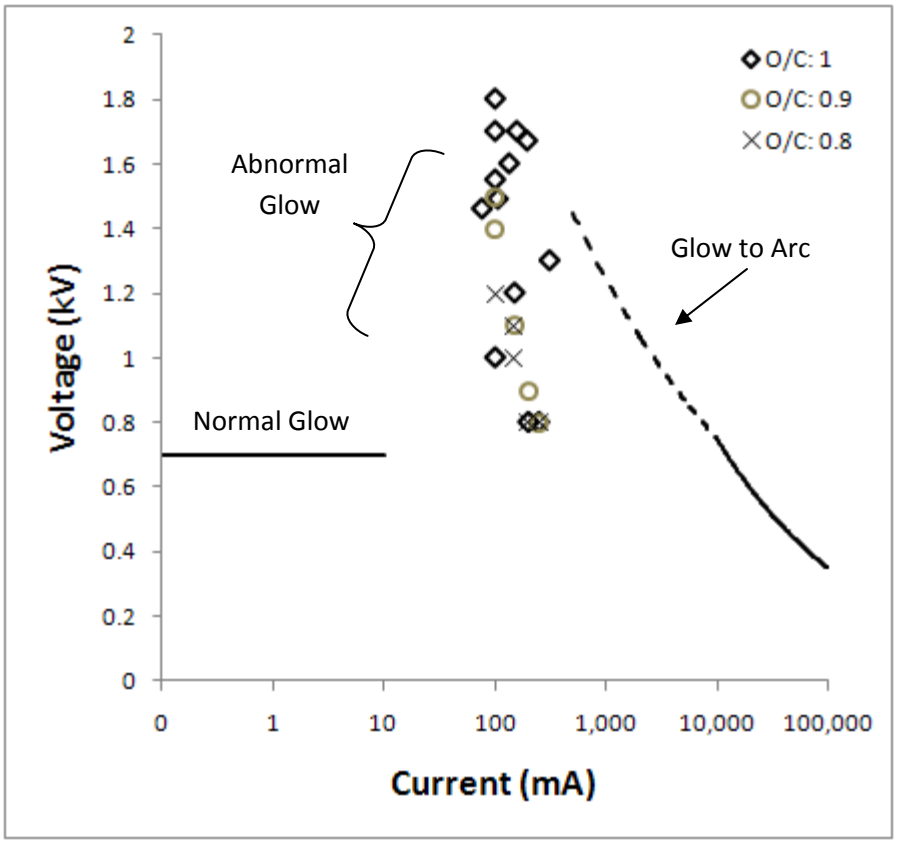

Figure 52. V-I Characteristics for the RVF-GA and GA-Plasmatron devices.

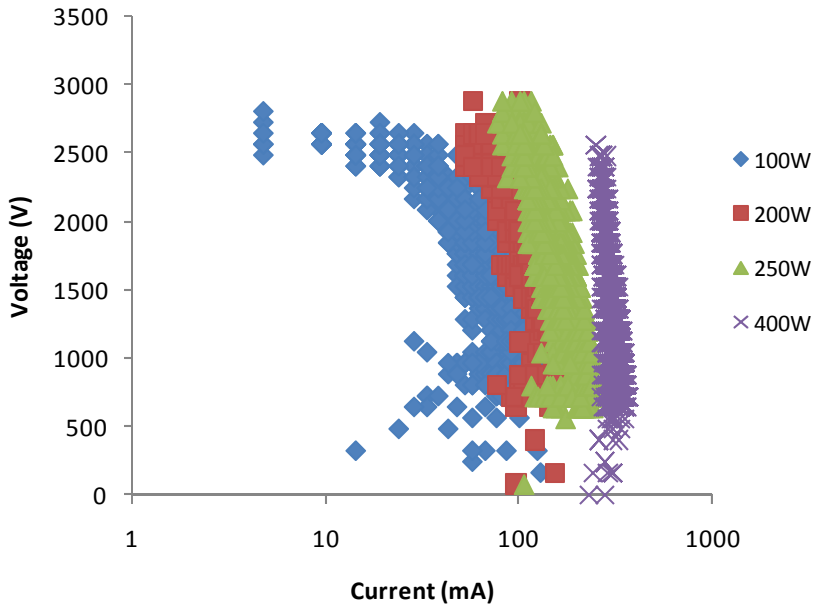

Figure 53. V-I characteristics of the RVF-GA reactor during partial oxidation of n-Tetradecane fuel at various average power levels.

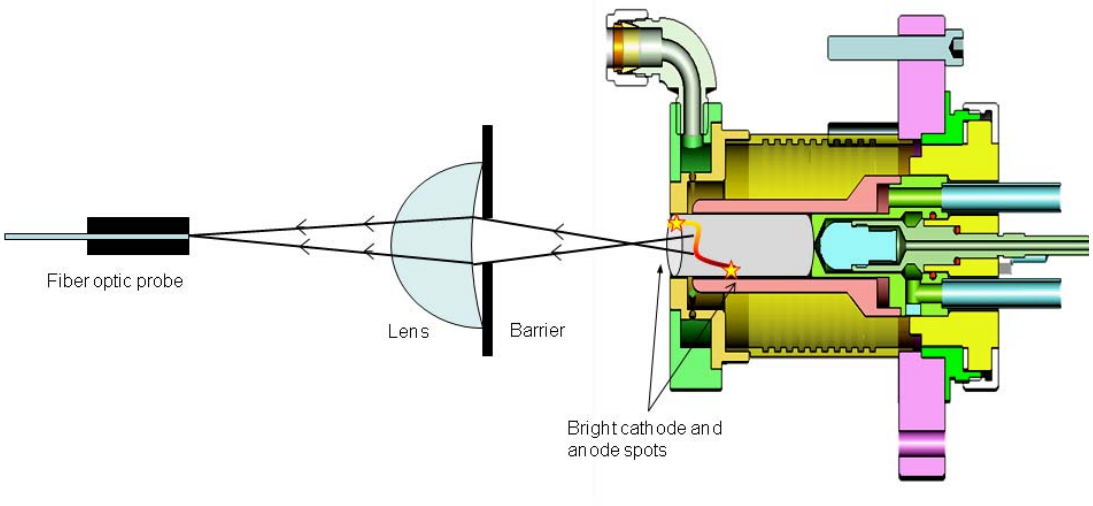

Figure 54. Comparison of the rotational energy spectral emission lines from theoretical and experimental spectrum for the 2nd positive system of N2.

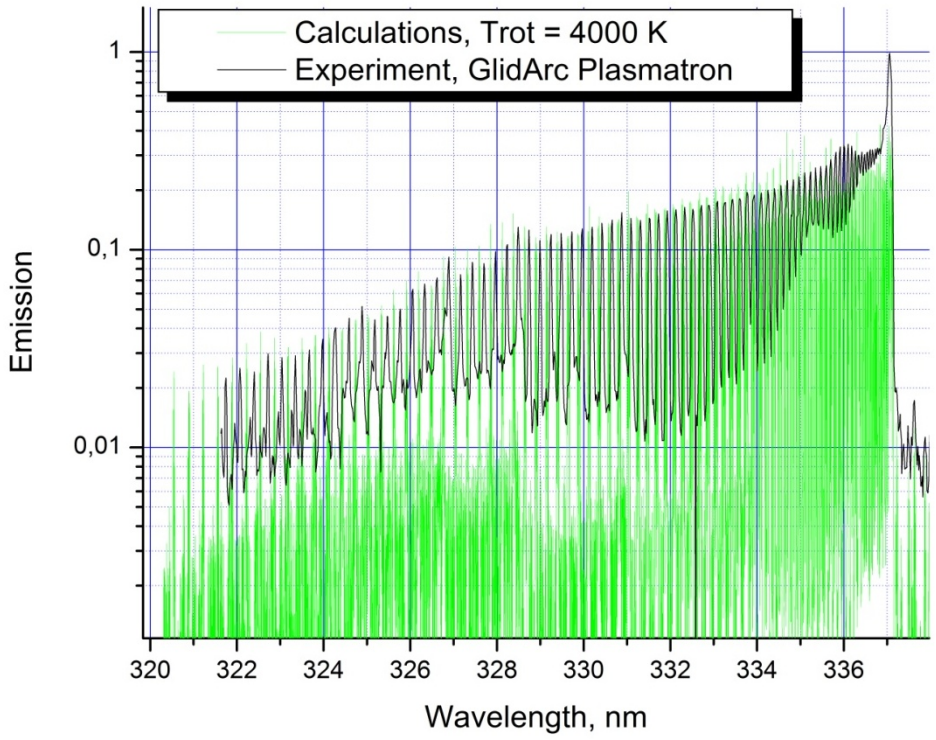

Figure 55. Optical focusing system designed to capture spectral emission from the positive column of the gliding arc discharge stabilized in vortex flow.

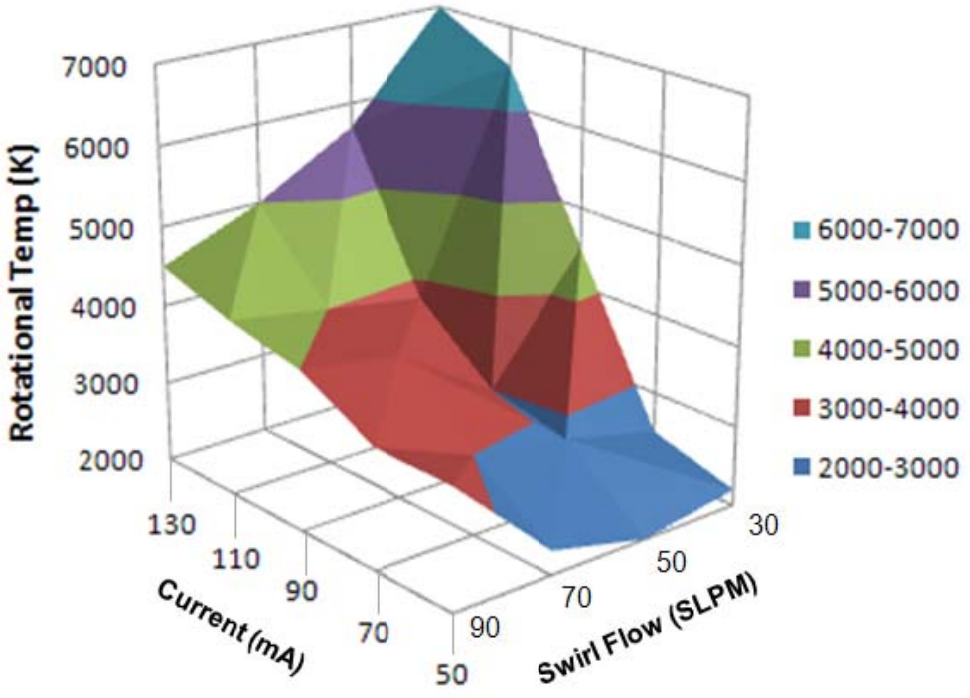

Figure 56. Surface plot showing the dependence of rotational gas temperatures of 2nd positive N2 on current and swirl flow for the GA-Plasmatron device.

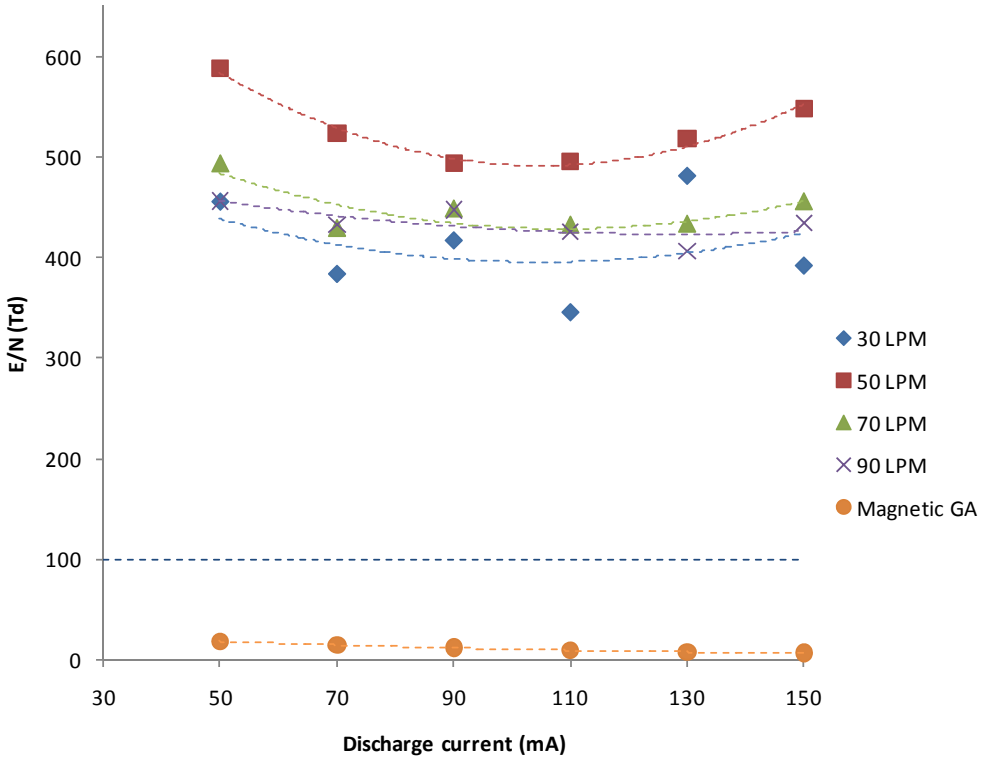

Figure 57. Estimations of the reduced electric field as a function of the discharge current for various cases of swirl flow for the GA-Plasmatron device.

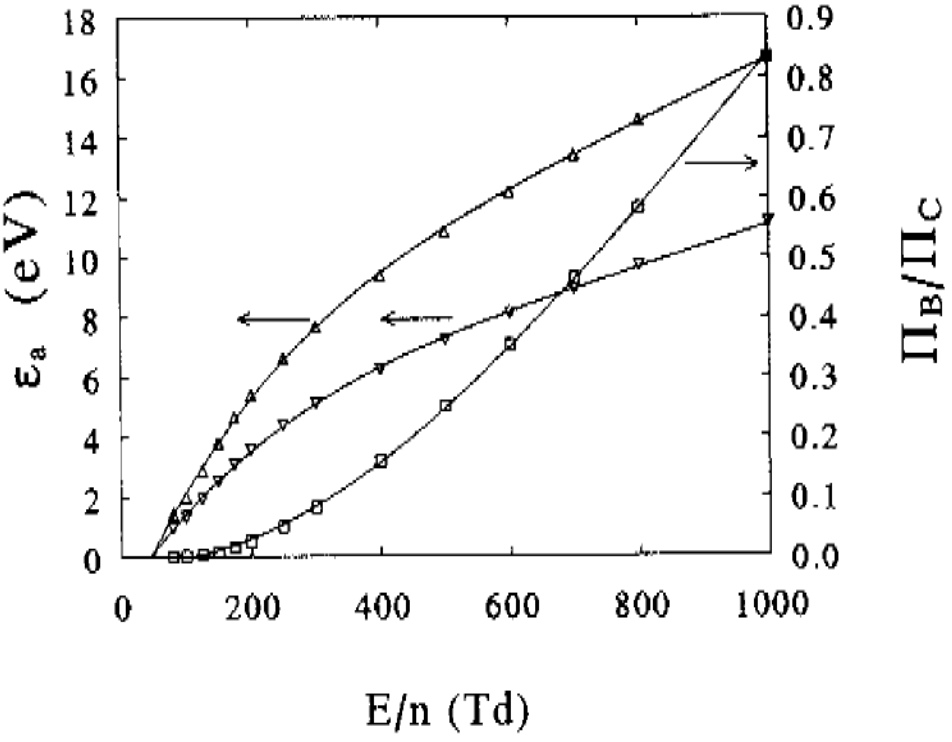

Figure 58. Correlation of the ratio of intensities (391/337) for nitrogen plasma (□) to the reduced electric field strength (E/n) and average electron energy (Δ).

5. Summary and Conclusions

In this thesis, the development and testing three vortex-based gliding arc plasma reformers was described in the framework of converting heavy hydrocarbon fuels into synthesis gas through partial oxidation and autothermal reforming. The ultimate goal of this research was to develop an advanced non-thermal plasma fuel reforming technology that could be combined with solid oxide fuel cells to create novel auxiliary power units for civilian and military transportation applications. Gliding arc plasma-assisted reformers have several advantages that are well suited for these goals, which include fast start time, stable operation with a wide variety of heavy hydrocarbons fuels, and low electrical energy consumption (2–5% of total chemical energy of the system). This is especially important when considering transportation-related applications where syngas is required to be generated on-board vehicles.

In chapter 2, an investigation of the plasma-assisted partial oxidation reforming of n-Tetradecane (a common surrogate for diesel fuel) included the effects of several parameters: the effect of increasing O/C ratio and plasma power, and adding polyaromatic compound additives to fuels. The results of the investigation were evaluated against the hydrogen and carbon monoxide yields, the energy conversion efficiency, and the specific energy requirement to generate syngas. The experimental results were also compared against the predicted yields and efficiencies expected if the system were to reach thermodynamic equilibrium conditions. The performance of these plasma fuel conversion systems has showed great promise in terms of efficient conversion of heavy hydrocarbons fuels to syngas products, even though there was a significant fraction light hydrocarbons that were preserved in the syngas product stream. These residual light hydrocarbons should not hinder the performance of a SOFC, since the majority of the hydrocarbons were comprised of methane. Researchers have shown that residual methane in the syngas product stream (up to 25% molar concentration) is beneficial to the thermal management

characteristics of a solid oxide fuel cell. This is because methane can be reformed in the high temperatures of the anode side of the fuel cell, where abundant H_2O is present. Overall, both the RVF-GA and GA-Plasmatron reformers (which were found to perform similarly) achieved approximately 50% efficiency with the formation of an additional fraction of light hydrocarbons that account for an additional 40% of the energy of the product stream. When the light hydrocarbons are included in the energy-mass balance with syngas, the energy conversion efficiency of both systems can be as high as 80–90%, which is very close to the thermodynamic equilibrium energy efficiency for conversion. Further work is needed to optimize these systems to minimize heat losses in the post-plasma treatment zone and increase residence time in the vicinity of the plasma discharge itself. Such modifications should improve syn-gas selectivity and yields. Furthermore, when considering that the residual light hydrocarbons may be fully converted within a SOFC, the energy conversion efficiency can then be increased from 50% to approximately 83%. Complete conversion (tetradecane-to-electricity) using the plasma reformers combined with a solid oxide fuel cell (with 50% maximum efficiency) would be then as high as 42%.

The results presented in chapter 3 describe the development and testing of a portable advanced auxiliary power unit (size: 150L) for military applications which included a gliding arc plasma reformer integrated with a solid oxide fuel cell. The system was operated near the autothermal regime by recirculating high temperature exhaust gases from the SOFC, thus providing conditions for improved energy conversion efficiency (as high as 105%) and energy costs (net enthalpy change of the process is zero). The experimental results show that the presence of SOFC exhaust gases improved energy conversion efficiency; however, increasingly higher amounts of SOFC exhaust gas recirculation caused a reduction in conversion. This result was attributed to a kinetic limitation in the system in which the higher recycle gas flow rates reduced the residence time required for reaction completion. Upon scaling back flow rates of all

reactants, thus increasing residence time, the energy conversion efficiency improved further, reaching as high as 80%. The integration of plasma fuel reformers within auxiliary power units for vehicles is in the early stage of development and the results look promising. Some improvement is needed to reduce low levels of C_2 hydrocarbons (C_2H_2, C_2H_4) that were detected in the product streams. The concentrations of these light hydrocarbons is low (1-2% in absolute concentration), but even small amounts of these compounds are known to cause degradation in the performance of the SOFC. Future efforts to optimize plasma fuel conversion systems may reduce these unconverted hydrocarbons and improve syngas yields, thereby eliminating this problem.

In the near future, some promising areas of study include investigating the fundamental mechanisms of plasma-assisted fuel conversion. Combustion researchers have identified several important plasma induced effects that can lower the required ignition temperature or extend the flammability limits of combustion processes. This research took a fundamental approach where advanced diagnostic systems provided a means to probe the types and concentrations of plasma active species produced and their effects on combustion reactions. Such an approach may help to shed light on the important species responsible for fuel-rich syngas production processes. This will ultimately help engineers to design more efficient systems in the future.

In addition, researchers have begun combining plasma technology with traditional catalysis and have identified synergistic effects that have the potential to reform fuels into syngas with greater efficiency than either technology alone. In general, the consensus among researchers seems to be that plasma is effective at increasing the internal energy of reactants and specifically stimulating vibrational excitation which can be effectively utilized in thermal catalysis reactions. Further research in this area may lead to newer reforming technologies that combine plasma with cheaper catalysts that have greatly extended lifetimes.

Bibliography

1. Haynes, D.J., Berry, D.A., Shekhawat D., Spivey J.J., Catalytic partial oxidation of n-tetradecane using pyrochlores: Effect of Rh and Sr substitution. Catalysis Today 2008. 136: p. 206-213.

2. Pena, M.A., Gomez, J.P., Fierro J.L.G., New catalytic routes for syn-gas and hydrogen production. Applied Catalysis A: General 1996. 144: p. 7-57.

3. Vernon, D.F., Green, M.L.H., Cheetham, A.K., Ashcroft A.T., Partial oxidation of methane to synthesis gas. Catalysis Letters 1990. 6: p. 181-186.

4. Dhamrat, R.S., Ellzey, J.L., Numerical and experimental study of the conversion of methane to hydrogen in a porous media reactor. Combustion and flame, 2006. 144: p. 698–709.

5. Al-Hamamre, Z., Vob, S., Trimis, D. , Hydrogen production by thermal partial oxidation of hydrocarbon fuels in porous media based reformer. International Journal of Hydrogen Energy, 2009. 34: p. 827-832.

6. Toledo, M., Bubnovich, V., Saveliev, A., Kennedy L. , Hydrogen production in ultra-rich combustion of hydrocarbon fuels in porous media. International Journal of Hydrogen Energy, 2009. 34: p. 1818–1827.

7. Rollier, J.D., Gonzalez-Aguilar, J., Petitpas, G., Darmon, A., Fulcheri, L., Metkemeijer, R., Experimental study on gasoline reforming assisted by nonthermal arc discharge. Energy and Fuels, 2008. 22: p. 556-560.

8. Czernichowski, A., GlidArc assisted production of the synthesis gas from natural and waste hydrocarbons gases. Oil and Science Technology, 2001. 56(2): p. 181-198.

9. Petitpas, G., Rollier, J.D., Darmon, A., Gonzalez-Aguilar, J., Metkemeijer, R., Fulcheri, L., A comparative study of non-thermal plasma assisted reforming technologies. International Journal of Hydrogen Energy, 2007. 32(14): p. 2848-2867.

10. Czernichowski, A., Gliding arc: Applications to engineering and environmental control. Pure and Applied Chemistry, 1994. 66(6): p. 1301.

11. Kalra, C.S., Gutsol, A.F., Fridman, A., Gliding arc discharges as a source of intermediate plasma for methane partial oxidation. IEEE Transactions on Plasma Science, 2005. 33(1): p. 32.

12. Kalra, C.S., Gliding Arc in Tornado (GAT) and its Application for Plasma Catalytic Partial Oxidation of Methane in Mechanical Engineering and Mechanics. 2004, Drexel University: Philadelphia.

13. Raizer, Y.P., Gas Discharge Physics, ed. J.E. Allen. 1991, Berlin: Springer-Verlag.

14. Starikovskii, A.Y., Plasma supported combustion. Proceedings of the Combustion Institute, 2005. 30(2): p. 2405-2417.

15. Fridman, A. and L.A. Kennedy, Plasma Physics and Engineering. 2004, New York: Taylor and Francis.

16. Fridman, A., Plasma Chemistry. 2008, New York: Cambridge University Press. 978.

17. Kuznetsova, I.V., Kalashnikov, N.Y., Gutsol, A.F., Fridman, A.A., Kennedy, L.A. , Effect of "overshooting" in the transitional regimes of the low-current gliding arc discharge. Journal of Applied Physics, 2002. 92(8): p. 4231-4237.

18. Gangoli, S., Experimental and Modeling Study of Warm Plasmas and their Applications, in Mechanical Engineering. 2007, Drexel University: Philadelphia.

19. Gallagher, J., Michael J., Geiger, R., Polevich, A., Rabinovich, A., Gutsol, A., Fridman, A., On-board plasma-assisted conversion of heavy hydrocarbons into synthesis gas. Fuel, 2010. in Press.

20. Givotov, V.K., Rusanov, V.D., Fridman, A., Diagnostics of non-equilibrium chemically active plasma, in Energoatomizdat. 1985b: Moscow.

21. Hocker, H., Plasma treatment of textile polymers. Pure and Applied Chemistry, 2002. 74(3): p. 423-427.

22. Gilman, A.B., Interaction of chemically active plasma with surfaces of synthetic materials, in Encyclopedia of low-temperature plasma, V.E. Fortov, Editor. 2000: Moscow.

23. Kogelschatz, U., Dielectric-barrier discharges: Their history, discharge physics, and industrial applications. Plasma chemistry and plasma processing, 2003. 23(1): p. 1-46.

24. Vezzo, G., Lopez, J.L., Freilich, A., Becker, K.H., Optimization of large-scale ozone generators. IEEE Transactions on Plasma Science, 2009. 37: p. 890-896.

25. Gallagher, M.J., et al., Rapid Inactivation of Airborne Bacteria using Atmospheric Pressure Dielectric Barrier Grating Discharge. IEEE Transactions on Plasma Science, 2007. 35(5): p. 1501-1510.

26. Eliasson, B., W. Egli, and U. Kogelschatz, Modelling of dielectric barrier discharge chemistry. Pure and Applied Chemistry, 1994. 66(6): p. 1275-1286.

27. Kosarev, I.N., Starikovskaia, S.M., Starikovskii, A.Y., Shock tube study of artificial ignition of N2O:O2:H2:Ar mixtures, in Shock Waves. 2009, Springer Berlin Heidelberg. p. 769-774.

28. Kolb, G., Fuel Processing for Fuel Cells. 2008, Weinheim: Wiley-VCH.

29. Mungen, R., Kratzer, M.B., Partial combustion of methane with oxygen. Industrial Engineering and Chemistry 1951. 43.

30. Mallens, E.P.J., Hoebink, J.H.B.J., Marin, G. B., The reaction mechanism of the partial oxidation of methane to synthesis gas: a transient kinetic study over rhodium and a comparison with platinum. Journal of Catalysis, 1997. 167: p. 43–56.

31. Rostrup-Nielsen, J.R., Syngas in perspective. Catalysis Today, 2002. 17: p. 243-247.

32. Zhu, J., Zhang, D., King, K.D., Reforming of CH4 by partial oxidation: thermodynamic and kinetic analysis. Fuel, 2001. 80: p. 899-905.

33. Talrose, V.L., Ph.D. Dissertation. 1952, N. N. Semenov Institute of Chemical Physics: Moscow.

34. Starikovskaia, S.M., Plasma assisted ignition and combustion. Journal of Physics D: Applied Physics, 2006. 39: p. 265-299.

35. Lou, G., Bao, A., Nishihara, M., Keshav, S., Utkin, Y.G., Rich, J.W., Lempert, W.R., Adamovich, I.V., Ignition of premixed hydrocarbon-air flows by repetitively pulsed, nanosecond pulse duration plasma. Proceedings of the Combustion Institute, 2007. 31(2): p. 3327-3334.

36. Anikin, N.B., Starikovskaia, S.M., Starikovskii, A.Yu. , Study of the oxidation of alkanes in their mixtures with oxygen and air under the action of pulsed volume nanosecond discharge. Plasma Physics Reports, 2004. 30: p. 1028-1042.

37. Ombrello, T., Qin, X., Ju, Y., Gutsol, A., Fridman, A., Carter, C., Combustion enhancement via stabilized piecewise nonequilibrium gliding arc plasma discharge. American Institute of Aeronautics and Astronautics (AIAA) Journal, 2006. 44: p. 142-150.

38. Kim, W., Do, H., Godfrey-Mungal, M., Cappelli, M.A., Plasma-discharge stabilization of jet diffusion flames. IEEE Transactions on Plasma Science, 2006. 34(6): p. 2545-2551.

39. Leonov, S.B., Yarantsev, D.A., Plasma-induced ignition and plasma-assisted combustion in high-speed flow. Plasma Sources Science and Technology, 2007. 16: p. 132-138.

40. Macheret, S.O., Shneider, M.N., Miles, R.B., Energy efficiency of plasma-assisted combustion in ram/scramjet engines, in 36th AIAA Plasmadynamics and Lasers Conference. 2005: Toronto, Canada.

41. Chintala, N., Bao, A., Lou, G., Adamovich, I.V., Measurements of combustion efficiency in nonequilibrium RF plasma-ignited flows. Combustion and flame, 2006. 144(4): p. 744-756.

42. Gorchakov, G., Lavrov, F. , in Acta Phisicochim. 1934, URSS. p. 139.

43. Plasma science committee and committee on atomic, m., and optical sciences, Database needs for modeling and simulation of plasma processing. 1996, National Research Council: Washington, D.C.

44. Nalbandjan, A., Acta Physicochimica URSS, 1934. 1: p. 305.

45. Dubovitsky, F., Acta Physicochimica URSS, 1935. 2: p. 361.

46. Haas, F.M., Plausibility analysis of branching radical reclamation from HO2 in plasma-stimulated ignition below the autoignition temperature threshold. 2006, Thesis, Drexel University.

47. Bozhenkov S., S., S.M., Starikovskii, A. Yu., Nanosecond gas discharge ignition of H2- and CH4- containing mixtures. Combustion and flame, 2003. 133: p. 133-146.

48. Kosarev, I.N., Starikovskii, A. Yu., Mechanism for electric breakdown in a chemically nonequilibrium system and the influence of the chain oxidation reaction in a H2-air mixture on the breakdown threshold. Plasma Physics Reports, 2000. 26(8): p. 701-709.

49. Campbell, C.S., Egolfopoulos, F.N., Combustion Science and Technology, 2005. 177: p. 2275.

50. Nozaki, T., Muto, N., Kado, S., Okazaki, K., Dissociation of vibrationally excited methane on Ni catalyst Part 1. Application to methane steam reforming. Catalysis Today, 2004. 89: p. 57-65.

51. Nair, S.A., Nozaki, T., Okazaki, K., In situ Fourier Transform Infrared (FTIR) study of nonthermal plasma-assisted methan oxidative conversion. Industrial and Engineering Chemistry Research, 2007. 46: p. 3486-3496.

52. Kovacs, T., Deam, R.T., Methane reformation using plasma: an initial study. Journal of Physics D: Applied Physics, 2006. 39: p. 2391-2400.

53. Mlotek, M., Sentek, J., Krawczyk, K., Schmidt-Szalowki, K. , The hydbrid plasma-catalytic process for non-oxidative methane coupling to ethylene and ethane. Applied Catalysis A: General, 2009. 366: p. 232-241.

54. Yang, Y., Direct non-oxidative methane conversion by non-thermal plasma: modeling study. Plasma chemistry and plasma processing, 2003. 23(2): p. 327-346.

55. Slovetskii, D.I., Plasma chemical processes in petroleum chemistry (review). Petroleum Chemistry, 2006. 46(5): p. 323-332.

56. Yao, S., Nakayama, A., Suzuki, E., Methane conversion using a high frequency pulsed plasma: important factors. American Insitute of Chemical Engineering Journal, 2001. 47(2): p. 413-418.

57. Rykalin, N.N., Tsvetkov, Yu.V., Petrunichev, V.A., Glushko, I.K., Physics, Engineering, and Application of Low-Temperature Plasma, ed. N. (Science). 1970, Kazakhstan: Alma-Ata. p.602.

58. Bromberg, L., Cohn, D.R., Rabinovich, A., Alexeev, N., Plasma catalytic reforming of methane. International Journal of Hydrogen Energy, 1999. 24: p. 1131-1137.

59. Luche, J., Aubry, O., Khacef, A., Cormier, J.M., Syngas production from methane oxidation using non-thermal plasma: experiments and kinetic modeling. Chemical Engineering Journal, 2009. 149: p. 35-41.

60. Czernichowski, A., Czernichowski, M., Czernichowski, P., Cooley, T., Reforming of methane into syngas in a plasma-assisted reactor. Fuel Chemistry Division Preprints, 2002. 47(1): p. 280.

61. Lee, D.H., Kim, K.T., Cha, M.S., Song, Y.H., Optimization scheme of a rotating gliding arc reactor for partial oxidation of methane. Proceedings of the Combustion Institute, 2007. 31: p. 3343-3351.

62. Pushkarev, A.I., Zhu, A.M., Li, X.S., Sazonov, R.V., Methane conversion in low-temperature plasma. High Energy Chemistry, 2009. 43(3): p. 156-162.

63. Cormier, J.M., Rusu, I., Syngas production via methane steam reforming with oxygen: plasma reactors versus chemical reactors. Journal of Physics D: Applied Physics, 2001. 34: p. 2798-2803.

64. Ouni, F., Khacef, A., Cormier, J.M., Effect of oxygen on methane steam reforming in a sliding discharge reactor. Chemical Engineering & Technology, 2005. 29(5): p. 604-609.

65. Nair, S.A., Nozaki, T., Okazaki, K., Methane oxidative conversion pathways in a dielectric barrier discharge reactor - Investigation of gas phase mechanism. Chemical Engineering Journal, 2007. 132: p. 85-95.

66. Givotov, V.K., Potapkin, B.V., Rusanov, V.D., Low-temperature plasma chemistry, in Encyclopedia of Low-Temperature Plasma Y.A. Lebedev, Plate, N.A., Fortov, V.E., Editor. 2005: Moscow.

67. Rusanov, V.D., Babaritskii, A.I., Baranov, I.E., Bibikov, M.B., Deminskii, M.A., Demkin, S.A., Zhivotov, V.K., Konovalov, G.M., Lysov, G.V., Moskovskii, A.S., Potapkin, B.V., Smirnov, R.V., Cheban'kov, F.N., Nonequilibrium effect of atmospheric-pressure microwave-discharge plasma on methane and kerosene conversion into synthesis gas. Doklady Chemistry, 2004. 395(2): p. 82-85.

68. Shekhawat, D., Berry, D.A., Gardner, T.H., Spivey, J.J., Catalytic reforming of liquid hydrocarbon fuels for fuel cell applications, in Catalysis, J.J. Spivey, Dooley, K.M., Editor. 2006, The Royal Society of Chemistry.

69. Shawal-Nasri, N., Jones, J.M., Dupont, V.A., Williams, A., A comparative study of sulfur poisoning and regeneration of precious-metal catalysts. Energy and Fuels, 1998. 12: p. 1130-1134.

70. Moulijn, J.A., van Diepen, A.E., Kapteijn, F., Catalyst deactivation: is it predictable? What to do? . Applied Catalysis A: General, 2001. 212: p. 3-16.

71. Gallagher, M.J., Geiger, R., Rabinovich, A., Fridman, A., Partial oxidation of heavy hydrocarbon fuels for auxiliary power units using non-thermal plasma, in American Institute of Chemical Engineers (AIChE) Spring National Meeting. 2009: Tampa, FL.

72. Nunnally, T., Gutsol, K., Rabinovich, A., Fridman, A., Starikovsky, A., Gutsol, A., Potter, R.W., Dissociation of H2S in non-equilibrium gliding arc "tornado" discharge. International Journal of Hydrogen Energy, 2009. 34(18): p. 7618-7625.

73. Asisov, R.I., Vakar, A.K., Gutsol, A.F., Givotov, V.K., Krasheninnikov, E.G., Krotov, M.F., Rusanov, V.D., Fridman, A.A., Sholin, G.V., Plasmachemical methods of energy carrier production. International Journal of Hydrogen Energy, 1985. 10(7/8): p. 475-477.

74. Harkness, J.B.L., Doctor, R.D., Plasma-chemical treatment of hydrogen sulfide in natural gas processing. 1993, Argonne National Laboratory, Gas Research Institute: Chicago, IL.

75. Benilov, M.S., Naidis, G.V., Modeling of hydrogen-rich gas production by plasma reforming of hydrocarbon fuels. International Journal of Hydrogen Energy, 2006. 31: p. 769-774.

76. Indarto, A., Choi, J.W., Lee, H., Song, H.K., Kinetic modeling of plasma methane conversion using gliding arc. Journal of Natural Gas Chemistry, 2005. 14: p. 13-21.

77. Babaritskii, A.I., Baranov, I.E., Bibikov, M.B., Demkin, S.A., Zhivotov, V.K., Konovalov, G.M., Lysov, G.V., Moskovskii, A.S., Rusanov, V.D., Smirnov, R.V., Cheban'kov, F.N., Partial hydrocarbon oxidation processes induced by atmospheric pressure microwave-discharge plasma. High Energy Chemistry, 2004. 38(6): p. 407-410.

78. Deminsky, M., Jivotov, V., Potapkin, B., Rusanov, V., Plasma-assisted production of hydrogen from hydrocarbons. Pure and Applied Chemistry, 2002. 74(3): p. 413-418.

79. Okumoto, M., Kim, H.H., Takashima, K., Katsura, S., Mizuno, A., IEEE Transactions on Industry Applications, 2001. 37: p. 1618.

80. Supat, K., Chavadej, S., Lobban, L.L., Mallinson, R.G., Combined steam reforming and partial oxidation of methane to synthesis gas under electrical discharge. Industrial and Engineering Chemistry Research, 2003. 42: p. 1654.

81. Fridman, A., Nester, S., Kennedy, L.A., Saveliev, A., Mutaf-Yardimci, O., Gliding arc gas discharge. Progress in Energy and Combustion Science, 1999. 25: p. 211-231.

82. Rusanov, V.D., Babaritskii, A.I., Gerasimov, E.N., Deminskii, M.A., Demkin, S.A., Zhivotov, V.K., Moskovskii, A.S., Potapkin, B.V., Smirnov, R.V., Strelkova, M.I., Doklady Akademii Nauk (Doklady Physical Chemistry), 2003. 389(3): p. 324.

83. Sekine, Y., Urasaki, K., Kado, S., Matsukata, M., Kikuchi, E., Nonequilibrium pulsed discharge: A novel method for steam reforming of hydrocarbons or alcohols. Energy and Fuels, 2004. 18: p. 455-459.

84. Kogelschatz, U., Zhou, L.M., Xue, B., Eliasson, B., Greenhouse gas control technologies, ed. B. Eliasson. 1999: Pergamon.

85. Gesser, H.D., Hunter N.R., Probawono D., , The CO2 reforming of natural gas in a silent discharge reactor. Plasma chemistry and plasma processing, 1998. 18: p. 241-245.

86. Song, H.K., Lee, H., Choi, J.W., Na, B., Effect of electrical pulse forms on the CO2 reforming of methane using atmospheric dielectric barrier discharge. Plasma chemistry and plasma processing, 2004. 24(1): p. 57.

87. Larkin, D.W., Caldwell, T.A., Lobban, L.L., Mallinson, R.G., Oxygen pathways and carbon dioxide utilization in methane partial oxidation in ambient temperature electric discharges. Energy and Fuels, 1998. 12: p. 740-744.

88. Mutaf-Yardimci, O., Saveliev, A.V., Fridman, A.A., Kennedy, L.A., Employing plasma as a catalyst in hydrogen production International Journal of Hydrogen Energy, 1998. 23(12): p. 1109-111.

89. Indarto, A., Kinetic of CO2 reduction by gliding arc plasma. Asian Journal of Water, Environment, and Pollution, 2006. 4(1): p. 191-194.

90. Lesueur, H., Czernichowski, A., Chapelle, J., Electrically assisted partial oxidation of methane. International Journal of Hydrogen Energy, 1994. 19: p. 139-144.

91. Indarto, A., Yang, D.R., Choi, J.W., Lee, H., Song, H.K., Gliding arc plasma processing of CO2 conversion. Journal of Hazardous Materials, 2006. 146(1/2): p. 309-315.

92. Czernichowski A., C.P., Wesolowska, K., Plasma-assisted reforming of some liquid fuels into synthesis gas, in 6th European SOFC Forum. 2004: Lucerne, Switzerland.

93. Paulmier, T., Fulcheri, L., Use of non-thermal plasma for hydrocarbon reforming. Chemical Engineering Journal, 2005. 106: p. 59-71.

94. Cohn, D.R., Rabinovich, A., Titus, C.H., Bromberg, L., Near-term possibilities for extremely low emission vehicles using onboard plasmatron generation of hydrogen. International Journal of Hydrogen Energy, 1997. 22(7): p. 715-723.

95. Horng, R.F., Wen, C.S., Liauh, C.T., Chao, Y., Huang, C.T., Driving characteristics of a motorcycle fuelled with hydrogen-rich gas produced by an onboard plasma reformer. International Journal of Hydrogen Energy, 2008. 33: p. 7619-7629.

96. Bromberg, L., Cohn, D.R., Heywood, J., Rabinovich, A., Onboard plasmatron generation of hydrogen rich gas for diesel engine exhaust aftertreatment and other applications. 2002, Massachusetts Institute of Technology, Plasma Science and Fusion Center.

97. Penetrante, B.M., Hsiao, M.C., Merritt, B.T., Vogtlin, G.E., Fundamental limits on NOx reduction by plasma, in SAE Meeting & Expo. 1997: Dearborn, MI.

98. Tonkyn, R.G., Barlow, S.E., Hoard, J.W., Reduction of NOX in synthetic diesel exhaust via two-step plasma-catalysis treatment. Applied Catalysis B: Environmental, 2003. 40(3): p. 207-217.

99. Mok, Y.S., Koh, D.J., Shin, D.N., Kim, K.T., Reduction of nitrogen oxides from simulated exhaust gas by using plasma-catalytic process. Fuels Processing Technology, 2004. 86(3): p. 303-317.

100. Bromberg, L., Crane, S., Rabinovich, A., Kong, Y., Cohn, D.R., Heywood, J., Alexeev, N., Samokhin, A., Hydrogen generation from plasmatron reformers: A promising technology for NOx adsorber regeneration and other automotive applications. 2003, Massachusetts Institute of Technology, Plasma Fusion and Science Center.

101. Bromberg, L., Cohn, D.R., Wong, V., Regeneration of diesel particulate filters with hydrogen rich gas. 2005, Massachusetts Institute of Technology, Plasma Fusion and Science Center.

102. Yoshida, K., Rajanikanth, B.S., Okubo, M., NO_X reduction and desorption studies under electric discharge plasma using a simulated gas mixture: a case study on the effect of corona electrodes. Plasma Science and Technology, 2009. 11: p. 327-333.

103. EG&G Technical Services, Fuel Cell Handbook. 2004, U.S. Department of Energy: Morgantown, WV. p. 8-64.

104. Bromberg, L., Cohn, D.R., Rabinovich, A., Alexeev, N., Samokhin, A., Hadidi, K., Palaia, J., Margarit-Bel, N., Onboard plasmatron hydrogen production for improved vehicles. 2006, Massachusetts Institute of Technology, Plasma Fusion and Science Center.

105. Long, H., Shang, S., Tao, X., Yin, Y., Dai, X., CO2 reforming of CH4 by combination of cold plasma jet and Ni/g-Al2O3 catalyst. International Journal of Hydrogen Energy, 2008. 33: p. 5510-5515.

106. Kraus, M., Eliasson, B., Kogelschatz, U., Wokaun, A., CO2 reforming of methane by the combination of dielectric-barrier discharges and catalysis. Physical Chemistry Chemical Physics, 2001. 3: p. 294-300.

107. Nozaki, T., Tsukijihara, H., Fukui, W., Okazaki, K., Kinetic analysis of the catalyst and nonthermal plasma hybrid reaction for methane steam reforming. Energy and Fuels, 2007. 21: p. 2525-2530.

108. Sekine, Y., Haraguchi, M., Tomioka, M., Matsukata, M., Kikuchi, E., Low-temperature hydrogen production by highly efficient catalytic system assisted by electric field. Journal of Physical Chemistry: A, 2009. in Press.

109. Pietruszka, B., Anklam, K., Heintze, M., Plasma-assisted partial oxidation of methane to synthesis gas in a dielectric barrier discharge. Applied Catalysis A: General, 2004. 261: p. 19-24.

110. Heintze, M., Pietruszka, B., Plasma catalytic conversion of methane into syngas: the combined effect of discharge activation and catalysis. Catalysis Today, 2004. 89: p. 21-25.

111. Horng, R.F., Huang, C.T. Lai, M.P., Wen, C.S., Chiu, W.C., Characteristics of hydrogen production by a plasma-catalyst hybrid converter with energy saving schemes under atmospheric pressure. International Journal of Hydrogen Energy, 2008. 33: p. 3719-3727.

112. Sobacchi, M.G., Saveliev, A.V., Fridman, A.A., Kennedy, L., Ahmed, S., Krause, T., Experimental assessment of a combined plasma/catalytic system for hydrogen production via partial oxidation of hydrocarbon fuels. International Journal of Hydrogen Energy, 2002. 27: p. 635-642.

113. Liu, C., Marafee, A., Mallinson, R., Lobban, L., Methane conversion to higher hydrocarbons in a corona discharge over metal oxide catalysts with OH groups. Applied Catalysis A: General, 1997. 164: p. 21-33.

114. Chen, H.L., Lee, H.M., Chen, S.H., Chao, Y., Chang, M.B., Review of plasma catalysis on hydrogen reforming for hydrogen production - Interaction, integration, and prospects. Applied Catalysis B: Environmental, 2008. 85: p. 1-9.

115. Nozaki, T., Muto, N., Kado, S., Okazaki, K., Minimum energy requirement for methane steam reforming in plasma-catalyst reactor. American Chemical Society, Division of Fuel Chemistry, 2004. 49(1): p. 179.

116. Nozaki, T., Muto, N., Kado, S., Okazaki, K., Dissociation of vibrationally excited methane on Ni catalyst Part 2. Process diagnostics by emission spectroscopy. Catalysis Today, 2004. 89: p. 67-74.

117. Gutsol, A.F., Bakken, J.F., , New vortex method of plasma insulation and explanation of the ranque effect. Journal of Physics D: Applied Physics, 1998. 31: p. 704-711.

118. Gutsol, A., Larjo, J., Hernberg, R., Comparative study of ICP generator with forward-vortex and reverse-vortex stabilization. Plasma chemistry and plasma processing, 2002. 22: p. 351-369.

119. Bromberg, L., CFD modeling of plasmatron methane reformer, in Plasma Science and Fusion Center Report JA-05-14. 2005.

120. Al-Hamamre, Z., Deizinger, S., Mach, A., Von Issendorf, F., Trimis, D., Thermal partial oxidation of diesel fuel in porous reactors for synthesis gas production. Clean Air, 2006. 7: p. 391-407.

121. Kalra, C.S., et. al. , Electrical discharges in the Reverse Vortex Flow – Tornado Discharges, in International Symposium on Plasma Chemistry. 2003: Taormina, Italy.

122. Nassar, H., Pellerin, S., Musiol, K., Martinie, O., Pellerin, N., Cormier, J.M., N2+/N2 ratio and temperature measurements based on the first negative N2+ and second positive N2 overlapped emission spectra. Journal of Physics D: Applied Physics, 2004. 37: p. 1904-1916.

123. Laux, C.O., Spence, T.G., Kruger, C.H., Zare, R.N., Optical diagnostics of atmospheric pressure air plasmas. Plasma Sources Science and Technology, 2003. 12: p. 125-138.

124. Starikovskii, A.Y., E/n from ratio of N2 spectra (337/391). 2009.

125. Creyghton, Y., Pulsed Positive Corona Discharges: Fundamental Study and Application to Flue Gas Treatment. 1994, Eindhoven University of Technology: Eindhoven.

Appendix A. Reverse Vortex Gliding Arc Reactor Design Details

Gliding Arc Diesel Reformation Reactor

Safety Calculations

Michael Gallagher, Alexander Gutsol

A. Description

This document describes safety calculations that are based on the Lawrence Livermore National Laboratory (LLNL) Environmental Safety and Health Manual, document 18.2: pressure vessel and system design [1]. Calculations were made for the Gliding Arc Diesel Reformation reactor designed by Drexel Plasma Institute. The reactor is cylindrical with a shell comprised of type 316 seamless stainless steel tubing and welded flanges on each end that include flanged/o-ring sealed lid. This study will evaluate the strength of the cylindrical shell including top and bottom flanges and bolts/nuts, as these are the only places where failure, if it occurs, can have an influence on surrounded environment. Note: calculations for outer shell strength do not consider operation of the vessel in a corroded condition.

B. Hazard

This reactor is designed to operate at a pressure of 15 psig and utilizes combustion or steam reforming of methane (model fuel) or gasified diesel fuel at an ultra-rich equivalence ratio. Mixtures of these fuels (especially methane) with air are considered reactive, flammable and even explosive, and therefore the experimental protocol for this device should be carefully followed in order to prevent catastrophic failure. Nevertheless, the reactor is designed to sustain this catastrophic failure. In the event of improper mixing of the feed gas, thermodynamic estimates conclude that volumetric expansion of the methane-air mixture will not exceed 10 times, which means that pressure will not exceed 300 psia.

C. Safety Calculation

For this vessel, the following design features will be analyzed:

1. Maximum Allowable Working Pressure (MAWP)
2. Top/Bottom Flange thickness

3. Bolt size & required area

4. Bolt/nut thread stress

Design details for this vessel are presented in the Figure 1.

Temperature operation range: 70°F to 1100°F (high temperature for the central part of the reactor only).

Outer cylinder material and specifications for 316 stainless steel seamless tube per SA-312:

- Tensile strength = 75,000 psig [2]
- Yield stress: Sy = 30,000 psig [2]
- Application and Max. Temp. limit: 1500ºF
- Maximum Allowable stress @1100 ºF: Sa = 11.1 ksig [2]

C.1 Maximum Allowable Working Pressure (MAWP)

For pressure vessels where $r_o/r_i \leq 1.1$, the thin-wall equation is used to calculate the MAWP due to cylindrical hoop stress [3].

$$MAWP = \frac{(S_a)Et}{r_i}$$

Where,

r_o = (76.2mm)/2 = 38.1mm

r_i = (73mm)/2 = 36.5mm

r_o / r_i = 38.1/36.5 = 1.043

Sa = allowable stress of material = 11.1 ksi @1100F [2]

E = joint efficiency factor = 1 for seamless pipe [4]

t = wall thickness = 1.65 mm

$$MAWP = \frac{(11{,}100\,psi) * 1.65mm}{36.5mm} = 501\,psi$$

The maximum allowable working pressure due to cylindrical hoop stress is 501 psi. The maximum allowable working pressure due to axial stress on the vessel was also

calculated for two cases; one case that considers the axial stress in the heated zone (T=1100F) and the other that considers the axial stress on the welded flanges in the cooler zone (T~200F). The formula for the maximum allowable pressure due to axial stress is the following [5]:

$$MAWP = \frac{2*(S_a)Et}{r_i}$$

For MAWP pressure due to axial stress in heated zone(T=1100F):

$$MAWP = \frac{2*(11{,}100\,psi)*1.65mm}{36.5mm} = 1003\,psi$$

Where E = 1 for the seamless pipe. For MAWP pressure due to axial stress in the cooled zone considering the joint efficiency factor (E=0.60) for welded flanges [4]:

$$MAWP = \frac{2*(0.60)*(18{,}800\,psi)*1.65mm}{36.5mm} = 1019\,psi$$

In conclusion, the overall MAWP of the vessel is 501 psi, which is 33 times higher than the design operating pressure of the reactor and higher than expected pressure in the case of catastrophic failure. Taking into account that tensile strength of material is much higher than yield stress (75,000 psig in comparison with 30,000 psig), the tensile strength for the vessel is also much higher than MAWP, therefore even catastrophic operational failure will not destroy the vessel.

C.2 Top/Bottom Flange Thickness

The top and bottom flanges have a bolted connection with a silicone o-ring. Both flanges should extend approximately 6 inches away the heat exchanger and therefore should be significantly cooler than the cylindrical body of the reactor. Figure 1 below depicts the connection type used for both flanges.

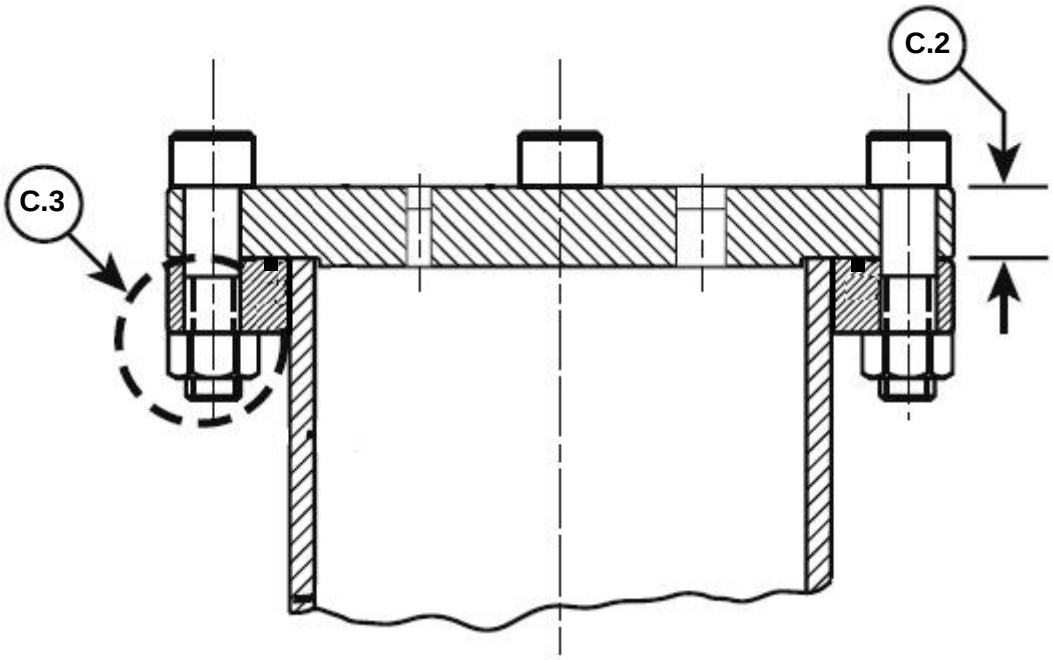

Figure 1. Flanged connection type for the outer shell of the Gliding Arc reactor

For a top and bottom flange thickness of 0.375" (9.4mm) the maximum working pressure is calculated from the following [6]:

$$P = \left[\frac{T^2}{d^2} - \frac{1.9Wh_g}{S_a d^3} \right] \frac{S_a}{c}$$

Where,

P = Maximum pressure for top/bottom flanges

d = 3.3"

P_m = Maximum allowable working pressure (MAWP) = 501 psi

H = Hydrostatic End Force = $\pi/4(d^2 * P_m)$ = 2565 lbs.

h_g = radial difference between bolt circle and pressure seal circle (flange moment arm) = (5" – 3")/2 = 1"

d = pressure seal diameter = 3.3”

Hp = 0 - for self-energizing seals (o-rings)

W = Flange design bolt load = H + Hp = 2565 + 0 = 2565 lbs.

C = attachment coefficient = 0.25

T = flange thickness = 0.375”

S_a = Allowable stress of flange (18800 psi @ 400K) [2]

Solving for P gives:

P = 724 psi ← The top/bottom flanges can withstand this pressure, since it is above the MAWP (501 psi) the flange thickness is acceptable.

C.3.1 Bolt size & required area

The bolts chosen are 3/8-16 stainless steel with minimum tensile strength 140,000 psi (part#: 96870A255). The bolting area is determined by the following:

A_m = total required area of bolting

= larger of : A_{m1} = (operating conditions)

A_{m2} = (gasket sealing)

S_a = Allowable bolt stress at atmospheric temperature = 25,000 psi [7]

S_b = Allowable bolt stress at operating temperature = 25,000 psi [7]

$S_a = S_b = S_{a-b}$

$A_{m1} = W/S_{a-b}$

A_{m1} = 2565 lbs. / 25000lbs/ in^2 = 0.1026 in^2

A_b = actual total area of bolting for 8 x 3/8-16 bolts = 8 x 0.0775 = 0.62 in^2 [8]

$A_b > A_m$, therefore the design bolting area is adequate for this vessel.

C.3.2 Bolt/Nut Thread Stress

The following formula was used to determine the pressure/stress relationship of the bolts & nuts used for the primary flanges of the vessel shell.

$$P = 8\left[\frac{S_a E L_e}{D^2}\right]$$

Where E = pitch diameter of the external thread (bolt) = 0.3287”

Le = thickness of nut = 0.3281”

D = o-ring seal diameter = 3.3”

For Bolts:

$$P = 8\left[\frac{(25{,}000 * 0.3287 * 0.3281)}{3.3^2}\right] = 1980\,psi$$

Bolts can withstand pressure of 1980 psi, which is significantly greater than the MAWP (501 psi).

For Nuts:

S_a = Allowable nut stress at operating temperature - Proof load (lbf) is used here, where Proof load = proof load stress (90,000 psi) * stress area of 3/8-16 nut (0.0775 in^2) = 6975 lbf [9]

E = 0.3287”

$$P = 8\left[\frac{6{,}975(.3287 * 0.3281)}{3.3^2}\right] = 552\,psi$$

Nuts can withstand pressure of 552 psi, which is greater than the MAWP (501 psi).

References

1. LLNL document 18.2. ES&H Manual, vol 2: Health & Safety Controls and Hazards, document 18.2: Pressure vessel and system design
2. 2004 ASME Boiler and Pressure Vessel Code, Section II, Table 1A Section I; Section III, Class 2 and 3; and Section VIII, Division 1 Maximum Allowable Stress Values S for Ferrous Materials, SA-312 seamless pipe, type 316
3. Roark R.J., Formulas for Stress and Strain, McGraw-Hill, New York, 1954.
4. Megyesy, Eugene F. Pressure Vessel Handbook, Pressure Vessel Handbook Publishing, Inc., Tulsa, OK, 1977.
5. Harvey, John F. Pressure Vessel Design, D. Van Nostrand Company, Inc., New York, NY, 1963.
6. LLNL document 18.2. ES&H Manual, vol 2: Health & Safety Controls and Hazards, document 18.2: Pressure vessel and system design: equation 10.
7. 2004 ASME Boiler and Pressure Vessel CodeTable 3, Section III, Class 2 and 3, and Section VIII, Divisions 1 and 2 Maximum Allowable Stress Values S for Bolting Materials.
8. Bolt Clamping Force Table. http://studentsections.asme.org/calpoly/bolttorquetable.htm
9. Stainless steel fasteners designers handbook. Specialty Steel Industry of North America. http://www.ssina.com/view_a_file/fasteners.pdf

Vita

Michael J. Gallagher, Jr.

Birthplace: Philadelphia, PA

Education

Ph.D. Mechanical Engineering, Drexel University 2005 – 2010

M.S. Mechanical Engineering, Drexel University 2003 – 2005
Dissertation: Effects of Dielectric Barrier Discharge Plasma on the Survivability of Airborne Bacteria

B.S. Commerce and Engineering, September 1996 – June 2000
Minor: Management Information Systems

Journal Publications

Gallagher, Jr. M.J., et al. "*Rapid Inactivation of Airborne Bacteria Using Atmospheric Pressure Dielectric Barrier Grating Discharge*." IEEE Transactions on Plasma Science, 35:5, pp. 1501-1510 (2007).

Gallagher, Jr. M.J., Geiger, R., Polevich, A., Rabinovich, A., Fridman, A. "*On-board Plasma-Assisted Conversion of Heavy Hydrocarbons into Synthesis Gas*," Fuel, (Article in Press, January 2010).

Gallagher, Jr. M.J., Geiger, R., Polevich, A., Rabinovich, A., Fridman, A. "*Autothermal reforming of diesel fuel using gliding arc plasma for solid oxide fuel cells*," International Journal of Hydrogen Energy, in preparation.

Book Chapter

Gallagher, Jr. M.J., Fridman A. "*Plasma reforming for H_2-rich synthesis gas*," Fuel Processing for Fuel Cell Applications. Eds. D. Shekhawat, D. Berry, J.J. Spivey. Elsevier, in review.